ITS INSTITUTE
Intelligent Transportation Systems

Enhanced Micro-Simulation Models for Accurate Safety Assessment of Traffic Management ITS Solutions

Final Report

Prepared by:

Wuping Xin
John Hourdos
Panos Michalopoulos

Department of Civil Engineering
University of Minnesota

CTS 08-17

Technical Report Documentation Page

1. Report No. CTS 08-17	2.	3. Recipients Accession No.
4. Title and Subtitle Enhanced Micro-Simulation Models for Accurate Safety Assessment of Traffic Management ITS Solutions		5. Report Date November 2008 6.
7. Author(s) Wuping Xin, John Hourdos, and Panos Michalopoulos		8. Performing Organization Report No.
9. Performing Organization Name and Address Department of Civil Engineering University of Minnesota 500 Pillsbury Drive S.E. Minneapolis, MN 55455-0116		10. Project/Task/Work Unit No. CTS project # 2006043 11. Contract (C) or Grant (G) No.
12. Sponsoring Organization Name and Address Intelligent Transportation Systems Institute University of Minnesota 200 Transportation and Safety Building 511 Washington Ave. SE Minneapolis, Minnesota 55455		13. Type of Report and Period Covered Final Report 14. Sponsoring Agency Code
15. Supplementary Notes http://www.cts.umn.edu/Publications/ResearchReports/		

16. Abstract (Limit: 200 words)

Much research has been conducted in the development, implementation, and evaluation of innovative ITS technologies aiming to improve traffic operations and driving safety. Existing micro-simulation modeling only describes normative car-following behaviors devoid of weakness and risks associated with real-life everyday driving. This research aims to develop a new behavioral car-following model that is pertinent to the true nature of everyday human driving. Unlike traditional car-following models that deliberately prohibit vehicle collisions, this new model builds upon multi-disciplinary findings explicitly taking into account perceptual thresholds, judgment errors, anisotropy of reaction times and driver inattention, in order to replicate “less-than-perfect” driving behavior with all its weakness and risks. Most importantly, all parameters of this model have direct physical meaning; this ensures vehicle collisions are replicated as a result of behavioral patterns rather than simply being numerical artifacts of the model. Meanwhile, vehicle trajectories were extracted from real-life crashes collected from a freeway section of I-94WB This is by far the first data collection efforts that aim to collect vehicle trajectories from real-life crashes to aid car-following modeling. These data were employed in this study to test, calibrate and validate the model. This new model is successful in replicating these vehicle trajectories as well as crashes.

17. Document Analysis/Descriptors Traffic simulation, driving behavior, car-following models, traffic safety, rear-end collisions, freeway traffic.		18. Availability Statement No restrictions. Document available from: National Technical Information Services, Springfield, Virginia 22161	
19. Security Class (this report) Unclassified	20. Security Class (this page) Unclassified	21. No. of Pages 107	22. Price

Enhanced Micro-Simulation Models for Accurate Safety Assessment of Traffic Management ITS Solutions

Final Report

Prepared by

Wuping Xin
John Hourdos
Panos Michalopoulos

November 2008

Published by

Intelligent Transportation Systems Institute
Center for Transportation Studies
University of Minnesota
200 Transportation and Safety Building
511 Washington Ave SE
Minneapolis, MN 55455

The contents of this report reflect the views of the authors, who are responsible for the facts and the accuracy of the information presented herein. This document is disseminated under the sponsorship of the Department of Transportation University Transportation Centers Program, in the interest of information exchange. The U.S. Government assumes no liability for the contents or use thereof. This report does not necessarily reflect the official views or policy of the Intelligent Transportation Systems Institute or the University of Minnesota.

The authors, the Intelligent Transportation Systems Institute, the University of Minnesota and the U.S. Government do not endorse products or manufacturers. Trade or manufacturers' names appear herein solely because they are considered essential to this report.

Acknowledgements

This study utilized the advanced detection and surveillance stations maintained by the Minnesota Traffic Observatory while support for this study was provided by the ITS Institute of the University of Minnesota. The authors wish to thank Professor Takashi Nakatsuji and Dr. Prakish Ranjitkar from Hokkaido University, Japan for providing the RTKGPS data. The NGSIM data were provided by the FHWA funded NGSIM project that maintains a comprehensive library of vehicle trajectories from freeways and arterial streets. Finally, the German autobahn data were graciously provided to us by the Robert Bosch GmbH through the German Aerospace Center.

The author(s) wish to acknowledge those who made this research possible. The study was funded by the Intelligent Transportation Systems (ITS) Institute, a program of the University of Minnesota's Center for Transportation Studies (CTS). Financial support was provided by the United States Department of Transportation Research and Innovative Technologies Administration (RITA).

Table of Contents

1 INTRODUCTION 1
1.1 Problem Statement 1
1.2 Research Objectives 2
1.3 Contributions 3
1.4 Outline 3
2 BACKGROUND 5
2.1 Overview of Car-following Modeling 5
2.2 Detailed Review of Existing Car-following Models 6
2.2.1 Deterministic Stimulus-Response Models 8
2.2.2 Optimal Velocity Model 13
2.3 Traffic Stability and Car-following Behavior 15
2.4 Conclusions 17
3 METHODOLOGY 18
3.1 Data Requirements 18
3.1.1 Non-Crash Data Collection 18
3.1.2 Crash Data Collection 20
3.2 Model Development 23
3.2.1 Empirics of Car-following Behavior 23
3.2.2 Review of Crash-prone Conditions 38
3.2.3 Conceptual Framework 44
3.2.4 Proposed Model 48
3.3 Model Calibration and Validation 53
3.3.1 Calibration Methodology 53
3.3.2 Validation Methodology 54
3.4 Stability Analysis Methodology 55
4 IMPLEMENTATION 57
4.1 Environment 57
4.2 Model Calibration and Validation Using Non-Crash Data 60
4.3 Model Calibration and Validation Using Crash Data 73
5 CONCLUDING REMARKS 91
REFERENCES 92

List of Tables

Table 2-1. Parameter Values Suggested by Gipps 12
Table 3-1. Specifications of Test Vehicles (Provided Courtesy of Dr. Ranjitkar) 19
Table 3-2. Drivers' Characteristics (Provided Courtesy of Dr. Ranjitkar) 19
Table 3-3. Statistics of Time Headway Distribution and Gamma Parameters of A100 Freeway Dataset 25
Table 3-4. Statistics of Time Headway Distribution and Gamma Parameters of RTKGPS Dataset 29
Table 3-5. Statistics of Reaction Time: NGSIM Data 36
Table 4-1. Calibrated Parameters for the Following Vehicles in the Platoon (RTKGPS Data) ... 61
Table 4-2. Statistics of Calibrated Parameters for Non-Crash Data (RTKGPS Data): Sample Size 9 65
Table 4-3. Validation Statistics (G01 is Platoon Leader) 66
Table 4-4. Validation Statistics (G03 is Platoon Leader) 66
Table 4-5. Summary of Crash/Near-Misses Cases Collected from Study Site 74
Table 4-6 (a). Calibrated Parameters for Crash Case CR-01 75
Table 4-6 (b). Calibrated Parameters for Crash Case #2 75
Table 4-6 (c). Calibrated Parameters for Crash Case #3 (Near-Miss) 75
Table 4-6 (d). Calibrated Parameters for Crash Case #4 76
Table 4-6 (e). Calibrated Parameters for Crash Case #5 76
Table 4-6 (f). Calibrated Parameters for Crash Case #6 (Near Misses) 76
Table 4-6 (g). Calibrated Parameters for Crash Case #7 77
Table 4-6 (h). Calibrated Parameters for Crash Case #9 (Vehicle 12 Near-Miss) 77
Table 4-6 (i). Calibrated Parameters for Crash Case #10 78
Table 4-6 (j). Calibrated Parameters for Crash Case #11 (Vehicle 11 Near-Miss) 78
Table 4-6 (k). Statistics of Calibrated Parameters for Crash Data (I94 Crash Trajectories) Sample Size: 48 Drivers 79
Table 4-7 (a). Validation Statistics for Crash Case CR-01 88
Table 4-7 (b). Validation Statistics for Crash Case #2 88
Table 4-7 (c). Validation Statistics for Crash Case #3 (Near-Miss) 88
Table 4-7 (d). Validation Statistics for Crash Case #4 89
Table 4-7 (e). Validation Statistics for Crash Case #5 89
Table 4-7 (f). Validation Statistics for Crash Case #6 (Near Misses) 89
Table 4-7 (g). Validation Statistics for Crash Case #7 89
Table 4-7 (h). Validation Statistics for Crash Case #9 (Vehicle 12 Near-Miss) 90
Table 4-7 (i). Validation Statistics for Crash Case #10 90
Table 4-7 (j). Validation Statistics for Crash Case #11 (Vehicle 11 Near-Miss) 90

List of Figures

Figure 2-1. A Typical Car-Following Situation with Two Interacting Vehicles 5
Figure 2-2. Classification Diagram of Existing Car-Following Models..... 7
Figure 2-3. Measured Car-Following Behavior. Data were Collected From a Japan Test Track using GPS 16
Figure 3-1. Schematic Layout of the Track at Hokkaido University (Ranjitkar 2004) 18
Figure 3-2. Lead Vehicle Speed Pattern 20
Figure 3-3. Selected Data Collection Site: A High Crash-Rate Section Of I-94 Westbound..... 21
Figure 3-4. Surveillance Cameras that Monitor the Site..... 21
Figure 3-5. Small Factor PCs used to Digitize and Store Video Data 23
Figure 3-6. A Sample of Extracted Vehicle Trajectory 23
Figure 3-7 (a). Distance-Headway and Velocity: A100 Freeway Dataset (Hifahrt) 25
Figure 3-7 (b). Distance-Headway and Velocity: A100 Freeway Dataset (Rueckfahrt)..... 25
Figure 3-8 (a). Time Headway Distribution: German Hifahrt Dataset (Speed > 5m/S)..... 26
Figure 3-8 (b). Time Headway Distribution: German Rueckfahrt Dataset (Speed > 5m/S) 26
Figure 3-9 (a). Oscillations Spirals: German Rueckfahrt Dataset 27
Figure 3-9 (b). Oscillations Spirals: German Hifahrt Dataset 27
Figure 3-10. Distance Headway and Speed Relationship: Japan Dataset (9 Vehicles On Test Track)..... 30
Figure 3-11. Time Headway Distribution Japan Data (9 Vehicles)..... 31
Figure 3-12. Oscillation Spirals 32
Figure 3-13 (a). Acceleration-Relative Speed-Distance Relationship..... 33
Figure 3-13 (b). Acceleration-Relative Speed-Distance Relationship..... 33
Figure 3-13 (c). Acceleration-Relative Speed-Distance Relationship..... 35
Figure 3-14 (a). Reaction Time Distribution: I-80 from 4:00-4:15 pm 37
Figure 3-14 (b). Reaction Time Distribution: I-80 from 5:00-5:15 pm 37
Figure 3-14 (c). Reaction Time Distribution: I-80 from 5:15-5:30 pm 38
Figure 3-15. Number of Crashes vs. Visibility 39
Figure 3-16. Poor Visibility Days..... 39
Figure 3-17. Crashes vs. Pavement Condition..... 39
Figure 3-18. Crash Cases vs. Sun Position 40
Figure 3-19. Collision Totals per Location..... 40
Figure 3-20. Crashes vs. Time 41
Figure 3-21. General Concept: Situational/Environmental Factors and DUV 45
Figure 3-22. Interactions between External World and DUV 45
Figure 3-23. Detailed Block Diagram of Longitudinal Driving Task 47
Figure 3-24. Visual Angle Subtended by the Image of an Object on the Retina and its Expansion Rate 49
Figure 3-25. Speed Profiles of Platoon Leader used in Mild and Severe Disturbance Scenarios..... 56
Figure 4-1. Snapshot of the CalibWizard Program Developed for Automating Parameter Calibration..... 57
Figure 4-2. Snapshot of the wxSim Program Developed for Testing the Proposed Car-Following Program 58
Figure 4-3. CalibWizard User Interface for Setting Up Parameters Feasible Region 59

Figure 4-4. Calibration Results 59
Figure 4-5. wxSim Loading Vehicle User Interface 60
Figure 4-6. Calibrated Scanning Intervals 61
Figure 4-7 (a). Validation Results (Lead Vehicle G01 Not Shown in the Figure) 63
Figure 4-7 (b). Validation Results (Lead Vehicle is G03 Not Shown in the Figure) 64
Figure 4-8 (a). Lead Vehicle (G01) Speed Profile 67
Figure 4-8 (b). Veh G02 Speed and Trajectory Profile: Real vs. Simulated 67
Figure 4-8 (c). Veh G03 Speed and Trajectory Profile: Real vs. Simulated 67
Figure 4-8 (d). Veh G04 Speed and Trajectory Profile: Real vs. Simulated 67
Figure 4-8 (e). Veh G05 Speed and Trajectory Profile: Real vs. Simulated 68
Figure 4-8 (f). Veh G06 Speed and Trajectory Profile: Real vs. Simulated 68
Figure 4-8 (g). Veh G07 Speed and Trajectory Profile: Real vs. Simulated 68
Figure 4-8 (h). Veh G08 Speed and Trajectory Profile: Real vs. Simulated 68
Figure 4-8 (i). Veh G09 Speed and Trajectory Profile: Real vs. Simulated 69
Figure 4-8 (j). Veh G10 Speed and Trajectory Profile: Real vs. Simulated 69
Figure 4-9 (a). Lead Vehicle (G03) Speed Profile 70
Figure 4-9 (b). Veh G04 Speed and Trajectory Profile: Real vs. Simulated 70
Figure 4-9 (c). Veh G05 Speed and Trajectory Profile: Real vs. Simulated 71
Figure 4-9 (d). Veh G06 Speed and Trajectory Profile: Real vs. Simulated 71
Figure 4-9 (e). Veh G07 Speed and Trajectory Profile: Real vs. Simulated 71
Figure 4-9 (f). Veh G08 Speed and Trajectory Profile: Real vs. Simulated 71
Figure 4-9 (g). Veh G09 Speed and Trajectory Profile: Real vs. Simulated 72
Figure 4-9 (h). Veh G10 Speed and Trajectory Profile: Real vs. Simulated 72
Figure 4-10 (a). Distribution of Calibrated Maximum Comfortable Acceleration 80
Figure 4-10 (b). Distribution of Calibrated Maximum Comfortable Deceleration 80
Figure 4-10 (c). Distribution of Calibrated Oscillation Acceleration 81
Figure 4-10 (d). Distribution of Calibrated Oscillation Deceleration 81
Figure 4-10 (e). Distribution of Calibrated Desired Following Gap Time 82
Figure 4-10 (f). Distribution of Calibrated Scanning Interval 82
Figure 4-11 (a). Simulated Trajectories (Dotted Line) vs. Real Trajectories (Solid Line) for Crash Case CR-01 83
Figure 4-11 (b). Simulated Trajectories (Dotted Line) vs. Real Trajectories (Solid Line) for Crash Case CR-02 83
Figure 4-11 (c). Simulated Trajectories (Dotted Line) vs. Real Trajectories (Solid Line) for Crash Case CR-03 84
Figure 4-11 (d). Simulated Trajectories (Dotted Line) vs. Real Trajectories (Solid Line) for Crash Case CR-04 84
Figure 4-11 (e). Simulated Trajectories (Dotted Line) vs. Real Trajectories (Solid Line) for Crash Case CR-05 85
Figure 4-11 (f). Simulated Trajectories (Dotted Line) vs. Real Trajectories (Solid Line) for Crash Case CR-06 85
Figure 4-11 (g). Simulated Trajectories (Dotted Line) vs. Real Trajectories (Solid Line) for Crash Case CR-07 86
Figure 4-11 (h). Simulated Trajectories (Dotted Line) vs. Real Trajectories (Solid Line) for Crash Case CR-09 86

Figure 4-11 (i). Simulated Trajectories (Dotted Line) vs. Real Trajectories (Solid Line) for Crash Case CR-10 87
Figure 4-11 (j). Simulated Trajectories (Dotted Line) Vs. Real Trajectories (Solid Line) for Crash Case CR-11 87

Executive Summary

Much research has been conducted in the development, implementation, and evaluation of innovative ITS technologies aiming to improve traffic operations and driving safety. As part of the process, micro-simulation has become an increasingly indispensable tool for assisting in system design and evaluation. It has become evident that existing micro-simulation models are deficient when evaluating sophisticated safety-related ITS techniques. This is because existing micro-simulation modeling only describes normative car-following behaviors devoid of weakness and risks associated with real-life everyday driving. This research aims to develop a new behavioral car-following model that is pertinent to the true nature of everyday human driving. This model is for the purpose of enabling micro-simulation as an effective and reliable tool to study crash mechanism and aid safety evaluations. Unlike traditional car-following models that deliberately prohibit vehicle collisions, this new model builds upon multi-disciplinary findings explicitly taking into account perceptual thresholds, judgment errors, anisotropy of reaction times and driver inattention, in order to replicate "less-than-perfect" driving behavior with all its weakness and risks. Most importantly, all parameters of this model have direct physical meaning; this ensures vehicle collisions are replicated as a result of behavioral patterns rather than simply being numerical artifacts of the model. Meanwhile, vehicle trajectories were extracted from real-life crashes collected from a freeway section of I-94WB This is by far the first data collection efforts that aim to collect vehicle trajectories from real-life crashes to aid car-following modeling. These data were employed in this study to test, calibrate and validate the model. This new model is successful in replicating these vehicle trajectories as well as crashes. The outcomes of this research will help advance the understanding of car-following behaviors while improving the micro-simulation modeling to facilitate assessing freeway safety concepts at the high definition microscopic level.

1 INTRODUCTION

1.1 Problem Statement

Rear-end crashes are a major freeway safety problem. Currently up to 25% of all crashes in the U.S. are rear-end collisions involving two or more vehicles. Albeit mostly non-fatal, rear-end collisions induce non-recurrent congestions causing substantial vehicle-delays while greatly degrading freeway performance. To be sure, approximately 157 million vehicle-hours of delay annually, or one-third of all crash-related delays in the United States are caused by rear-end collisions (Brown et al. 2000).

Over the past ten years, various safety countermeasures and ITS techniques have been developed and/or deployed trying to reduce collision occurrences and improve safety. In spite of some successful implementations, it has been found that expected safety improvements from a particular ITS technique or safety countermeasure could turn out to diminished, sometimes even negative safety gain due to behavioral adaptation or unforeseen factors (Ledoux and Archer 1999). This suggests that a clear understanding of crash mechanism at microscopic (i.e., individual driver-vehicle) behavioral level is critical for developing effective safety treatments, while any proposed countermeasure should be comprehensively assessed, tested and tuned prior to actual field deployment in order to achieve optimal safety benefits. To this end, a realistic and reliable modeling tool is needed that can help understand crash mechanism and assist testing, verification, and improving safety concepts and technical solutions without resorting to prohibitive and potentially hazardous field experimentation.

Microscopic traffic simulation is *potentially* one of the most viable tools of choice for studying crash mechanism and assessing proposed safety concepts. Specifically, vehicle interactions are captured through two basic types of models i.e., car-following and lane-changing models to describe vehicle movements in longitudinal and lateral dimensions. Detailed information such as acceleration, velocity, and position can be tracked for every vehicle during the study period, while measures of effectiveness (MOE's) such as *Total Travel Time*, *Total Travel*, *Vehicle Delays*, and *Number of Stops*, that are practically hard to obtain can be easily derived from simulation outputs to aid operational analysis. Due to its level of detail, modeling realism and ease of use, micro-simulation has emerged as an invaluable tool for traffic researchers and practical engineers worldwide. However, while being successfully in many applications, micro-simulation has been insufficient for safety-related studies and its applications have long been limited to collision-free scenarios. In fact, most existing micro-simulation models (i.e., car-following and lane-changing models) *by design* target only *normal* driver behavior in *typical* traffic conditions. To be sure, these models are mostly developed based on Newton's physical law with *limited* human performance factors taken into account. In other words, contrary to their real-world counterparts, virtual vehicles/drivers in simulation environment do not have human errors or perception limits. For example, lapse of attention which is a common limitation of human driving and often reported as contributing to rear-end collisions, does not occur in simulation. As a result, vehicle crashes are deliberately prohibited in existing simulation models. This is akin to assuming safe driving behavior in micro-simulation for all drivers under study; as such, micro-simulation becomes insufficient when *unsafe* driving behavior is desired in order to study causes and dynamics of crashes and evaluate the effects of proposed safety treatments.

Recognizing potential advantages of applying micro-simulation approach in freeway safety analysis, some recent research efforts have been directed to *enhancing* existing micro-simulation models by developing *conflict statistics* and *safety surrogates* to enable safety-related assessments (Hunuenin et al. 2005; Kosonen 1999; Kosonen and Ree 2000; Ledoux and Archer 1999; Mehmood et al. 2001; Torday et al. 2003). Yet due to the constraints that crash occurrence is deliberately excluded in (current) micro-simulation, it has been difficult to test and validate the correlation between *extracted* conflict statistics/surrogate measures with *actual* crash potential. This inevitably tainted the reliability of safety-performance conclusions obtained by use of micro-simulation.

Clearly, there is a critical need for enhancing *basic simulation modeling* in order to enable micro-simulation as an effective and reliable tool in safety-related studies. Otherwise stated, a new behavioral car-following model is needed that targets both safe and unsafe driving behavior. Further, in order for this new model to be able to capture real-life "less-than-perfect" driving behavior, adequate human performance factors need to be incorporated to overcome shortcomings of existing car-following models. Most importantly, the new model should be able to *realistically* replicate real-life crashes with parameters that are *identifiable from empirical data*. This means**,** this new model should be able to replicate vehicle collisions (i.e., in terms of zero or negative distance headway) as a result of certain behavioral pattern rather than numerical artifact carrying no behavioral/physical connection with real-life driving.

1.2 Research Objectives

The primary goal of this research is to develop a new behavioral car-following model that is pertinent to the true nature of everyday human driving. This model is for the purpose of enabling micro-simulation as an effective and reliable tool to study crash mechanism and aid safety evaluations. This boils down to three specific objectives that are related to data collection, model development, model calibration and validation:

1) **Collect vehicle trajectories from real-life crashes**
   Vehicle trajectories refer to time-dependent vehicles position, velocity, and acceleration data collected from field. Such data are critical for model development, calibration and validation. In this research, two types of trajectories, i.e., non-crash and crash trajectories are required as both safe and unsafe driving behavior need to be modeled. Non-crash trajectories are readily available from earlier studies. However, there are no existing crash trajectories hence these data need to be collected in this study. It should be pointed out that this is so far the first data collection efforts aiming to collect crash trajectories from real-life crashes.

2) **Develop new behavioral car-following model**
   Unlike existing car-following models that build on simplistic behavioral assumptions and deliberately prohibit vehicle collisions, this new model needs to incorporate adequate human performance factors in order to replicate "less-than-perfect" driving behavior. Also the proposed model is to be calibrated and validated using both non-crash and crash trajectories. This ensures that the new model is not only capable of replicating normal driving behavior but also unsafe behavior that could lead to crashes.

3) **Propose calibration/validation methodologies and test the proposed model**
Another important objective of this study is to develop an effective and computationally efficient calibration/validation methodology. This methodology is to be used for estimating optimal parameters and deriving distribution for general use. Moreover, the proposed model will be tested to examine its capability of replicating typical macroscopic traffic flow patterns such as fundamental diagrams and shockwave propagations.

1.3 Contributions

Existing micro-simulation modeling only describes normative car-following behaviors devoid of weakness and risks associated with real-life driving. To date, realistic car-following models pertinent to the true nature of driver behaviors thus suitable for safety studies are still lacking. In this study, a new behavioral car-following model is proposed to overcome the insufficiencies of existing car-following models. Specifically, major contributions of this research include:

1) High-resolution vehicle trajectories were collected from real-life crashes. This is so far the *first* data collection efforts aiming to collect vehicle trajectories from *real-life* crashes. Furthermore, state-of-the-art vehicle tracking techniques were employed to extract trajectories from crash videos. Finally, the extracted trajectories have been used in this study to aid model development, calibration and validation. More than that, these data are also suitable for traffic safety or engineering studies with other objectives.

2) For the first time in the literature, adequate human performance factors are integrated to allow for "less-then-perfect" driving behavior, whereas all parameters are *physically meaningful* with behavioral connections to real-life driving. Mostly importantly, all parameters are *identifiable* from empirical data while vehicle collisions are generated as *a result of behavioral patterns* rather than numerical artifacts of the model.

3) The proposed model was calibrated and validated using both non-crash and crashed data. Again, this is by far the first modeling efforts that try to replicate freeway rear-end collisions using microscopic car-following modeling that incorporates adequate human factor components. The will help advance the understanding of unsafe car-following behaviors and provide insights for crash-mechanism at microscopic (individual vehicle) level. Essentially, this improves existing micro-simulation modeling technique to facilitate assessing freeway safety concepts at high definition microscopic level.

1.4 Outline

This report is organized as follows. Chapter 2 presents a detailed review of existing car-following models. Feasibility of applying these models to safety studies is discussed where appropriate. Chapter 3 details research methodology which involves data collection, model development, and model calibration/validation. Specifically, in Chapter 3, data collection efforts are documented explaining the specific techniques used to collect and extract vehicle trajectories. Capitalized on collected empirical data as well as research results from earlier studies, a comprehensive conceptual framework describing driving tasks is formulated. Based on the conceptual framework a new behavioral car-following model is proposed. This model incorporates adequate human performance factors in order to allow "less-then-perfect" driving behavior thus capture the weakness and risks associated with real-life driving. Calibration and

validation approaches are also presented in Chapter 3. In Chapter 4, the proposed model is calibrated and validated using both crash-free and crash-inclusive trajectories. Concluding remarks are given in Chapter 5, particularly discussed are the requirements for applying the proposed model, and feasibility of integrating the proposed model with existing commercial simulators such as VISSIM and AIMSUN.

2 BACKGROUND

2.1 Overview of Car-following Modeling

Car-following models have been the subject of numerous research efforts since 1950s'. The motivation arises from the need to model individual vehicle movements as realistically as possible. In contrast to lane-changing models, car following models deal with longitudinal direction of driving. In conjunction with lane-changing algorithm, car following modeling forms the cornerstone of microscopic simulation tools and is of particular importance for studying rear-end collisions. Figure 2-1 illustrates a typical car-following situation with two interacting vehicles on a single lane. Notations in this figure are detailed in forthcoming sections.

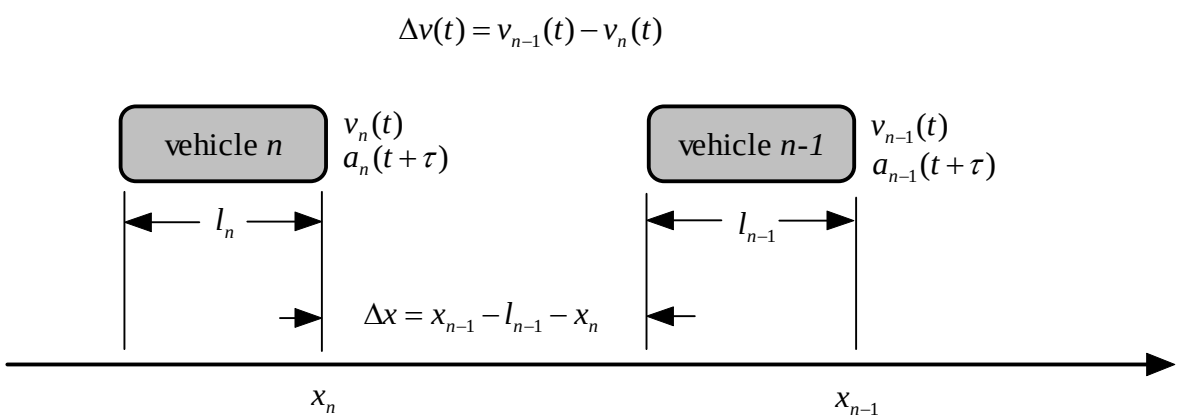

Figure 2-1. A Typical Car-Following Situation with Two Interacting Vehicles

Essentially, most of existing car-following models can be represented as:

$$a_n(t+\tau) = f(\Delta x, v, \Delta v, \Delta a, a; t) \tag{0.0.1}$$

or

$$a_n(t+\tau) = f(\Delta x, v, \Delta v, \Delta a, a; t) + \varepsilon \tag{0.0.2}$$

with

$$\Delta x(t) = x_{n-1}(t) - l_{n-1} - x_n(t)$$
$$\Delta v = v_{n-1}(t) - v_n(t)$$
$$\Delta a(t) = a_{n-1}(t) - a_n(t)$$

where

- a_{n-1} : Acceleration of lead vehicle;
- a_n : Acceleration of following vehicle;
- Δa : Relative acceleration between lead and following vehicles;
- l_{n-1} : Length of lead vehicle;
- l_n : Length of following vehicle;
- $n-1$: Index of lead vehicle;
- n : Index of following vehicle;
- τ : Reaction delay of following vehicle;
- v_{n-1} : Instantaneous speed of lead vehicle;

v_n : Instantaneous speed of following vehicle;
Δv : Relative speed between lead and following vehicles;
x_{n-1} : Position of lead vehicle's bumper;
x_n : Position of following vehicle's bumper;
Δx : Bumper to rear distance between lead and following vehicles;
ε : Noise term.

These models can be either deterministic as described by Equation (0.0.1), or stochastic as by Equation (0.0.2) where a certain noise term ε is added, making them discontinuous in time. In addition, taking the driver and vehicle as one integrated unit, most classical car-following models incorporate reaction time delay into the dynamics. This reaction time delay is defined as the time lag between a stimuli effected by lead vehicle (e.g., braking) and a response by the subject vehicle. Usually it encompasses *perception, recognition, decision time* plus *neural-muscle response time*, sometimes also includes vehicle's *mechanical response delay*. Typically, most classical car-following models assumed constant reaction delay time for all drivers, while implemented in some recent studies is *variable* delay time that varies with different drivers, or depends on limited traffic situations (Toledo 2003; TSS 2005; Wang 2005; Wang et al. 2006)

Beyond classical car following paradigms, there is also a notable line of developments termed *psycho-physical* modeling that cannot be represented by Equation (0.0.1) or (0.0.2). Specifically, this type of models assumes vehicle acceleration is more or less constant until a certain action-point is reached (therefore, these models are sometimes referred to as action point models). Todesiev (Todesiev 1963) was among the first using action points to characterize car-following process; while the most successful action-point models include Wiedsmann (Wiedemann and U.Reiter 1992) and Fritzsche model (Fritzsche 1994); variants of these two models are implemented in two widely-used commercial micro-simulators, i.e., *VISSIM*™ and *PARAMICS*™ , respectively.

2.2 Detailed Review of Existing Car-following Models

Despite of large difference in approach and scope, existing car-following models can be classified as

1) Deterministic Stimulus-Response Models
2) Safety Distance Car-following Models
3) Optimal Velocity Car-following Models
4) Cellular Automata Models
5) Psycho-physical Car-following Models (Action Point Models)
6) Fuzzy-logic Car-following Models

Note this classification is similar to that of (Brackstone and McDonald 1999). Also this classification makes no claim to be exhaustive while various other categories of car-following models have been proposed in the literature. Figure 2-2 presents a diagram demonstrating the above classification including representative models of each class. Main characteristic as well as shortcomings of these models are reviewed in forthcoming sections. In particular, feasibility of applying these models in traffic safety studies is discussed where appropriate. Also it is worthwhile to note that "subject vehicle", "following vehicle", or "lag vehicle" are used

interchangeably henceforth to refer to the vehicle that is *following* another vehicle on a single lane. This vehicle is indexed by integer n and represents the "response" side of car-following interactions. Likewise, "lead vehicle", "preceding vehicle", "immediately next vehicle ahead" or "immediate front vehicle" refers to the single vehicle that moves in front of the subject vehicle and represents the "stimulus" side of car-following interactions. While following vehicle is represented by integer n, lead vehicle is indexed by $n-1$ throughout this paper.

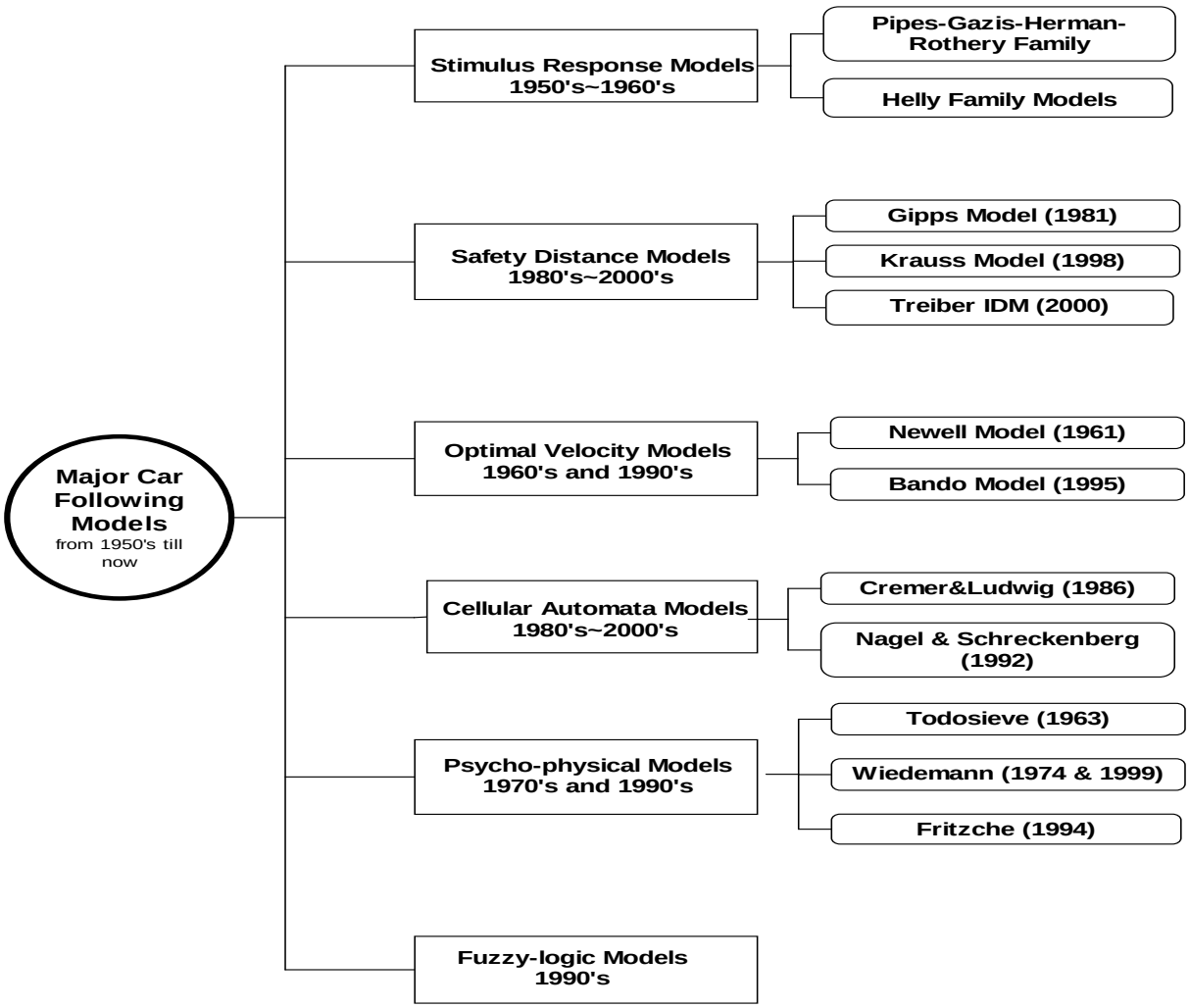

Figure 2-2. Classification Diagram of Existing Car-Following Models

2.2.1 Deterministic Stimulus-Response Models

Pipes-Gazis-Herman-Rothery Family

Stimulus-response models assume that the following vehicle's acceleration is a quantitative response to the stimulus (e.g., relative speed) administered by the immediate front vehicle. The first dynamical equations describing this relationship was proposed by Pipes (Pipes 1953), presuming that for every 10 mph increment of speed the following vehicle should leave a distance headway equivalent to one car's length, i.e.,

$$x_{n-1} = x_n + s_0 + l_{n-1} + \tau v_n \tag{0.0.3}$$

where s_0 is the distance headway at standstill; x_{n-1} is the position of lead vehicle, x_n the position of subject vehicle; l_{n-1} is the length of lead vehicle; τ is a constant in time unit; v_n is velocity of following vehicle.

Equation (0.0.3) can be rewritten as

$$v_n = \frac{x_{n-1}(t) - x_n(t) - s_0 - l_{n-1}}{\tau} \tag{0.0.4}$$

Differentiating Equation (0.0.4) gives the original dynamical equation proposed by Pipes:

$$\frac{dv_n(t)}{dt} = \frac{v_{n-1}(t) - v_n(t)}{\tau} \tag{0.0.5}$$

where $v_n(t)$ is the velocity of following vehicle, $v_{n-1}(t)$ preceding vehicle. Solving Equation (0.0.5) one immediately arrives at the conclusion that steady state solution, where all vehicles move at the same speed, is always stable. Moreover, vehicle collisions never occur with Pipe's model. This is because the lag vehicle can respond *immediately* to the lead vehicle without any reaction delay while deceleration rate is unbounded in Equation (0.0.5) thus safe following distance can always be maintained. Also due to the absence of reaction delay, this model cannot replicate *clustering effects* or s*hockwaves* as occurred in real-life traffic.

Chandler et al. (1958) introduced a finite time delay *T* into Equation(0.0.5), leading to

$$\frac{dv_n(t+T)}{dt} = \frac{v_{n-1}(t) - v_n(t)}{\tau} \tag{0.0.6}$$

Analytical analysis of Equation (0.0.6) indicates that the system reaches its stability limit when $\frac{T}{\tau} = 0.5$. Beyond this limit, i.e., when $\frac{T}{\tau} > 0.5$ the system becomes unstable and vehicle collisions could occur if lead vehicle decelerates abruptly while distance headway happens to be short enough. However, this model is independent of distance headway, which greatly restricted

the model's applicability. For example, the fundamental speed-density relationship cannot be derived from the model.

Gazis et at (1959) introduced into the model a dependence on the distance headway by defining:

$$\frac{dv_n(t+T)}{dt} = \alpha \frac{v_{n-1}(t) - v_n(t)}{x_{n-1} - x_n} \tag{0.0.7}$$

Integrating Equation (0.0.7) leads to the steady state speed-density relationship consistent with Greenberg's macroscopic theory (Greenberg 1959):

$$v \propto \ln(\frac{\rho_{jam}}{\rho}) \tag{0.0.8}$$

Following this, Edie (Edie 1961) assumed that the acceleration function should also be dependent on the momentary velocity of the following vehicle. Further, in order to replicate the discontinuity between free flow and congested flow in the fundamental diagram, he proposed the following dynamical equation:

$$\frac{dv_n(t+T)}{dt} = \alpha v_n(t) \frac{v_{n-1}(t) - v_n(t)}{(x_{n-1} - x_n)^2} \tag{0.0.9}$$

where the sensitivity coefficient α has two different values for free-flow and congestion regimes.

Gazis, Herman and Rothery (Gazis et al. 1961) unified and generalized the above formulations by allowing the sensitivity coefficient α dependent on arbitrary powers of spacing and momentary velocity:

$$\frac{dv_n(t+T)}{dt} = \alpha v_n(t)^m \frac{v_{n-1}(t) - v_n(t)}{(x_{n-1} - x_n)^l} \tag{0.0.10}$$

where the exponents l and m are free calibration parameters. When $l = 2$ and $m = 0$, steady-state speed-density relationship can be derived which is in agreement with Greenshields formula (Greenshields 1934).

Gazis-Herman-Rothery model has been criticized as not suitable for describing very low traffic where drivers accelerate to their desired free-flow velocity. Meanwhile, the car-following behavior in dense traffic is also unrealistic. For example, acceleration rate remains zero as long as velocity difference is zero regardless of the distance gap between vehicles. Further, parameters calibration remains an issue since all of them are phenomenological without explicit physical meaning. In addition, this model results in symmetric acceleration/deceleration. This means, with two relative velocities differing only in direction, the model would predict the same acceleration and deceleration rates (in terms of absolute value). This is not consistent with real-life driving since drivers usually employ higher rates when decelerating.

In order to capture more complex traffic flow patterns that exhibit capacity drops and hysteresis loops, following Pipes assumption, Zhang (Zhang and Kim 2005) recently proposed a new car following theory for multiphase vehicular flow:

$$v_n(t+T) = \frac{d_n(t)}{\gamma_n(t)} \tag{0.0.11}$$

where d_n is the distance separation between vehicles; γ_n is the desired gap time for the follower to travel the distance separation. Rather than using a constant gap-time for γ_n, γ_n (t) is assumed to be dependent on both gap-distance and the traffic phase. One of the possible definitions for γ_n is

$$\begin{aligned}
\gamma_n &= \frac{d_n(t)}{v_f}, \text{ if } d_1 \le d_n(t) \\
&= \gamma_1, \quad \text{if } 0 \le d_n(t) \le d_0 \\
&= \frac{d_n(t)}{v_f} \quad \text{if } d_0 \le d_n(t) < d_1 \text{ and } v_{n-1}(t) = v_f \\
&= \gamma_1, \quad \text{if } d_0 \le d_n(t) < d_1 \text{ and } v_{n-1}(t) < v_f
\end{aligned}$$

where v_f is free-flow speed, $d_{0,}d_1$ are thresholds for distance separation. Zhang's model is able to replicate complex traffic patterns such as capacity drop and traffic hyesteresis. However, this model resulted in unrealistic accelerations in some cases. For example, assuming a typical free flow speed v_f = 30 m/s (67.5 mph), and a reaction time T = 1.8 s. According to Equation(0.0.11), a free vehicle with initial speed 0 can achieve a free-flow speed of 30 m/s in just 1.8 seconds. This would require an unrealistically high acceleration of 30/1.8 = 16.67 m/s^2. This limitation was also confirmed by simulations (Wang 2005).

Helly Family

Starting from Pipes original dynamical equation, Helly (Helly 1959) added an additional linear term to account for gap distance between vehicles:

$$a_n(t+T) = \frac{dv_n(t)}{dt} = C_1[v_{n-1}(t) - v_n(t)] + C_2[x_{n-1}(t) - x_n(t) - d_n(t)] \tag{0.0.12}$$

where C_1, C_2 are constant coefficients, $d_n(t)$ is time dependent desired following distance given as:

$$d_n(t) = \alpha + \beta v_n(t) + \gamma a_n(t) \tag{0.0.13}$$

One notable feature of Helly model is that once an acceleration or deceleration rate is determined from Equation(0.0.12), the driver will not update the value till relative velocity or gap distance deviates substantially from the predicted value. Helly-like models also include the model proposed by Xing (Xing 1995), which combines Gazis-Herman-Rothery model with Helly's concept allowing for different states such as standard driving, acceleration from standing queue,

acceleration in free flow etc. The commercial Cube Dynasim simulator also employs a Helly-like model.

Safety Distance Car Following Models

Safety distance car following models start from the assumption that drivers try to keep a safe following distance from preceding car in order to avoid potential collisions. The first major development was made by Gipps (Gipps 1981)). Recent developments include Krauss (Krauss 1998) and the so-called Intelligent Driver Model (Treiber et al, 2000). These models are detailed next.

Gipps Model

Gipps model is the underlying car-following algorithm for the widely-used AIMSUN simulator(Barcelo 2001). This model is based on two velocity updating rule:

$$v_n^a(t+\tau) = v_n(t) + 2.5a_n^{\max}\tau[1-\frac{v_n(t)}{V_n}]\sqrt{0.025+\frac{v_n(t)}{V_n}} \qquad (0.0.14)$$

$$v_n^b(t+\tau) = b_n^{\max}\tau + \sqrt{(b_n^{\max}\tau)^2 - b_n^{\max}\{2[x_{n-1}(t)-l_{n-1}-s_n-x_n(t)]-v_n(t)\tau-\frac{v_{n-1}^2(t)}{b^{'}}\}} \qquad (0.0.15)$$

$$v_n(t+\tau) = \min\{v_n^a(t+\tau), v_n^b(t+\tau)\} \qquad (0.0.16)$$

Where

τ is reaction time; it is assumed to be the same for all drivers;

$a_n^{\max}$ is the maximum comfortable acceleration rate for vehicle *n*;

$b_n^{\max}$ is the maximum comfortable braking rate for vehicle *n*;

x_n, x_{n-1} are position of vehicle n and n-1, respectively;

$b^{'}$ is driver *n*'s estimation for vehicle *n-1* ' maximum comfortable braking rate;

V_n is the desired free-flow speed of vehicle *n;*

s_n is the standstill bumper to rear distance of vehicle *n*

Equation (0.0.14) describes vehicle's acceleration behavior in free flow when there is no constraints from the preceding vehicle, i.e., vehicle *n* is free to accelerate to its desired free-flow speed V_n; while Equation (0.0.15) describes car following behavior in dense traffic, that is, vehicle *n* (the follower) chooses a speed that ensures a safe stopping distance from preceding vehicle *n-1* , such that even if vehicle $n-1$ applies an emergent braking, vehicle *n* is still able to bring to a full stop before colliding into vehicle *n-1*.

Gipps showed that this model is *collision-free* as long as drivers don't underestimate the comfortable braking rate $b^{'}$ of the preceding vehicle. Gipps offered no calibration of his parameters. Instead, he performed simulations using realistic values and found that the model produced realistic macroscopic patterns and individual behaviors. It should be pointed out that all parameters of Gipps model have realistic physical meanings, thus virtually obviating the need for

elaborate calibration. This is a major advantage of Gipps model. Table 2-1 summarizes parameter values suggested by Gipps(Gipps 1981).

Gipps further pointed out that collective behavior of vehicles is controlled by reaction time τ, the ratio of $b_n^{\max}/b'$ and the distribution of desired free-flow speed V_n. On the other hand, individual vehicle behavior is affected by maximum comfortable acceleration $a_n^{\max}$, maximum comfortable deceleration $b_n^{\max}$, and the effective vehicle length ($l_n + s_n$). Critiques to Gipps model are mostly directed towards the magnitudes of the reaction time parameter τ, for which all drivers use the same value (Ehlert 2004). In fact, different reaction times for an individual driver (intra-driver) or varying reaction times over the driver population (inter-driver) seem more realistic. Also, in real traffic it is observed that drivers do not necessarily keep a safe headway, while the overall behavior generated by Gipps model becomes too stable especially when an accurate estimation of lead vehicle's braking rate is given.

Table 2-1. Parameter Values Suggested by Gipps

Parameters	Description	Suggested Distribution
$a_n^{\max}$	Maximum comfortable acceleration for vehicle *n*	$\sim N(1.7, 0.9)\ \ m/s^2$
$b_n^{\max}$	Maximum comfortable deceleration for vehicle *n*	-2.0 $a_n^{\max}$
$s_n + l_n$	Effective vehicle length	$\sim N(6.5, 0.09)\ \ m$
V_n	Desired free-flow speed for vehicle *n*	
τ	Reaction time for all drivers	$2/3$ sec
b'	Driver *n*'s estimation of vehicle *n-1's* maximum comfortable deceleration	$\min[-3.0, (b_n^{\max} - 3.0)/2]\ m/s^2$

Krauss Model

Krauss proposed a similar car following model parallel to Gipps model (Krauss 1998) . The velocity updating rules is given as:

$$v_n^{safe}(t) = v_{n-1}(t) + \frac{d_n(t) - d^{des}(t)}{\tau_b + \tau} \tag{0.0.17}$$

$$v_n^{des}(t + \Delta t) = \min[v_n^{\max}, v(t) + a\Delta t, v_n^{safe}(t)] \tag{0.0.18}$$

$$v_n(t + \Delta t) = \max[0, v_n^{des}(t + \Delta t) - \eta] \tag{0.0.19}$$

where $d_n(t)$ is the actual gap distance for vehicle *n*; $d^{des}(t)$ is the desired gap distance; Δt is updating interval; τ is driver reaction time; time scale τ_b is defined as $(v_n + v_{n-1})/2b$, b is the

maximum deceleration rate, a is maximum acceleration rate; η is stochastic perturbation which is assumed to be δ correlated in time. Krauss model is collision-free as vehicle speed is bounded by a safe velocity at each updating step. Meanwhile, this model can address capacity drop and the stability of wide jams (i.e., jams propagating upstream with low shockwave speed).

Intelligent Driver Model

Intelligent Driver Model (IDM) defines an acceleration function in relation to momentary vehicle velocity, gap distance and relative velocity (Treiber et al. 2000) :

$$\frac{dv_n(t)}{dt} = a[1-(\frac{v_n(t)}{v_0})^{\delta} - (\frac{s^*}{s})^2] \tag{0.0.20}$$

$$s^*(t) = s_0 + v_n(t)T + \frac{v_n(t)[v_{n-1}(t) - v_n(t)]}{2\sqrt{ab}} \tag{0.0.21}$$

where

s^* is the desired gap distance;
T is safe time headway;
a is maximum acceleration;
b is desired deceleration;
s_0 is jam space headway;
v_0 is desired free-flow velocity;
δ acceleration exponent.

IDM is collision-free and can capture complex traffic patterns including the so-called *self-organized characteristic traffic constants* (Kerner 1998), hysteresis effects and states transition. Importantly, all model parameters have meaningful interpretations and are empirically measurable.

2.2.2 Optimal Velocity Model

Bando Model

Optimal velocity models assume that drivers select their velocity according to a hypothetical "optimal" velocity function, i.e.,

$$\frac{dv_n(t)}{dt} = \frac{V^{opt} - v_n(t)}{\tau} \tag{0.0.22}$$

One representative optimal velocity model was proposed by Bando, where the optimal velocity function is assumed to be:

$$V(\Delta x) = \tanh(\Delta x) \tag{0.0.23}$$

Here Δx is gap distance. Clearly, as $\Delta x \to 0$, $V(\Delta x) \to 0$. This actually prescribes a speed-density relationship $V(\Delta x)$. Bando's model is widely used by physicists to study traffic phenomenon due

to its analytical properties. It is collision-free if reaction time $\tau < 0.9$ s. However, acceleration and deceleration rates are symmetric with respect to the deviation from optimal velocity. This is unrealistic as the absolute value of deceleration rate is usually higher than that of acceleration. Helbing and Tilch (Helbing and Tilch 1998) proposed the *Generalized Force Model* (GFM) to overcome the shortcomings of Bando's model. GFM incorporated reactions to both relative velocity and gap distance, and agrees with empirical data fairly well. However, according to (Jiang et al. 2001), GFM may produce low congestion wave propagation speed (12.11 km/h compared to empirically observed 17~23 km).

Newell Model

Newell used an exponential function to prescribe the optimal velocity (Newell 1961):

$$v_n(t+T) = V^{opt}(\Delta x) = v_0\{1 - e^{-[(x_{n-1}-x_n)-s_0]/v_0 T}\} \qquad (0.0.24)$$

As specified by Equation(0.0.24), optimal velocity approaches free-flow speed v_0 for vanishing interactions ($\Delta x \to 0$), thus this model can both capture dense traffic interactions as well as low traffic interactions. The model is collision-free; while acceleration rate predicted by the model have been found unrealistically high, typically of the order v_0/T.

Cellular Automata Model

Cellular Automata models features a coarse description of driving behaviors by discretizing both time and space. However, since the whole traffic dynamics is obtained through integer operations of cellular automata unit, these models are noted for computational efficiency especially when large-scale transportation networks are involved.

The first cellular automaton model applied in traffic simulation was proposed by Cremer and Ludwig (Cremer and Ludwig, 1986). However, the most widely-used cellular automaton traffic model was proposed by Nagel and Schreckenberg (Nagel and Schreckenberg 1992). In this model, roadway is discretized into cells corresponding to segment of 7.5 meters in length. The cell has two states: empty or occupied, depending on the presence of a vehicle. Vehicle velocity is characterized by the number of cells it "hops" at every time step. Each time step a vehicle's velocity and position is updated based on its maximum desired velocity and whether there is a vehicle blocking its movement in front. Stochastic perturbations are introduced into Nagel-Schreckenberg model as a noise term in the updating rules. N-S model can produce empirical speed-density relationship and spontaneous clustering fairly well.

As mentioned earlier, Cellular Automata models are noted for its computational efficiency and simple updating rules; therefore they are suitable for simulating large road networks when computing efficiency is of an issue. However, it seems insufficient to help understand detailed traffic dynamics and its behavioral foundations, as the underlying rules of Cellular Automata models are over-simplified with very few behavioral elements taken into account. Cellular Automata model is the underlying algorithm for TRANSIMS simulator developed at Los Alamos National Lab.

Action Point Model

Action point model describes car following behavior on the basis that the following vehicle attempts to maintain a desired gap distance and alters its acceleration response only when certain perceptual thresholds (action points) are exceeded. This approach was initiated by Todosiev (Todosiev, 1963) and expanded by Michaels and Cozan (Michaels and Cozon, 1962). Several existing microscopic traffic simulators including *Paramics* (Fritzche 1994) and *VISSIM* (Wiedemann, 1974) incorporated this approach. Specifically, for Wiedemann model, four thresholds are used (Wiedemann and U.Reiter 1970s):

(1). Minimum desired following distance $S^{\min}$

$S^{\min}(v) = S_0 + \alpha \sqrt{v}$

where S_0 is the desired spacing at rest, α is a coefficient. Both S_0 and α are probabilistically distributed; v is velocity.

(2). Maximum desired following distance $S^{\max}$

$S^{\max}(v) = S_0 + \alpha \sqrt{\beta . v}$, where β is a coefficient which is also probabilistically distributed.

(3). Threshold for recognizing small negative (i.e., closing) relative speed:

$V^{cl}(\Delta x) = -\frac{(\Delta x)^2}{\kappa^2}$, where Δx is the gap distance, κ is a coefficient randomly distributed among driver population.

(4). Threshold for the perception of small positive (i.e., opening) relative speed:

$V^{op}(\Delta x) = \frac{(\Delta x)^2}{\mu^2}$, where Δx is the gap distance, μ is a coefficient randomly distributed among driver population.

On crossing these thresholds, a driver may perceive an unacceptable change in relative speed or gap distance, and will initiate a change in the sign of his acceleration in the order of 0.2 m/s^2.

Fuzzy Logic Models

Fuzzy logic car following models describe the car following phenomenon through a set of "IF…THEN" rules. For example, IF "not close" AND "opening" THEN "accelerate". Chakroborty and Kikuchi first proposed fuzzy-logic based car following model (Chakroborty and Kikuchi 1999). Unfortunately, this type of models is computationally expensive, hard to calibrate, and not applicable to large network simulation.

2.3 Traffic Stability and Car-following Behavior

Considerable research efforts have been devoted to investigate microscopic foundations of individual vehicle dynamics and its correlation to traffic instabilities which could lead to crashes. This is usually done through analyzing fixed points stability of the dynamical equation

describing car-following process. For example, it has been shown that the fixed point $\Delta v = 0$ for the Gazis model (Gazis et al. 1959):

$$a(t) = \alpha \frac{[v(t)]^l}{[\Delta x(t-\tau)]^m} \Delta v(t-\tau) \tag{0.0.25}$$

become locally unstable for vehicle pairs when $\alpha\tau \frac{v_0^l}{\Delta x_0^m} > \frac{\pi}{2}$ (Gazis et al. 1961); or asymptotically unstable for vehicle platoons if $\alpha\tau \frac{v_0^l}{\Delta x_0^m} > \frac{1}{2}$ (Gazis et al. 1961; Zhang and Jarrett 1997), where α is sensitivity coefficient, l and m are free calibration parameters, τ is reaction time delay, v_0 and x_0 are initial speed and initial space headway respectively. Usually the instability is attributed to *collective motion* of car ensemble. Such instability is considered as the cause of non-damped oscillations in the relative motion of vehicles (See Figure 2-3). Moreover, (linear) stability analysis has indicated that when the magnitude of disturbances become sufficiently large, negative space headway could take place somewhere in between a platoon of vehicles indicating occurrence of vehicle crashes (Gazis et al. 1959; Gazis et al. 1961). This suggests that there exist collision-prone situations where traffic conditions develop so fast that the driver cannot effectively convert information into control maneuvers in sufficient time, which could possibly lead into multiple rear-end collisions in high-density traffic characterized by successive short time headways. In such situations, *an initial flow perturbation results in accumulated response time leaving no hope for collision avoidance for the drivers* who by chance or by choice drive at short time headways well below his physical reaction time. Similar line of reasoning has been employed to help explain identified common freeway accident mechanism as collective effects in (Davis and Swenson 2004). Henceforth in this paper, instability of this type is termed as *Structural Instability* because it is determined from physical laws expressed in structural dynamical equations describing car-following dynamics.

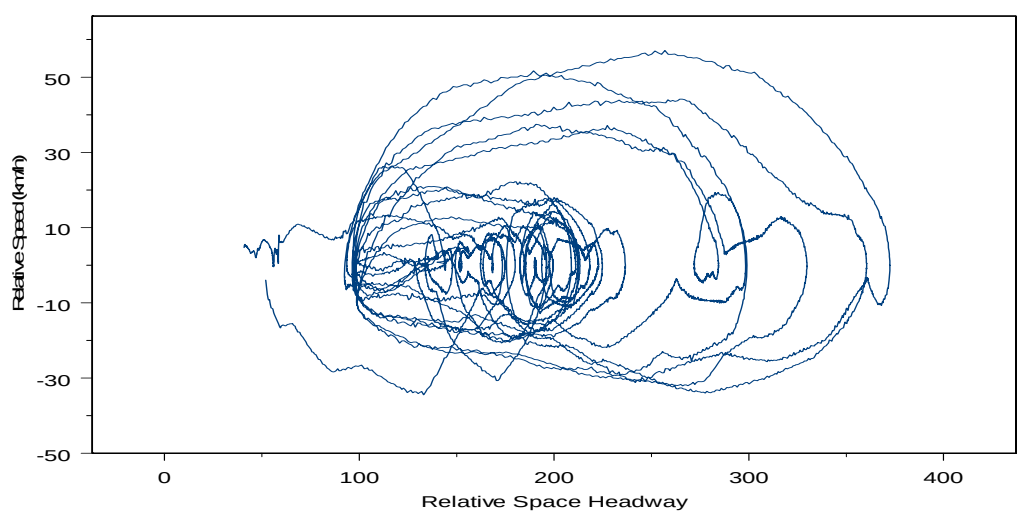

Figure 2-3. Measured Car-Following Behavior. Data were Collected from a Japan Test Track Using GPS

This type of non-damped oscillations is typical of car-following process, sometimes referred to as “closing following spirals”

There could be other factors causing traffic instabilities besides collective effects. If traffic instability is treated as solely collective effects, then any dynamical equations similar to Equation (0.0.1) can hardly predict the instability of a lag vehicle when the lead vehicle is driving at a constant speed, i.e., no oscillation spirals will appear. However, this is not in accordance to empirical observations as shown in Figure 2-3. Indeed, the pattern shown in this figure can not be simply explained as a fixed point dynamical process disturbed with noises either (Equation (0.0.2)); as in this case the oscillating spirals should distribute evenly around fixed points. Clearly, in addition to the collective *structural instability*, there is *an instability mechanism inherent to individual vehicle-driver-unit* not related to collective effects. In fact, the oscillatory pattern has long been observed and pointed out in earlier studies (Brackstone et al. 2002; Lubashevsky et al. 2003; Todesiev 1963; Wiedemann and U.Reiter 1970s). Such instability mechanism is unlikely a result of physical process; rather, driver-performance factors such as human visual perception process and decision errors may be vital. In order to realistically simulate real-life collision occurrences, it is essential that a high fidelity car-following model takes into account both structural and human-performance related instability and validates its parameters extensively against crash trajectory data.

2.4 Conclusions

In this chapter the most known and currently used car-following models were presented. The reason for this review was primarily to bring the reader up to speed for the state-of-the-art in car following models which are the cornerstone of today’s microscopic simulation applications but also in order to illustrate that the inability of these applications to emulate vehicle crashes realistically stems from the nature of these underlying car-following models. As stated in the previous chapter the goal of this research is to develop a new car-following model that can emulate realistically the conditions and behaviors leading to car-following type crashes. As it will be presented later, some of the fundamentals of the existing models are valid and will be utilized as the base upon which the new model will be based.

3 METHODOLOGY

This chapter describes the three main elements necessary in the development of a new crash-inclusive car-following model. These elements are data collection, model framework development, and model validation methodology. Data collection and analysis is one of the most important steps since it is the base of understanding the mechanisms involved both in normal driving and crash sequences. Data from various sources are analyzed to identify driving behavior characteristics and limits. The model framework is developed from the knowledge described in the previous chapter as well as the understanding of the mechanism the data analysis has offered. Finally, the available data as well as the structure of the proposed crash inclusive car-following model will dictate the development of the most appropriate validation framework.

3.1 Data Requirements

Two types of trajectories, i.e., non-crash and crash trajectories are required in this study as both normal driving behavior and unsafe behavior need to be modeled. Non-crash trajectories are readily available from earlier studies. However, there are no existing crash trajectories hence these data need to be collected. As stressed earlier, this is so far the first data collection effort aiming to collect detailed crash trajectories from real-life crashes. These data will be employed to aid develop, calibrate and validate a new car-following model in this study; however, it should be noted that they are not limited to this study; they are also suitable for general use with other objectives.

3.1.1 Non-Crash Data Collection

Data Collection Site

Non-crash car-following data are obtained from Hokkaido University, Japan. Specifically, these data were collected from car following experiments on a test track. Figure 3-1 illustrates the schematic layout of the site. As shown in this figure, the test track consists of two straight sections, each 1200 meters (2 miles) in length, and two semicircular curves with a radius of 50 meters. Total length of the track amounts to 2714 meters (8904 feet).

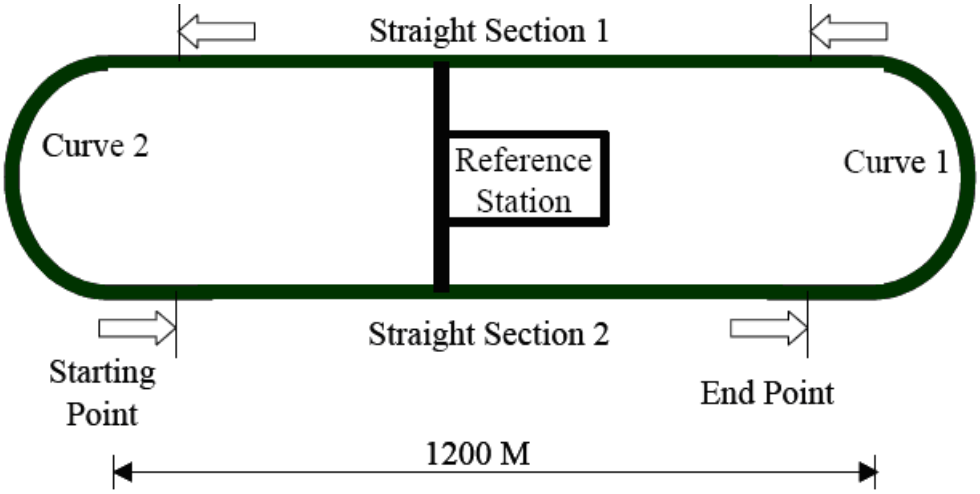

Figure 3-1. Schematic Layout of the Track at Hokkaido University (Ranjitkar 2004)

Instruments

Ten passenger cars participated in the car-following experiments. These vehicles were equipped with *Real-time Kinematics* (RTK) GPS receivers that output vehicle position and speed data every 0.1 second. The position data have an accuracy of 10mm+ 2ppm, while speed data less than 0.02 m/s (0.18 ft/s). Table 3-1 summarizes the specifications of the vehicles participated in the experiments. Table 3-2 provides additional information about individual drivers.

Table 3-1. Specifications of Test Vehicles (Provided Courtesy of Dr. Ranjitkar)

Car No.	Driver No.	Year	Model	Length m	ANT (m)
G01	D1	1988	Safari	4.80	3.0
G02	D2	1991	Highjendo	3.29	2.0
G03	D3	2000	Capera	4.59	2.5
G04	D4	1998	Roreru	4.74	2.5
G05	D5	1998	Cefiro	4.78	2.5
G06	D6	2000	Bluebird	4.56	2.5
G07	D7	2000	Skyline	4.70	2.5
G08	D8	1998	Primera	4.43	2.5
G09	D9	2000	Abeniru Fucon	4.65	2.5
G10	D10	1985	Bisuta	4.43	2.5

Table 3-2. Drivers' Characteristics (Provided Courtesy of Dr. Ranjitkar)

Driver/Car No.	Driving Experience	Driver's Age
D1	40	60
D2	10	30
D3	3	21
D4	3	25
D5	5	24
D6	7	25
D7	3	23
D8	2	22
D9	3	24
D10	10	30

A unique feature of these RTKGPS car-following data is that lead vehicle had designed speed profiles covering the full spectrum of accelerating, decelerating and cruising states (See Figure 3-2). This virtually generated a wide range of uninterrupted driving conditions with speed ranging from 20 km/h (12.4 mph) to 100 km/h (62mph) and spacing ranging from 10 m to 70 m.

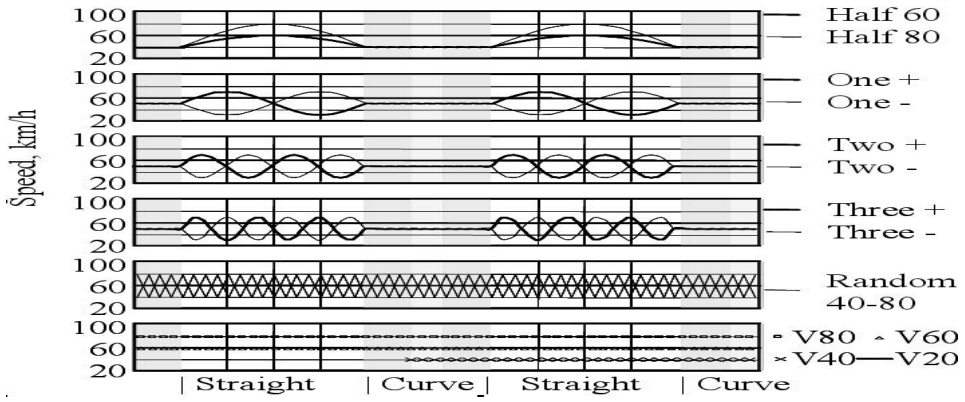

Figure 3-2. Lead Vehicle Speed Pattern

3.1.2 Crash Data Collection

Data Collection Site

As pointed earlier, crash data, i.e., vehicle trajectories from crashes, do not exist hence must be collected in this study. To do that, a freeway section from I-94 westbound between Park Ave and 3rd Ave in downtown Minneapolis was selected as data collection site. This section has a crash rate of 4.81 crashes per million-vehicle-miles (MnDOT 2004). In short, this is the highest crash rate location in the Twin Cities metropolitan area. Further, this section carries an average daily traffic in excess of 80,000 vehicles between downtown Saint Paul and Minneapolis, and is often congested especially during afternoon peak periods. Figure 3-3 illustrates an aerial view of this site.

The site is ideal for the collection of crash data due to the high crash rate experienced. Although non-crash data can be also easily collected in this site the presence of a number of overpasses and the roadway geometry does not allow an easy collection of long length (space) data sets like the one collected in the track or the one collected during the NGSIM project. Regardless, the site can be utilized for the collection of detailed merging and lane changing trajectories for crash and non-crash conditions.

Figure 3-3. Selected Data Collection Site: a High Crash-Rate Section of I-94 Westbound

Instruments

The data collection site was monitored using surveillance cameras. With these cameras, traffic was recorded from 11am to 8pm on a daily basis during a three-month period from June to August in 2006. Figure 3-4 shows the picture of two cameras at the site.

Figure 3-4. Surveillance Cameras that Monitor the Site

Figure 3-5. Small Factor PCs Used to Digitize and Store Video Data

Raw Data Collected

Video recordings were digitized and stored with a resolution of 640×480/10 fps in small factor PCs deployed in the field. The videos were visually examined on a daily basis to screen if any vehicle crashes or near misses had occurred during the day. In the end, a total of 7 crashes and 4 near-misses were successfully identified. Following this, these crashes/near-misses video recordings were further processed, i.e., two types of video clips were produced. The first type is one-hour-long video for *each* crash/near-miss case, covering traffic situation 45 minutes *before* and 15 minutes *after* the time the crash/near-miss occurred, while the second type is minute-long video clip that only includes 1-minute traffic situation before the crash/near-miss occurred. The first type provides comprehensive visual information regarding traffic dynamics before and after crashes, while the second are used to extract crash trajectories.

Trajectories Extraction

State-of-the-art vehicle-tracking algorithm was employed to extract vehicle trajectories from crash videos. Specifically, *NG-VIDEO*, meaning *Next Generation Vehicle Interaction and Detection Environment* for *Operations*, was employed in this study. NG-VIDEO program is developed specifically for extracting vehicle trajectories from videos captured from multiple cameras (Systematics 2006). This program integrates *Berkeley Vehicle Tracking Algorithm* developed at University of California, Berkeley (Kim et al. 2005; Kim and Malik 2003a; Kim and Malik 2003b). Meanwhile, *NG-VIDEO* features an efficient user interface to import accurate GIS coordinates, and convenient data storage and retrieval using MySQL database.

NG-VIDEO tracking algorithm is based on the *correlation matching of intensity pixels*. Importantly, the algorithm overcomes the limitations of previous machine vision algorithms that have difficulty to obtain accurate vehicle positions in the presence of shadows and occlusions. Prior to its application in this study, *NG-VIDEO* has been successfully applied in FHWA-funded NGSIM project, generating trajectories of over 4,700 individual vehicles, which is the largest and most comprehensive trajectories dataset ever produced. Figure 3.6 illustrates a sample of extracted trajectory data.

CR1_V1_S_A

	A	B	C	D	E	F	G	H	I
1	Time (sec)	Position (ft)	Speed (ft/sec)	Acceleration (ft/sec^2)					
2	25.7	220.213	49.7083	-1.76587					
3	25.8	226.706	49.2915	-7.44092					
4	25.9	233.177	48.6173	-12.5288					
5	26	237.673	47.6707	-16.1023					
6	26.1	241.169	46.8356	-15.2609					
7	26.2	246.165	45.7512	-14.5042					
8	26.3	249.662	44.8458	-11.0257					
9	26.4	254.639	43.6196	-8.25383					
10	26.5	258.137	42.6401	-2.50069					
11	26.6	262.134	42.2162	1.54767					
12	26.7	266.131	42.5377	3.06856					
13	26.8	271.611	42.7183	2.10282					
14	26.9	275.109	42.8794	3.36572					
15	27	280.106	43.1498	2.23782					
16	27.1	283.104	43.137	1.66844					
17	27.2	288.087	42.9958	-2.27174					
18	27.3	292.585	42.7492	-3.87371					
19	27.4	297.582	42.2543	-5.37102					
20	27.5	301.081	41.6508	-5.3965					
21	27.6	306.065	41.3657	-6.89477					
22	27.7	310.064	40.8857	-6.44809					
23	27.8	314.063	40.4962	-7.53274					
24	27.9	317.062	39.5281	-6.96641					
25	28	321.56	38.5519	-7.5433					
26	28.1	325.059	37.5039	-8.27803					
27	28.2	329.046	36.5843	-10.1529					
28	28.3	333.045	35.44	-10.3226					

CR1_V1_S_A

Figure 3-6. A Sample of Extracted Vehicle Trajectory

3.2 Model Development

3.2.1 Empirics of Car-following Behavior

This section summarizes the empirics of car-following behavior. This renders an empirical foundation for developing a realistic behavioral car-following model. Specifically, this includes empirical observations regarding the relationship between following distance and instantaneous speed, car-following oscillation spirals, distribution of time headways and reaction time. The datasets employed include the aforementioned RTKGPS test track data, NGSIM dataset, and the car-following dataset collected from German freeways.

3.2.1.1 Car-following Empirics from German A100 Freeway

Data Description

These data were collected using an instrumented vehicle equipped with a *differential GPS (DGPS)*, 4 radar sensors, and 2 video cameras recording the view in front of and behind the vehicle. The DGPS provides information of vehicle location, speed, acceleration and distance covered, whereas the radar sensors record the relative position and relative speed of every object in front of and behind the vehicle in a distance range of about 2 to 150 meters. Also the recorded data has been synchronized with the video recording so that the objects picked up by the radar system can be identified from the VCR pictures.

The data collection experiment was conducted at freeway A100 on a day in January 2004 during a drive from *Institute of Transport Research, Germany Aerospace Center* in Berlin to the Berlin-Tegel airport and back again. The drive was performed in the afternoon rush-hour when all roads

were heavily used. Further, the weather conditions are classified as dry. The following information was collected:

- id - internally used constant number
- $d(m)$ - total distance traveled since the start of recording
- $time(s)$ - time stamp
- $speed(m/s)$ - speed of the instrumented vehicle
- $x, y(m)$ - distance of the lead car from the instrumented car. x is the distance in driving direction, while is the perpendicular distance; positive values are in front and negative values correspond to cars behind.
- $vx, vy(m/s)$ - relative speed in x and y direction.

Data Analysis

The A100 freeway car-following dataset has two parts, i.e., hifahrt dataset and rueckfahrt, corresponding to the drives *to* and *from* the airport respectively. The following analysis results are based on these two parts separately. Note the data were collected using probe vehicle so the results are solely related to that probe vehicle.

Figure 3-7 plots the dependence of distance headway upon instantaneous speed. It can be seen from the figure that when instantaneous speed increases, the distance headway increases as well. This reflects the fact that drivers tend to leave larger distance gap at higher speed for safety reasons. Thus a driver might have a "desired" following distance dependent on his instantaneous speed. It is also indicated from the figure that there distance variance at higher speed is much larger than at lower speed, viz. the data points are more scattering at higher speed than when at lower speed. This suggests that at higher speed, drivers are less accurate in performing distance control to achieve desired following distance, which can be attributed to human's inability to accurately determine distance headway when speed is high and when distance is already large enough. As will become clearer in forthcoming sections, the desired space headway (hence desired following gap time) is an individual characteristic.

In Figure 3-8, the time headway distributions are depicted. Time headway refers to the gross following time headway $T = D/V$, where D is bumper-to-bumper distance from current vehicle to its preceding one, and V is the instantaneous speed of the current vehicle. It has been hypothesized in literature that for medium traffic time headway distribution is *Pearson type III* or gamma distributed(Rothery 1999):

$$P = \frac{\beta^{\alpha}}{\Gamma(\alpha)}(t-T)^{\alpha-1}e^{-\beta(t-T)}, t \geq T \qquad (0.0.26)$$

where T is cut-off time headway.

Table 3-3 summarizes the statistics of time headway distribution.

Table 3-3. Statistics of Time Headway Distribution and Gamma Parameters of A100 Freeway Dataset

Dataset	Minimum	25%	Median	75%	Mean	Var	α	β
Hifahrt	0.37s	1.17s	1.85s	2.79s	2.16s	1.64s	1.95	1.09
Rueckfahrt	0.32s	1.28s	1.83s	2.69s	2.20s	2.22s	1.60	0.85

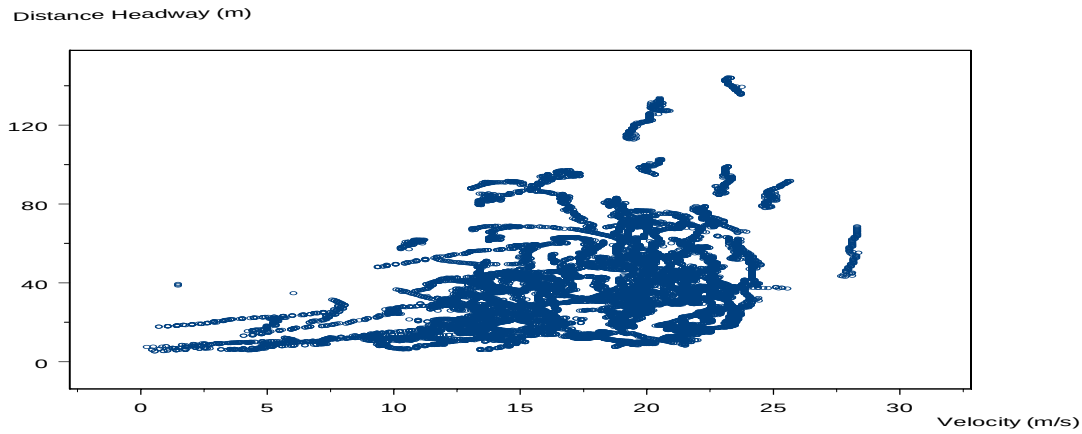

Figure 3-7 (a). Distance-Headway and Velocity: A100 Freeway Dataset (hifahrt)

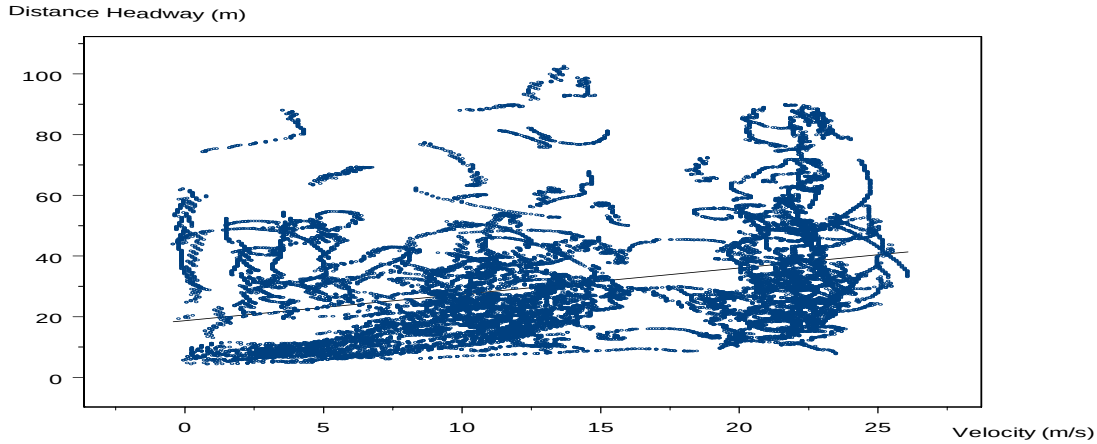

Figure 3-7 (b). Distance-Headway and Velocity: A100 Freeway Dataset (rueckfahrt)

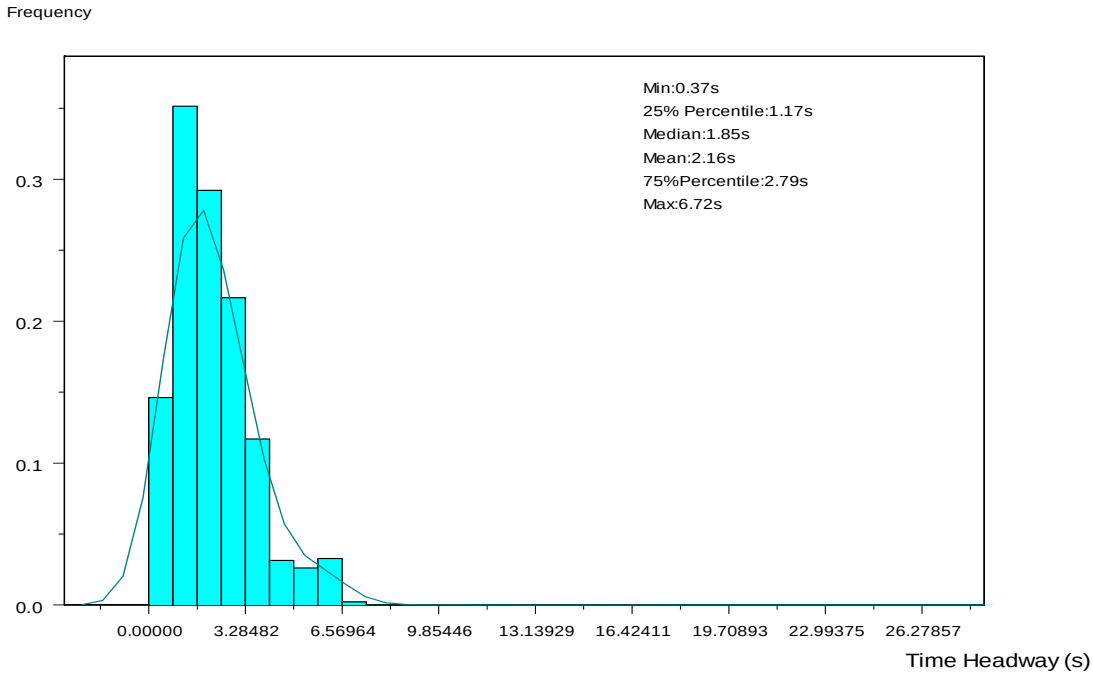

Figure 3-8 (a). Time Headway Distribution: German Hifahrt Dataset (Speed > 5m/s)

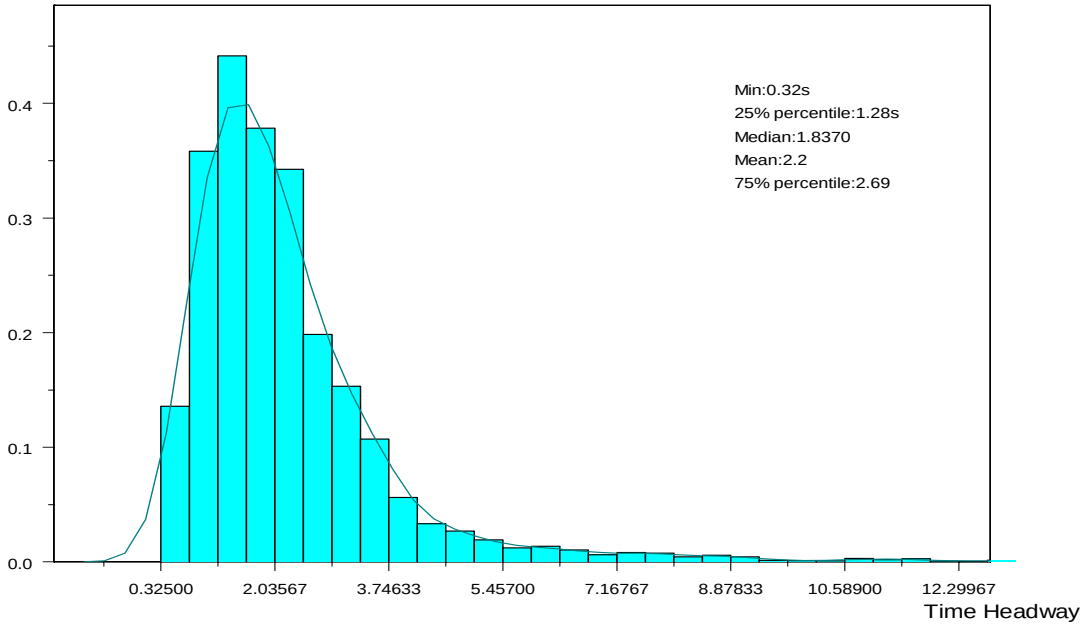

Figure 3-8 (b). Time Headway Distribution: German Rueckfahrt Dataset (Speed > 5m/s)

The distribution of relative speed in relation to relative distance is plotted in Figure 3-9 as oscillation spirals. As suggested in this figure, the oscillations are not real oscillations in the sense of a limit cycle (system reaching a prescribed movement boundary), otherwise, the spirals would stop at the stable point where $\Delta v = 0$. Further the spirals are scattering around $\Delta v = 0$ in a non-analytic way (no indication of harmonic oscillations); this indicate that there should be something beyond physical regularities involved in the process, thus it is not possible to have a fixed point $\Delta v = 0$ plus some white noise disturbing the system. Such non-physical regularities should be related to human-driver's incapability's in perceiving driving complex and accurately performing control tasks.

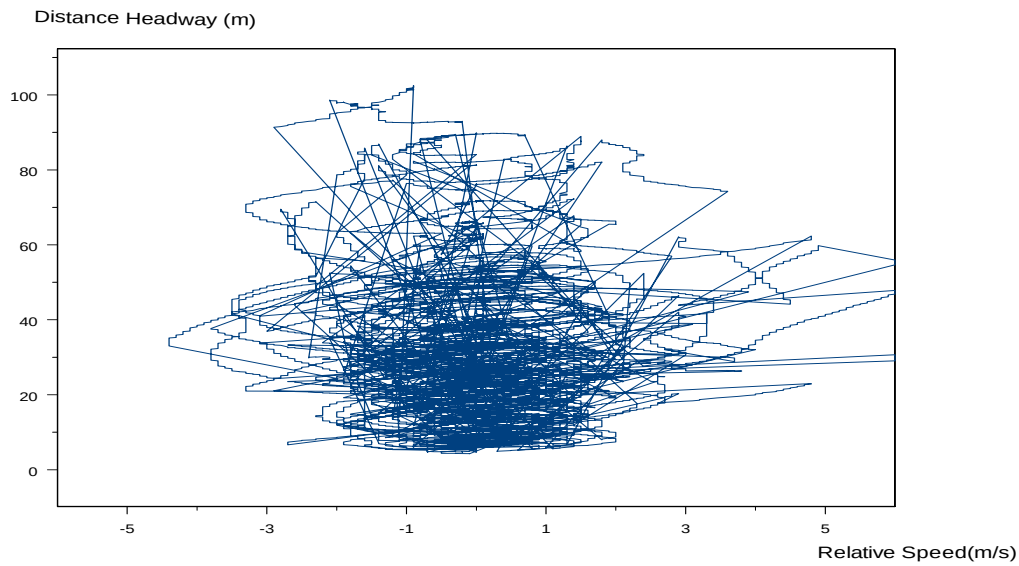

Figure 3-9 (a). Oscillations Spirals: German Rueckfahrt Dataset

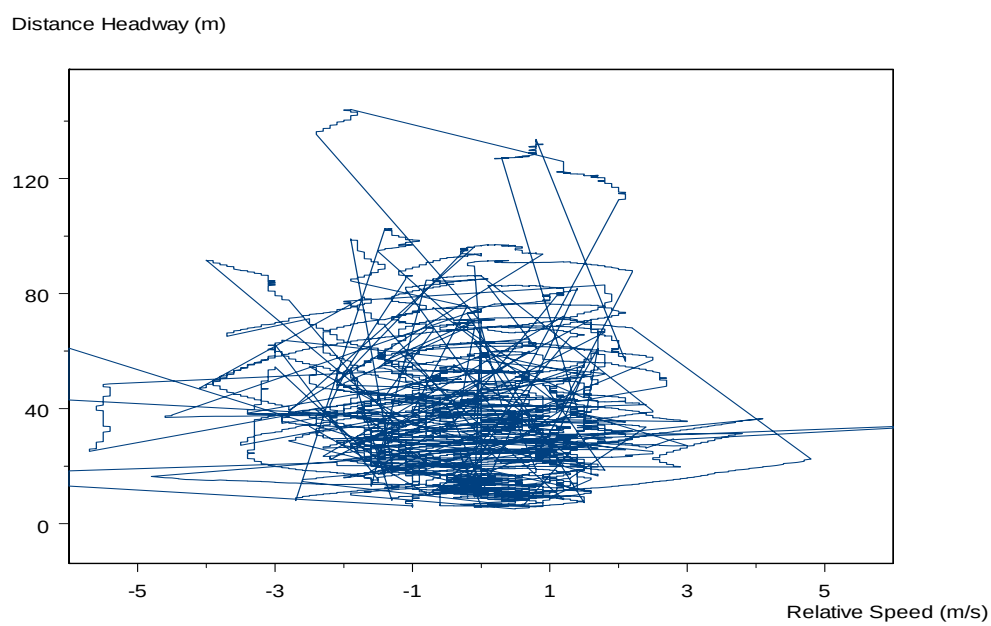

Figure 3-9 (b). Oscillations Spirals: German Hifahrt Dataset

3.2.1.2 Car-following Empirics from RTKGPS Test Track Data

RTKGPS data are the data to be used in this study to aid model development, calibration and validation. These data have been introduced in Section 3.1.1; thus detailed description is omitted here.

Data Analysis

Figure 3-10 plots the relationship between distance headway and instantaneous speed. In RTKGPS dataset, a platoon of 10 vehicles were running on a test track. In this Figure, Vehicle 1, i.e., the lead vehicle is excluded from analysis. Further, in this figure, the y-axis represents the instantaneous speed, and the x-axis the distance headway. It can be seen from the figure that when instantaneous speed increases, the distance headway increases as well. This is consistent with the well-accepted hypothesis that drivers tend to leave larger distance gap at higher speed for safety reasons. Furthermore, it is clearly shown in the figure that different driver has different patters in the relationship between distance headway and instantaneous speed; this suggests that such relationship is a driver-specific characteristics. Similar to the A100 freeway dataset, Figure 3-10 indicated that at higher speed there is bigger variance of distance headway. This suggests that drivers are less accurate in performing distance control to achieve desired following distance when speed is increasing, which can be attributed to human's inability to accurately determine distance headway when speed is high and when distance is already large enough.

In Figure 3-11, the time headway distributions are depicted. As mentioned earlier, time headway means the gross following time headway $T = D/V$, where D is bumper-to-bumper distance from current vehicle to its preceding one, and V is the instantaneous speed of the current vehicle. Table 3-4 summarizes the statistics of time headway distribution and gamma parameters. An interesting observation is that the variance of the time headway with all the 9 vehicles is much smaller than that of the probe vehicle in German A100 freeway data dataset. This can be explained since A100 freeway data were collected from real life traffic and RTKGPS data from test track; the former embodies much more varied traffic situations than the latter hence the time headway selection is less constrained.

The distribution of relative speed in relation to relative distance is plotted in Figure 3-12. The observations presented in Figure 3-12 are consistent with those with Figure 3-9. Once again, it is indicated that the oscillations are not real oscillations in the sense of a limit cycle, otherwise, the spirals would stop at the stable point where $\Delta v = 0$. Further the spirals are scattering around $\Delta v = 0$ in a non-analytic way; this indicate that the driving process could possibly is a mixture of physical regularities that determines vehicle mechanical dynamics together with human-factors. This is because if this is a pure fixed point process plus white noise disturbing the system, then such spirals would not have existed.

Figure 3-13 illustrates the relationship between acceleration, relative speed, and distance headway for all 9 vehicles. The z-axis is the acceleration rate adopted by the vehicle, y-axis is the distance headway and x-axis is relative speed. As clearly demonstrated by the figure, the acceleration rate points cluster around where $\Delta v = 0$; but the centered distance headway is not fixed with each vehicle. This means during the driving process each vehicle tries to maintain zero relative speed with regard to its preceding vehicle while keeping characteristic distance headway. The characteristic distance headway is driver specific. Also from the figure, it can be

seen that qualitatively acceleration is related to both distance headway and relative speed. This should be incorporated when developing new car-following models.

Table 3-4. Statistics of Time Headway Distribution and Gamma Parameters of RTKGPS Dataset

Dataset	Minimum (sec)	25% (sec)	Median (sec)	75% (sec)	Mean (sec)	Var	α	β
Vehicle 2	0.637	1.35	1.59	1.97	1.69	0.232	12.31078	7.284483
Vehicle 3	0.637	1.34	1.61	1.96	1.69	0.230	12.41783	7.347826
Vehicle 4	0.462	1.44	1.65	1.93	1.75	0.256	11.96289	6.835938
Vehicle 5	1.05	1.49	1.65	1.92	1.77	0.20	15.6645	8.85
Vehicle 6	1.08	1.72	1.97	2.29	2.05	0.257	16.35214	7.976654
Vehicle 7	1.27	1.99	2.27	2.56	2.35	0.328	16.83689	7.164634
Vehicle 8	1.11	1.81	2.08	2.47	2.20	0.323	14.98452	6.811146
Vehicle 9	0.86	1.98	2.35	2.82	2.48	0.546	11.26447	4.542125
Vehicle 10	0.96	1.68	1.93	2.36	2.10	0.543	8.121547	3.867403

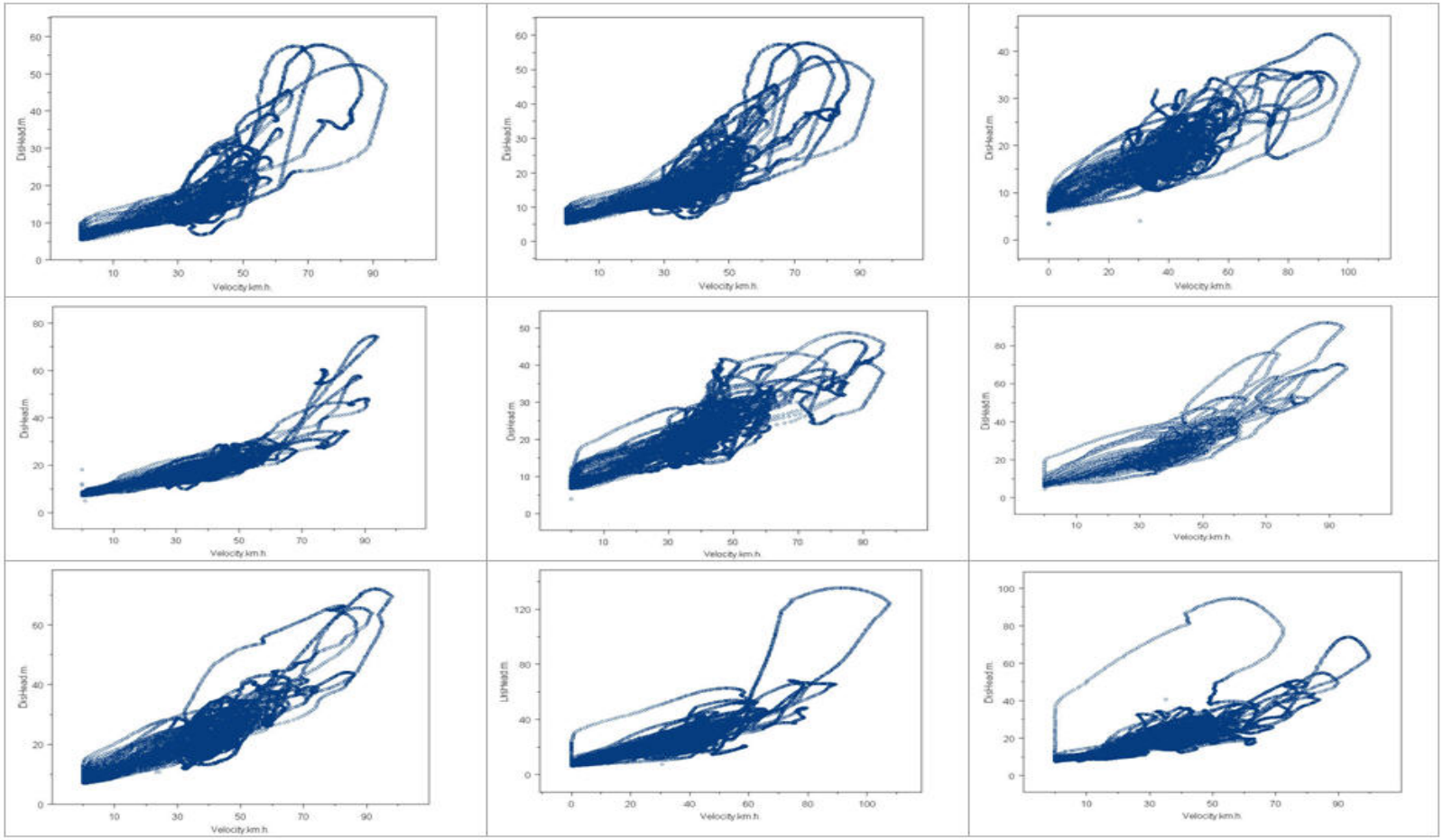

Figure 3-10. Distance Headway and Speed Relationship: Japan Dataset (9 Vehicles on Test Track)

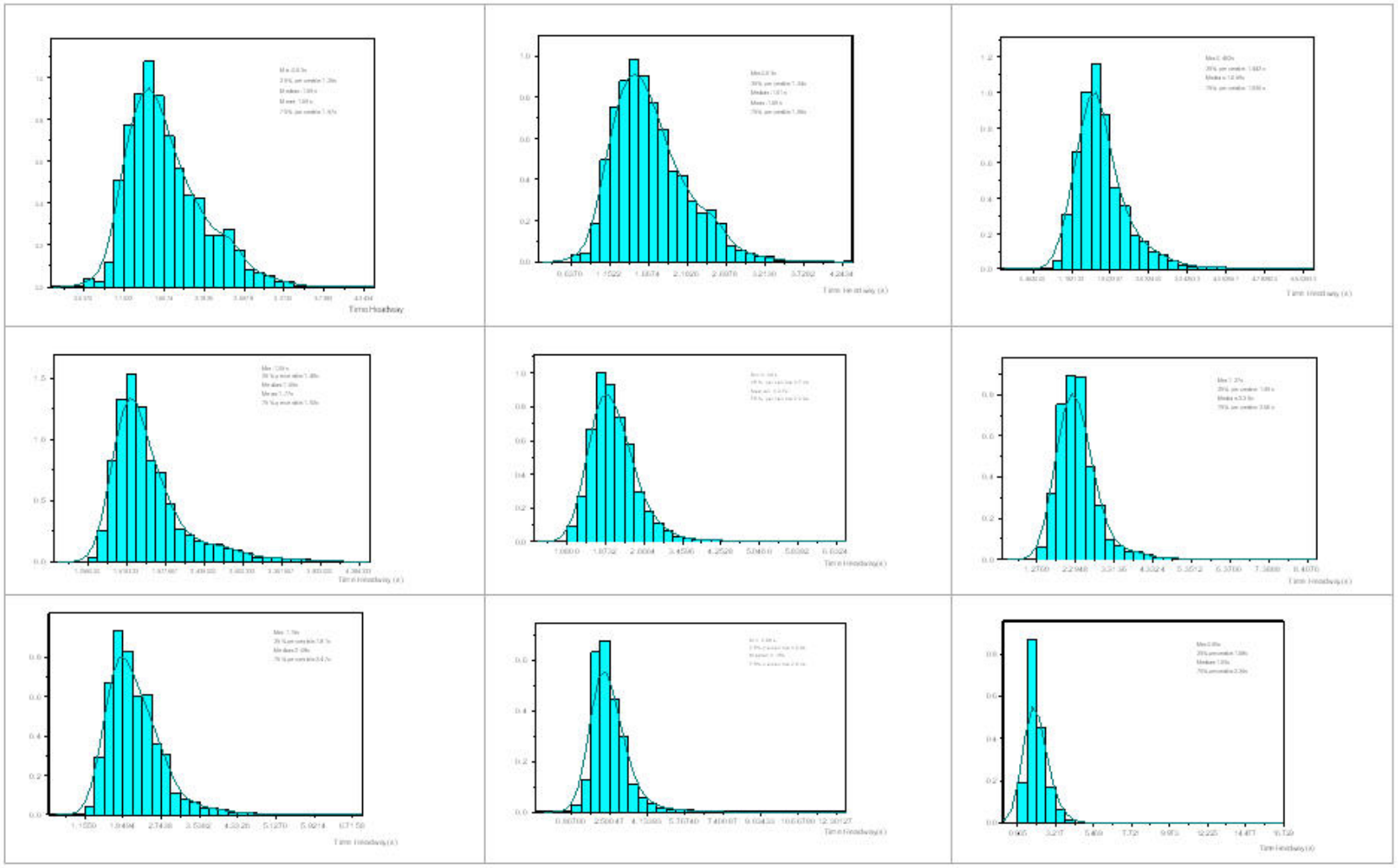

Figure 3-11. Time Headway Distribution Japan Data (9 Vehicles)

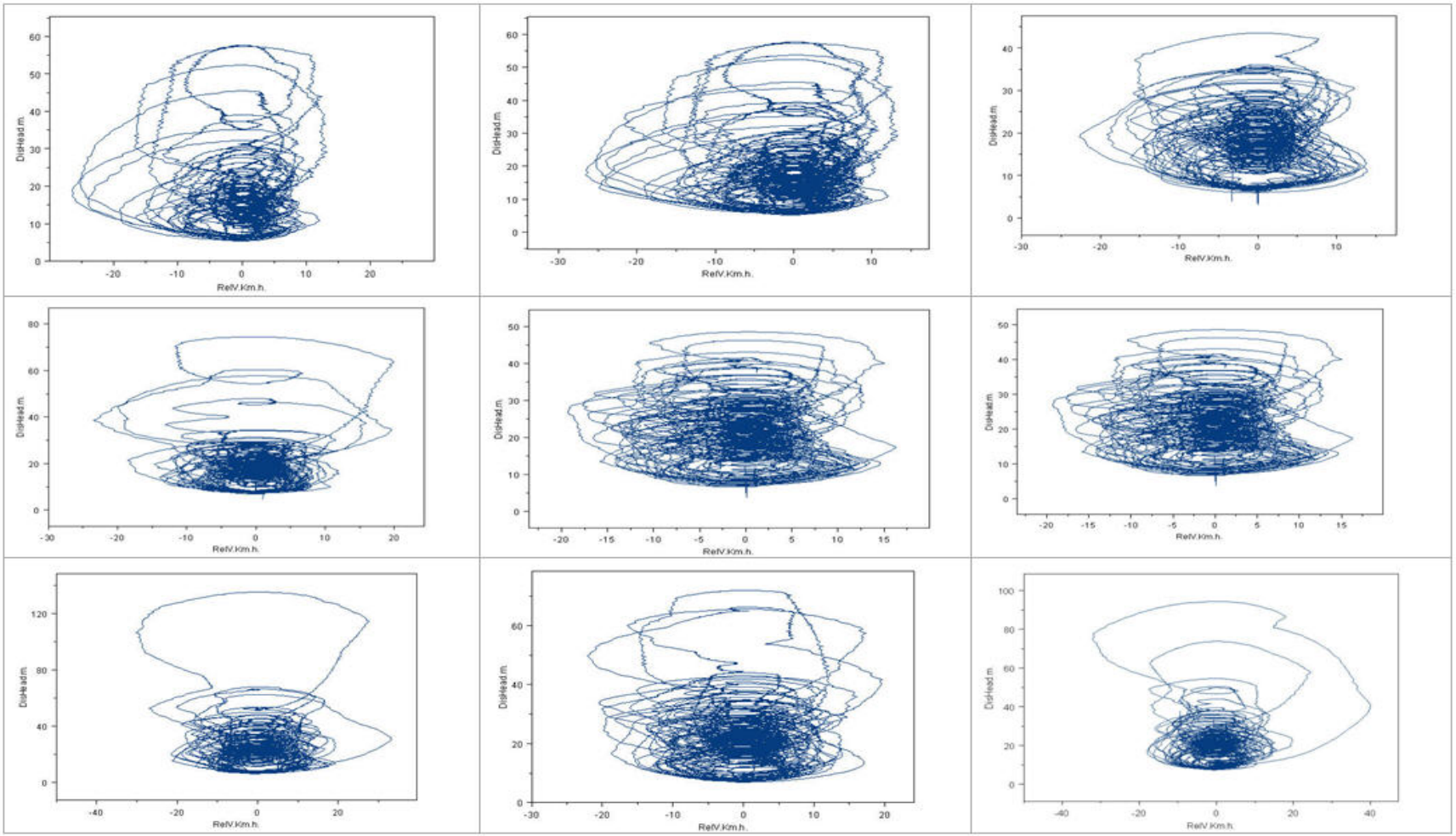

Figure 3-12. Oscillation Spirals

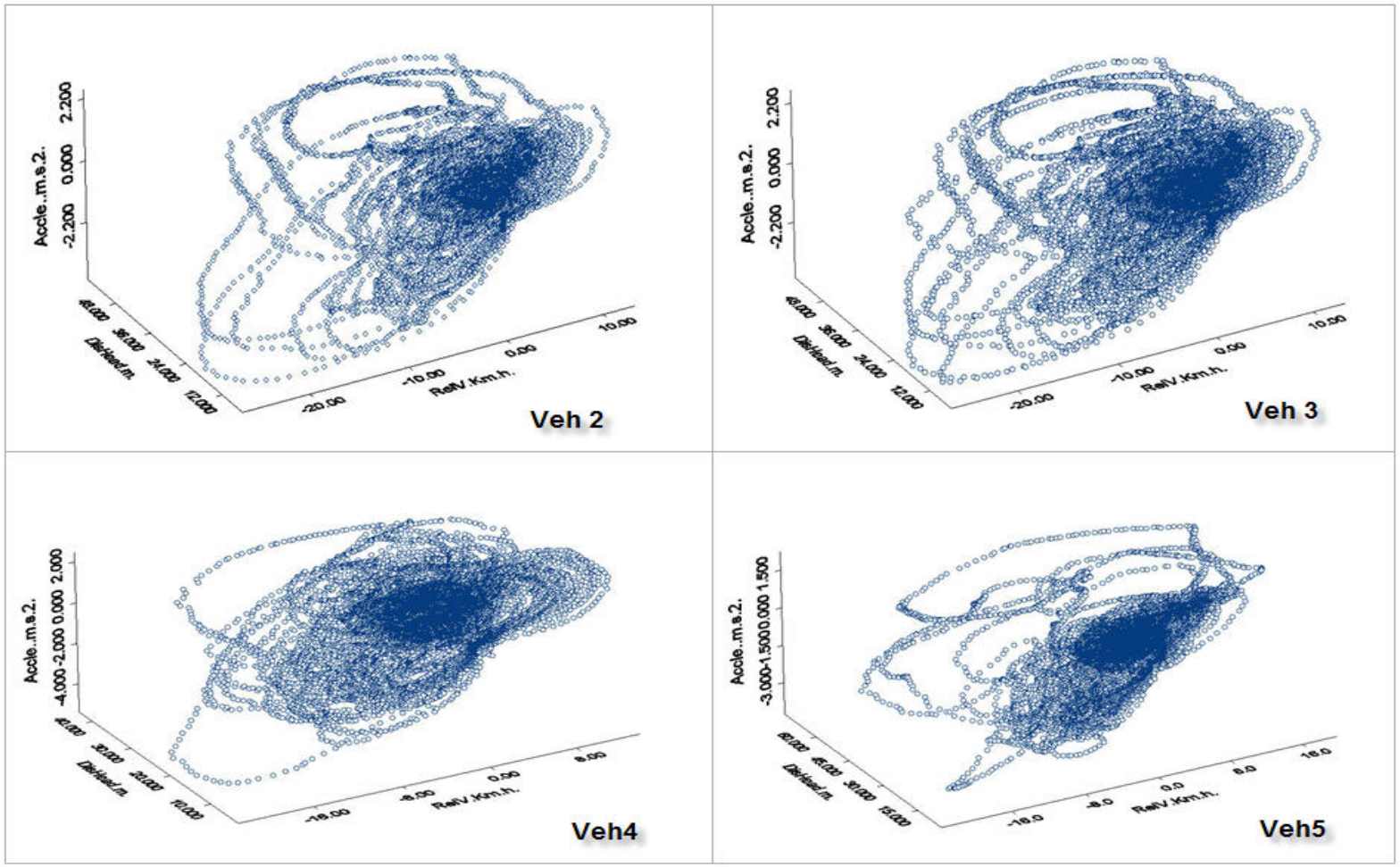

Figure 3-13 (a). Acceleration-Relative Speed-Distance Relationship

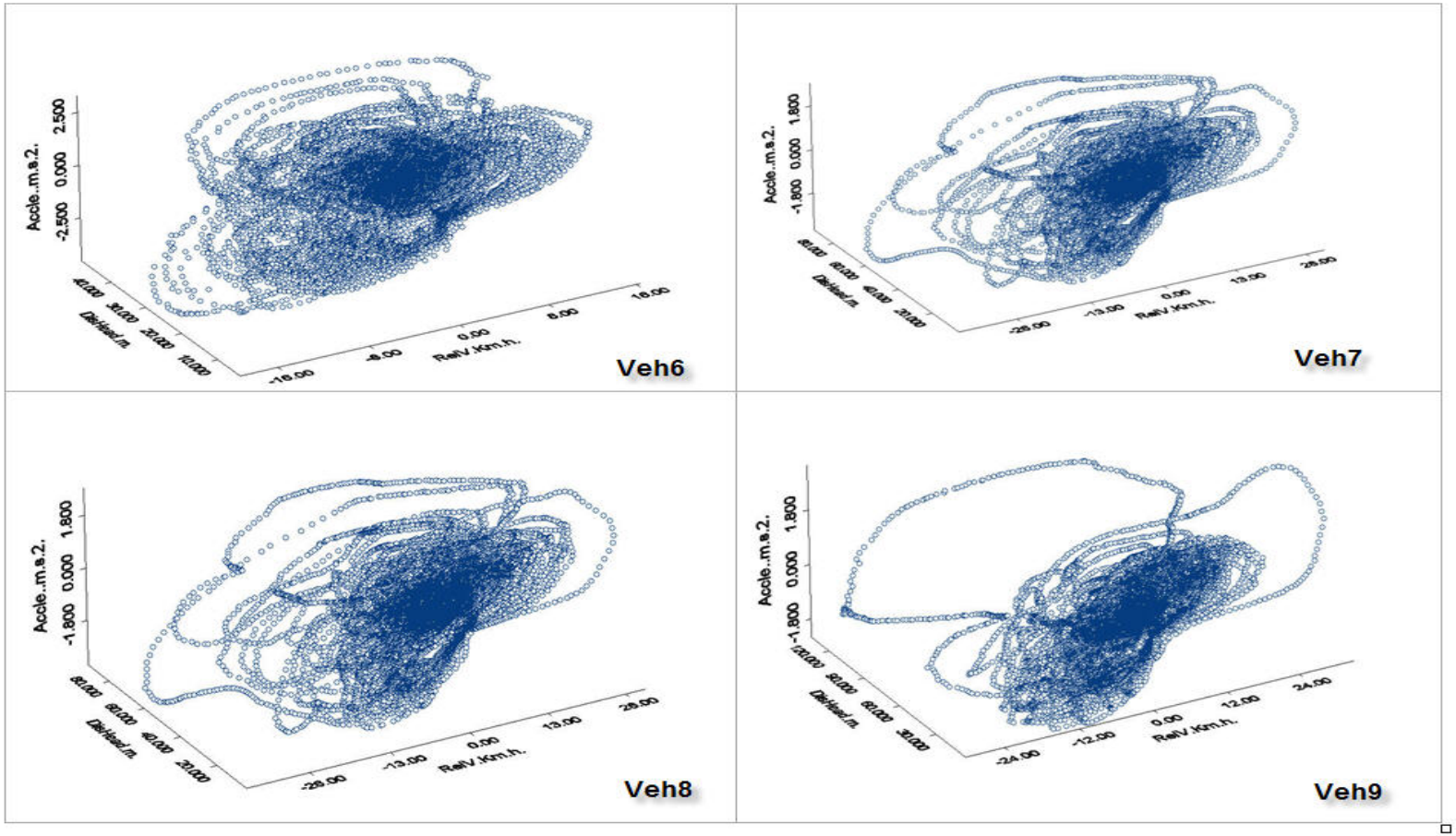

Figure 3-13 (b). Acceleration-Relative Speed-Distance Relationship

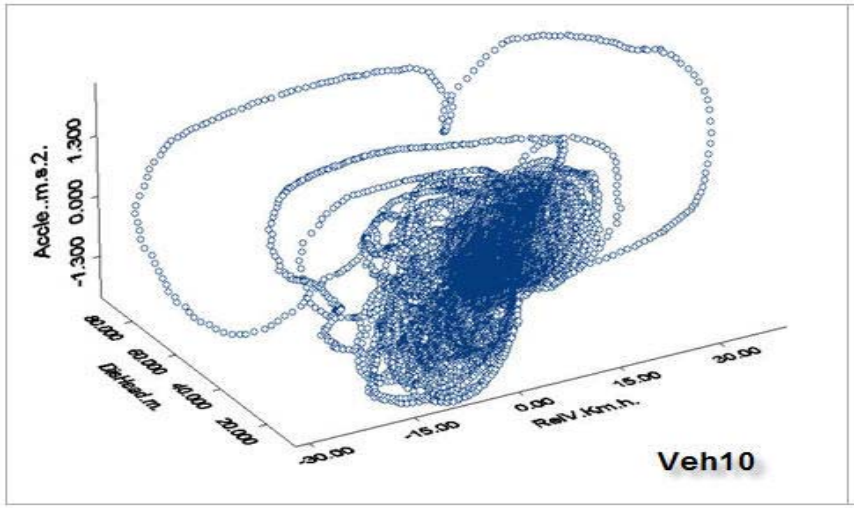

Figure 3-13 (c). Acceleration-Relative Speed-Distance Relationship

3.2.1.3 Car-following Empirics from NGSIM Data

The objective of the *Next Generation Simulation (NGSIM)* program is to develop a core of open behavioral algorithms in support of traffic simulation with a primary focus on microscopic modeling, including supporting documentation and validation data sets that describe the interactions of multi-modal travelers, vehicles and highway systems, and interactions presented to them from traffic control devices, delineation, congestion and other features of the environment. These products will be openly distributed and made freely available to the broad transportation community. The dataset used here is the 45 min data collected during the afternoon peak period on a segment of Interstate 80 in Emeryville (San Francisco), California. The dataset consists of detailed vehicle trajectory data, wide-area detector data and supporting data needed for behavioral algorithm research on a merge section of eastbound I-80. Within the dataset, three separate 15 minute periods of data are available: 1) 4:00 p.m. to 4:15 p.m.; 2) 5:00 p.m. to 5:15 p.m.; and 3) 5:15 p.m. to 5:30 p.m. All were collected on April 13th, 2005. The data for the 4:00 p.m. to 4:15 p.m. period primarily represent transitional traffic conditions during the build-up to congestion. The remaining two periods represent congested traffic conditions.

Reaction time is usually hypnotized to be lognormal distributed as in Equation (0.0.27)

$$P = \frac{1}{(t-T)\sigma\sqrt{2\pi}} e^{-[\frac{\ln(t-T)-\mu}{\sigma}]^2/2} \qquad (0.0.27)$$

Table 3-5 summarizes the statistics of reaction times derived from the I-80 dataset. This includes the mean, variance and estimated parameters for the underlying lognormal distribution. Specifically, the reaction time is computed using a conventional "traffic engineering" approach, i.e., vehicle pairs (lead vehicle, lag vehicle) are first screened from the dataset, then correlation coefficient between the lead and lag vehicle's speed profiles are computed. The time lag that gives the maximum correlation coefficient is assumed to be the (characteristic) reaction time of the following vehicle. Finally, a total of 2050 vehicles in 4:00-4:15pm dataset, 1831 vehicles in 05:00-05:15pm dataset, and 1787 vehicles in 05:15-05:30pm dataset are employed in this computation.

Table 3-5. Statistics of Reaction Time: NGSIM Data

Dataset	Mean	Var	T	σ	μ
4:00-4:15pm	2.087s	1.04	0.3s	0.11	0.73
5:00-5:15pm	1.987s	0.97	0.3s	0.31	0.64
5:15-5:30pm	2.007	0.88	0.3s	0.34	0.64

Compared to earlier studies, both the mean and variance of reaction times presented in Table 3-5 appears to be fairly large. For example, in (Rong et al. 2006), reaction time computed from normal motor way traffic ranges from 1.07 to 1.67 with variance ranging from 0.45 to 0.48. This

can be attributed to the fact that I-80 NGSIM data were collected from heavily congested traffic where stop-and-go phenomenon is not uncommon. Under such conditions, drivers usually have longer reaction time than under normal traffic with higher speeds. Figure 3-14 plots the reaction time distribution with each part of data. As shown in this figure, reaction time distribution features a high density area around its mean values while generally the distribution skewed towards right with longer "tails" spreading higher reaction time values (See Figure 3-14). This is a typical pattern consistent with earlier studies in the literature.

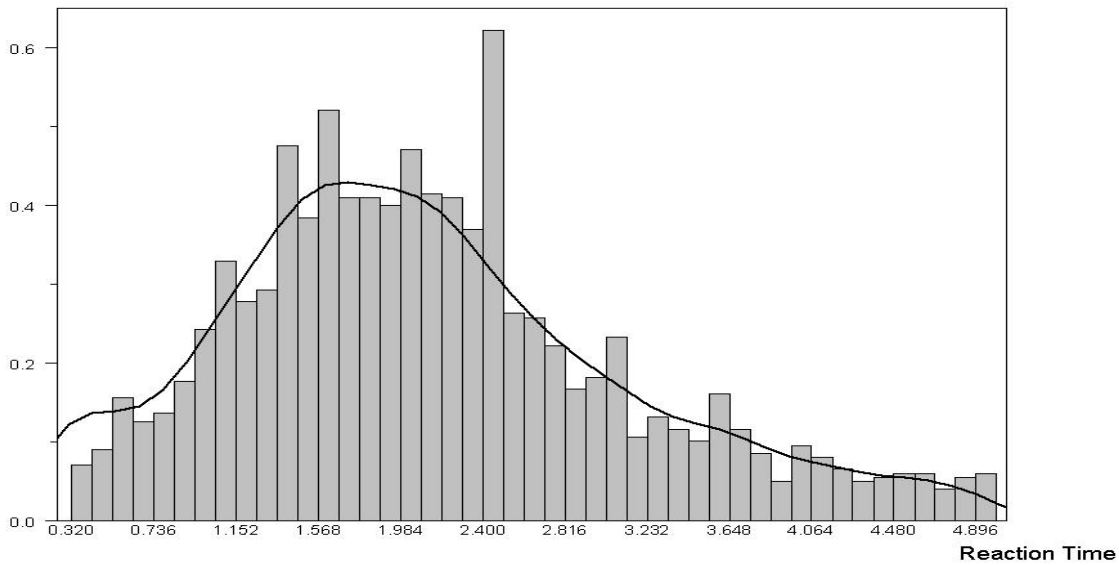

Figure 3-14 (a). Reaction Time Distribution: I-80 from 4:00-4:15 pm

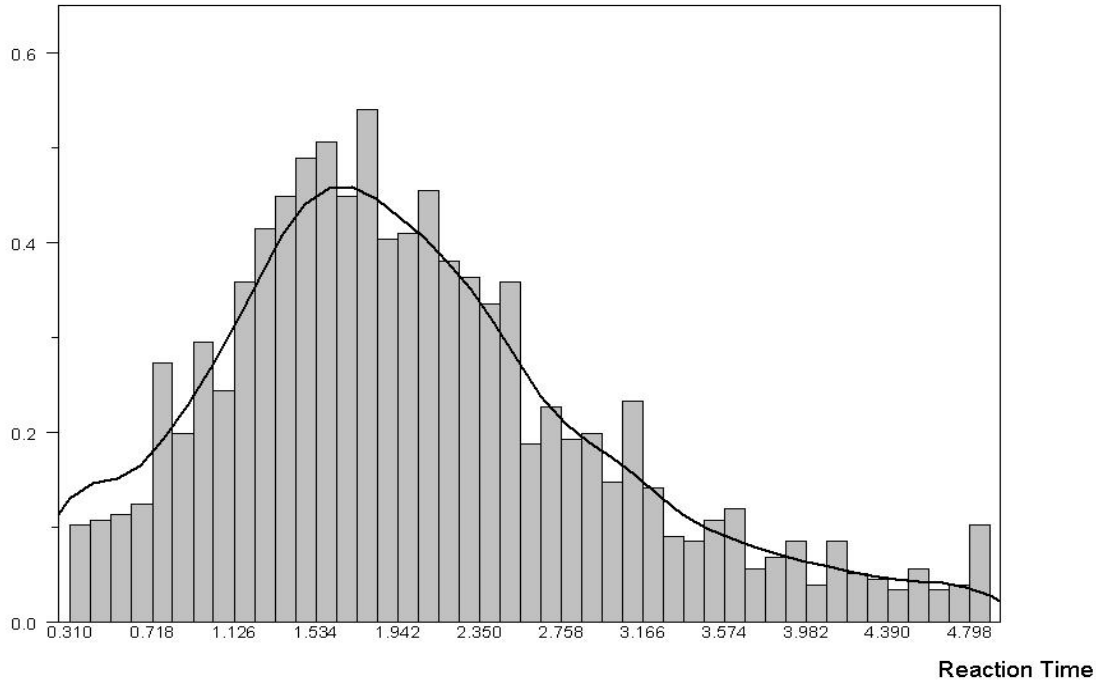

Figure 3-14 (b). Reaction Time Distribution: I-80 from 5:00-5:15 pm

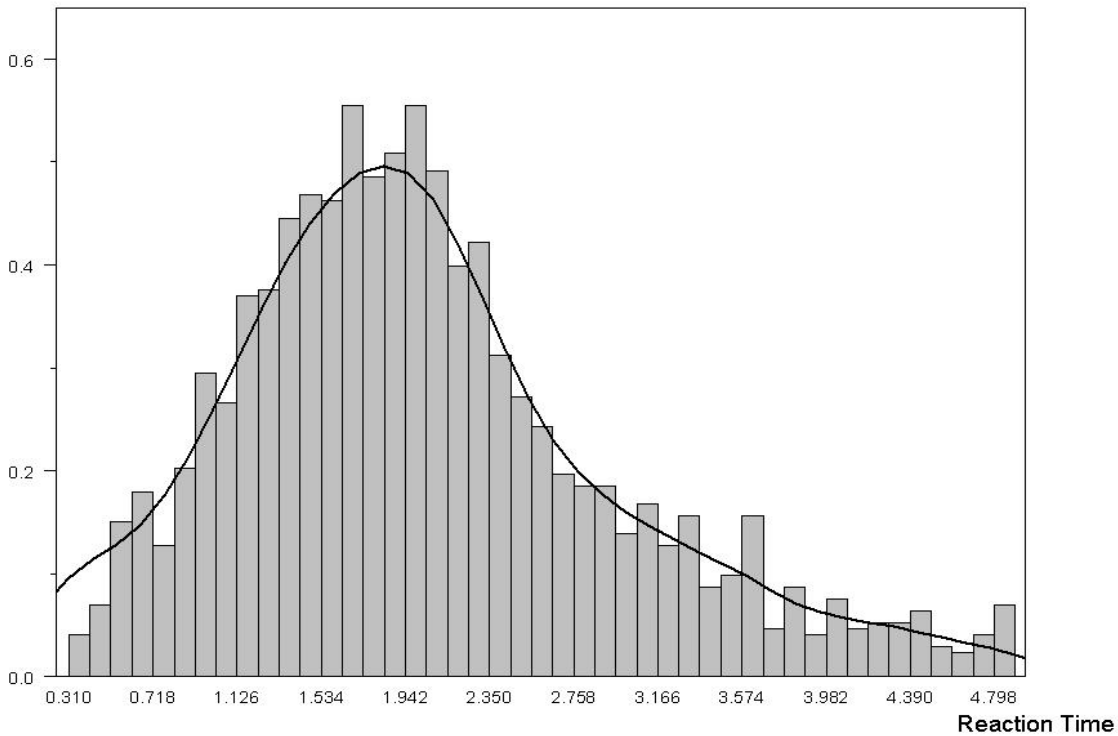

Figure 3-14 (c). Reaction Time Distribution: I-80 from 5:15-5:30 pm

3.2.2 Review of Crash-prone Conditions

Hourdos (Hourdos 2005) has examined various conditions that are possibly crash-related. In this section, major conclusions from (Hourdos 2005) are summarized. These conclusions render empirical insights for building collision-inclusive car-following models. Note, the crash cases mentioned below occurred during 2002~2003 at the crash data collection site from I94WB. This crash data collection site has been introduced in Section 3.1.2.

Visibility Conditions (weather)

Visibility does not appear to have a strong correlation with crash occurrences. Though, in rain or snow conditions visibility is significantly reduced, interfering with driver ability to see ahead, to recognize the edge of the road, and to keep a safe distance from other vehicles. However, drivers compensate this by driving in a more cautious manner, e.g., drive with much slower speed and/or keep longer distance headway. Figure 3-15 shows the number of crash cases in relation to visibility conditions.

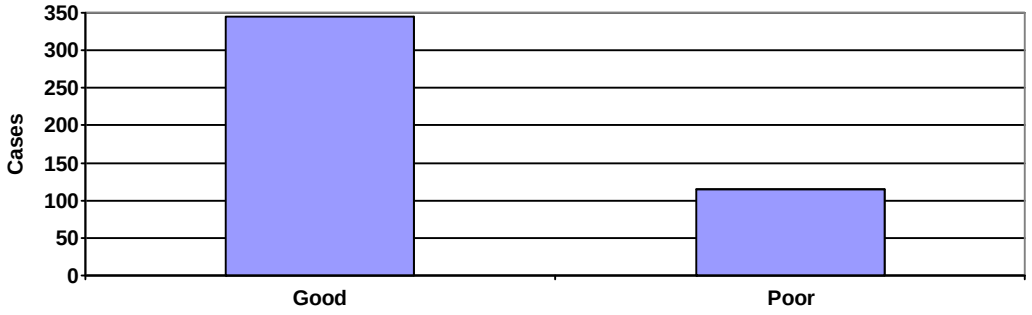

Figure 3-15. Number of Crashes vs. Visibility

Since the above chart does not take into consideration the percent of poor visibility days during the study year (i.e., 2002~2003), Figure 3-16 adds some clarification on the possible effect visibility conditions have on crashes.

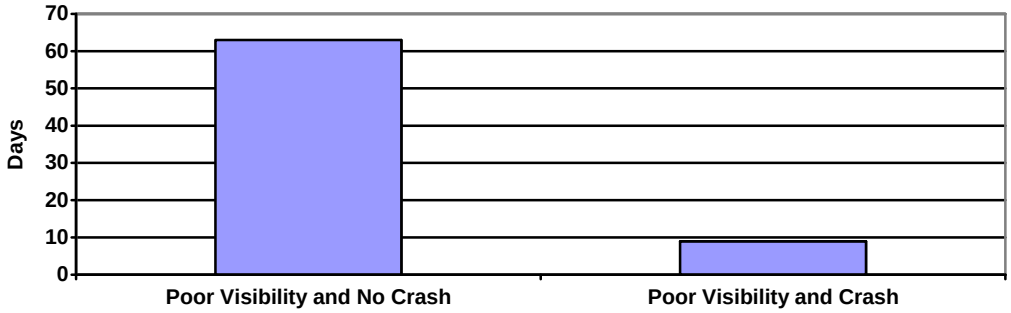

Figure 3-16. Poor Visibility Days

Pavement Conditions

Pavement conditions affect the friction between tires and road surface, thus determines the maximum deceleration rate a vehicle can actually implement. This in turn determines minimum stopping distance. Furthermore, driving behavior changes in locations with wet and icy pavement. Figure 3-17 depicts the number of crash cases in relation to pavement conditions. It has been observed that about 10% of the crashes and near-misses occurred during rain/snow or with wet pavement.

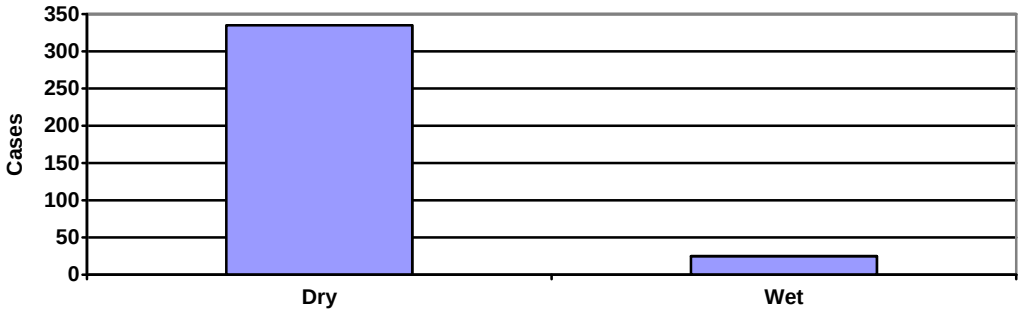

Figure 3-17. Crashes vs. Pavement Condition

Sun Glare

It was observed that during certain periods the sun is facing the driver causing glare on the windshield. This glare significantly impedes driver ability to recognize braking lights of the lead vehicle. Figure 3-18 illustrates the number of cases in relation to sun position.

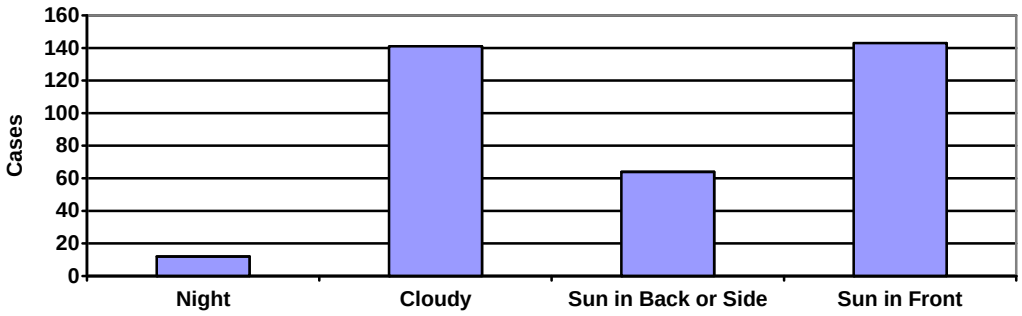

Figure 3-18. Crash Cases vs. Sun Position

Lane Position

For the crashes/near-misses captured from surveillance cameras during 2002 to 2003, 90 % of the collisions and 100% of the near –misses occurred in the right lane. Of all the crashes/near-misses cases, 18% took place upstream of Portland Avenue while 80% took place at Portland and only 2% downstream. The location of collisions relative to the Portland overpass is illustrated in Figure 3-19.

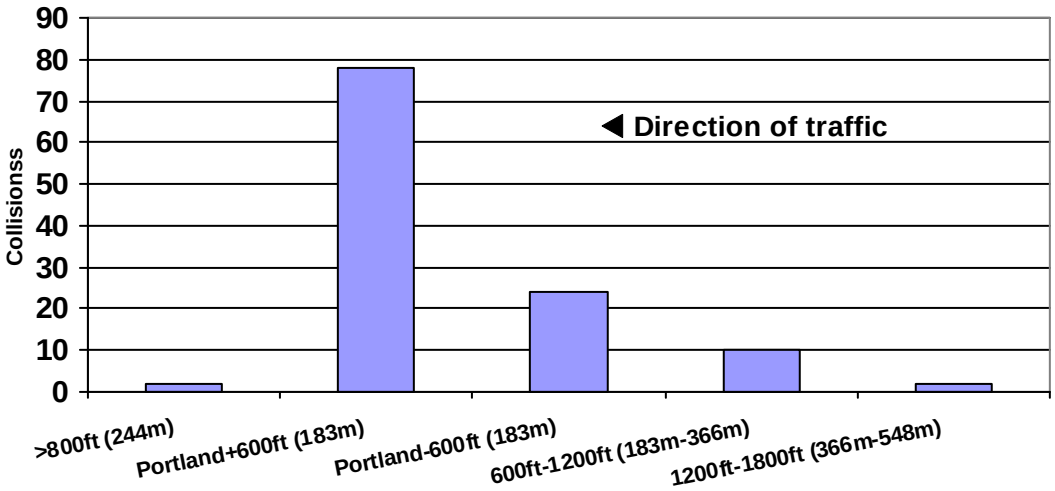

Figure 3-19. Collision Totals per Location

Meanwhile, it is interesting to point out that the downgrade and turn of the roadway in this section occurs 600 feet (183 meters) after where the majority of these crashes take place. At the beginning of the downgrade, driving visibility improves due to elevated line of sight relative to the vehicle in front. Additionally, for a brief instance it is possible to see traffic ahead as the driver approaches the turn.

From the video recordings, the specific location with highest crash rate is at 500 feet (152m) downstream of the lane drop. No crash was observed due to late merge from the auxiliary lane on the right. The collisions on the middle and left lanes generally occur slightly upstream of the majority of crashes in the right lane; but no farther than 1000 feet (304m) from the Portland overpass.

Crash Time

This particular freeway section carries high volumes during both morning and evening peak periods. The evening peak period is considerably longer than the morning and the congestion can extend to well after 7 p.m. Although congestion usually does not begin until 3 or 4 p.m., however, as can be seen in Figure 3-20, a large number of crashes occur early in the afternoon before the assumed start of the peak period (e.g., freeway ramp control operates from 15:00 to 18:00). The number of crashes during the morning peak is considerably fewer. This can be attributed to the different traffic patterns observed during the morning.

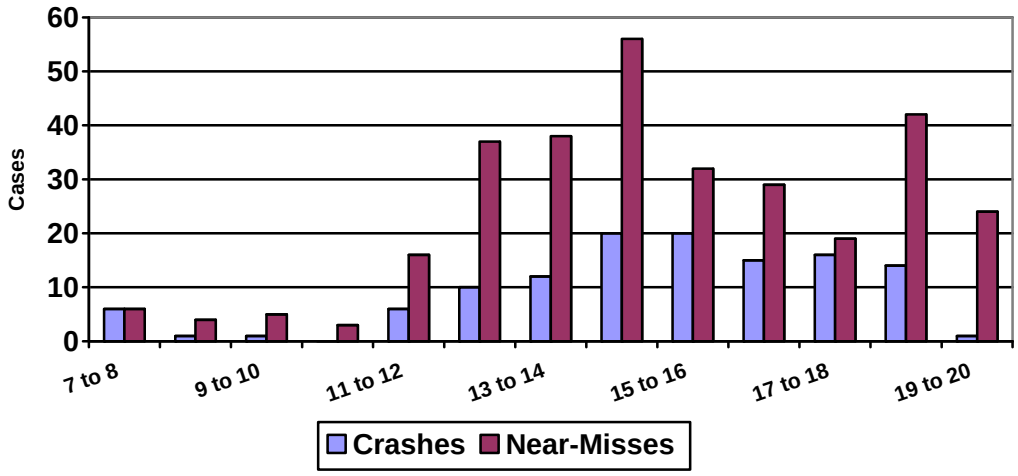

Figure 3-20. Crashes vs. Time

Traffic Dynamics

The study section of I-94 westbound presents a number of interesting traffic dynamics due to complex geometries and complicated O/D paths. In particular, due to the different origins and destinations served through this section a considerable amount of weaving takes place within a relatively short distance. To better understand the different traffic dynamics in this section, the origins and destinations served can be broken down as follows:

- Destinations in succession according to traffic direction (Westbound):
  - ✓ I-35W southbound exit. This left-hand exit terminates the short auxiliary lane in the first part of the study section. With a very short ramp it leads to the I-35W section that runs in parallel with the I-94 freeway. This is the only access toward the south of the metro and it is heavily used throughout the day.

- ✓ 11th Street. This is a right-hand exit to the local streets of the south downtown area. This exit is usually congested during the morning peak period with a queue frequently extending into the auxiliary lane of the freeway mainline. During the evening peak this exit exhibits very low volumes. The auxiliary, fourth lane on the second part of the study section ends at this exit.
- ✓ Hennepin/Lyndale Avenues exit. This is a multiple destination two lane right-hand exit leading both south, towards the uptown area, as well as towards the southwest area of downtown. This exit exhibits high volumes during both morning and evening peak periods. This exit can also be used as an alternate route towards I-394 or even I-94 west for vehicles prohibited from using the Lowry Hill Tunnel. The auxiliary, fourth lane on the third part of the study section ends at this exit.
- ✓ I-394 exit. Immediately after the Lowry Hill Tunnel there is a right hand, two lane exit towards the I-394 freeway. Although generally a high volume destination, this exit exhibits even higher volumes during the evening peak period.

- Origins in succession according to traffic direction (Westbound):
  - ✓ I-94 mainline from St. Paul. I-94 is the only freeway directly connecting downtown St Paul with downtown Minneapolis. The only other choice would involve a considerable trip north to I-35W and then south towards Minneapolis. Additionally, the three preceding entrances to I-94 serve the University of Minnesota campus, a considerable producer of work, school, and leisure related trips. During the morning peak period, traffic from this part of the freeway is directed towards the downtown area through the 11th Street and Hennepin exits. During the evening peak a large percentage of the traffic of I-94 is directed towards the I-394 freeway and the west side of the metro region. Especially in the case of the I-394 destination there are no other alternative routes that involve a freeway. The next choice would involve the 494/694 ring road. This puts a lot of pressure on the right lane of the entire section since this is the only one leading towards I-394. Signs to that exit start half way before the study section.
  - ✓ Southbound I-35W, TH-55, and local streets combined entrance ramp. This entrance ramp joins the mainline through the fourth, auxiliary lane on the middle part of the study section. This entrance combines traffic from three major origins. First origin is the I-35W southbound freeway. Traffic from this origin is mainly directed towards the I-394 freeway destination and the northwest part of the metro region. Additionally, traffic from North I-35W can also be directed towards the Hennepin/Lyndale exit or the 11th Street exit, but for both of these destinations there are other, alternate, routes that are usually more attractive. In fact no other freeway routes connect I-35W with either I-394 or the north part of I-94. The second origin is TH-55 or Hiawatha Avenue. Considering the other available routes from TH-55 the entrance ramp to the study section is primarily used for traffic that is either directed towards I-394 or to north I-94. It leaves no doubt that these are also the primary destinations of the local roads using this entrance ramp. The result is that, the vast majority of the traffic using this ramp must perform one lane change before the drop of the 1,200 feet (366m) long auxiliary lane and one more if they are not headed towards I-394.

- ✓ Northbound I-35W, 3rd Avenue combined entrance ramp. Approximately 1,500 feet (457m) after the drop of the aforementioned auxiliary lane, another one begins at the combined entrances of I-35W northbound and 3rd Avenue downtown, ending approximately 2,000 feet (609m) later at the Hennepin/Lyndale exit. The traffic using the I-94 flyover, the name given to the ramp coming from I-35W because it passes above I-94, will most likely not exit on Hennepin since an alternate route towards the downtown area is available and is considerably shorter. In contrast, the only alternate route to I-394 or north I-94 will require traversing the entire downtown area. Traffic from 3rd Avenue, being already in the Downtown area will probably not be directed towards the I-394 or the Hennepin/Lyndale exit. Similar to the previous auxiliary lane, the traffic using this one primarily will have to make one or even two lane changes before the tunnel entrance.

From reviewing thousands of hours of video records of the study section, a number of interesting traffic patterns have been observed. For most of these observations, corroborating evidence based on measurements can be found from (Hourdos 2005). Specifically, the following observations added to the general knowledge of the study section:

Of the majority of crashes observed, a compression wave was observed propagating backwards. Originally it was assumed that these waves are caused by the I-394 exit, since it has been noted that exit traffic generates congestion in the tunnel. When the video coverage was extended beyond 3rd Avenue, along with data from the detector measurements, it was confirmed that the section between that entrance and the tunnel exhibits lower densities than the traffic in the tunnel or the merge area of 3rd Avenue. Additionally, no significant numbers of compression waves were observed traversing this section. After further observation it was evident that the bottleneck causing the compression waves is the merge immediately after the 3rd Avenue entrance ramp.

Furthermore, it was also observed that the auxiliary lane between 3rd Avenue and the Hennepin/Lyndale exit is underutilized by the merging traffic. There is an obvious tendency of drivers using the I-94 flyover to merge quickly to the right regardless of whether there are more favorable merging conditions downstream. By contrast, drivers originating from the 3rd Avenue part of the ramp (right side) are merging much later and with fewer consequences to the mainline traffic.

Video recordings and detector measurements indicated that drivers on the right lane downstream of Portland have very short time headways. Regardless, it has been found that in many crash cases, following gap between the two colliding vehicles were sufficient for the following vehicle to apply an emergency stop, yet collision still took place. One possible explanation is that the driver of the second vehicle was not attentive to the driving task or had his focus elsewhere. Considering the speed difference between the lanes, the lane changing task is considerably harder than normal. Drivers must spend more time looking to the left and behind for an appropriate gap, and less time looking forward.

Conclusion

From the statistics presented above, one can observe a tendency for poor visibility/wet pavement conditions to discourage crashes (Hourdos 2005). This observation is in agreement with previous findings by (Edwards 1998) and (Lee et al. 2002). The low numbers during low light conditions can be attributed in the fact that the leading vehicles' break lights can be noticed faster even from the drivers' peripheral vision (not looking straight ahead). Similar findings can be found in several human factors studies on crashes (Marshal and Mahack 1998). Of course one has to be careful in generally associating bad weather with low crash risk since crashes are not always caused by inattention and the severity of a crash has been proven to increase during adverse conditions (Khattak et al. 1998). Further, in (Hourdos 2005), real-time measurements from the detection and surveillance stations and from loops are also analyzed to identify corroborating evidence that supports the observations summarized here and uncovers additional traffic dynamics possibly associated with crash prone conditions. Interested readers are encouraged to refer to (Hourdos 2005).

3.2.3 Conceptual Framework

Based on the car-following empirics summarized in Section 3.2.1 and crash-prone conditions in Section 3.2.2, a conceptual framework describing driving tasks are proposed. Specifically, driving process is *prescribed* as a *negative feedback system* with interactions between *external world* and *driver-vehicle-unit (DVU).* External world is composed of situational factors representing vehicle interactions and environmental factors such as roadway and weather conditions. DVU refers to an integrated unit when driver and vehicle are considered as a whole. This means a DUV has two components, i.e., driver performance component characterized by a human perception and decision-making process, and vehicle mechanics component, representing the mechanics of the vehicle. Figure 3-21 illustrates this concept. As shown in this figure, a DUV interacts with situational factors while acquiring environmental information by sampling the driving surroundings. This concept is further detailed next.

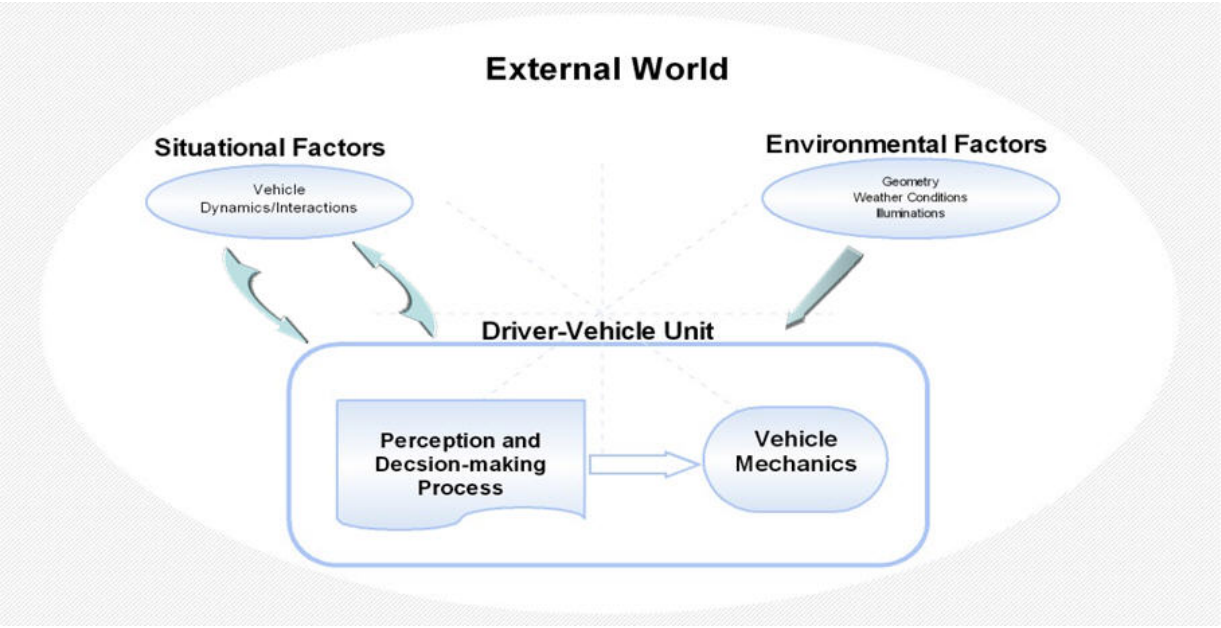

Figure 3-21. General Concept: Situational/Environmental Factors and DUV

3.2.3.1 External World

Situational Factors

In the context of this research, the influence of external world on driving process is exemplified via various situational and environmental factors. Situational factors refer to single-lane dynamics (i.e., velocity, relative velocity, space headway etc) of preceding and following vehicles, as well as that of vehicles on adjacent lanes. Such factors reflect interactions between vehicles during car-following process. In other words, a following car is not only influenced by the vehicle immediately in front, but could also be influenced by several vehicles ahead on the same lane, and likely vehicles on adjacent lanes. Such multilane-effect and anticipatory-behavior are typical in car-following process.

Environmental Factors

Environmental factors that could influence driving process include roadway conditions such as geometry features or illumination, weather conditions such as rain, fog, snow, or sun glare. These factors influence driver's perception-response process as well as vehicle control process (See Figure 3-22).

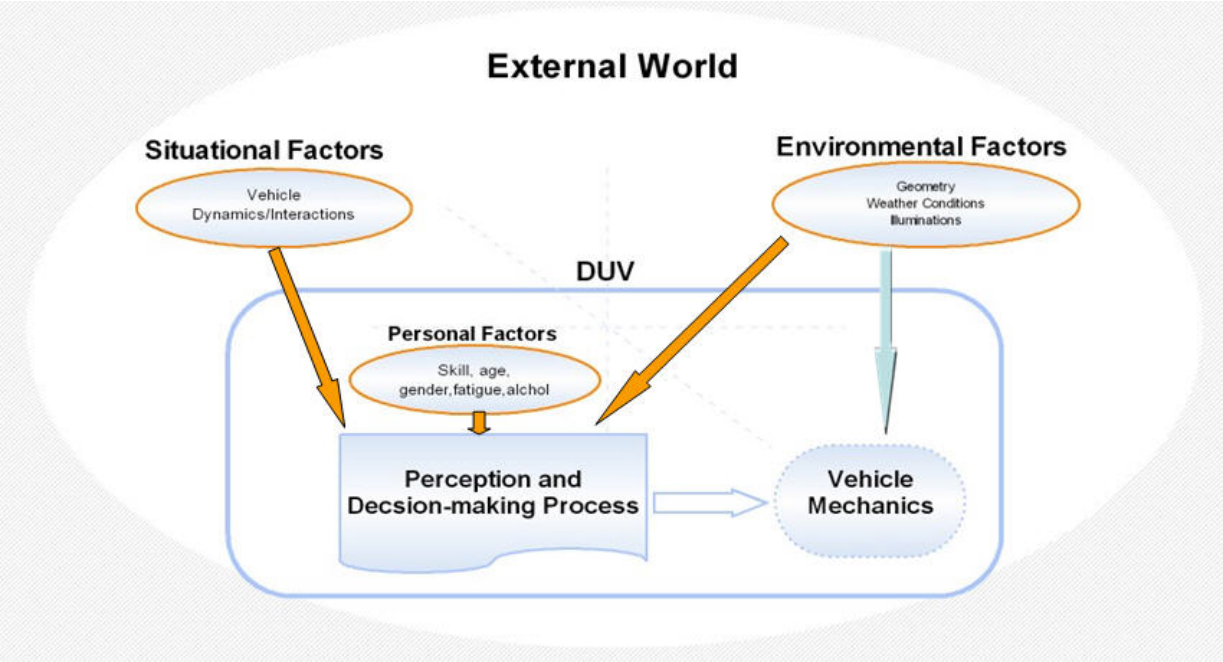

Figure 3-22. Interactions between External World and DUV

Driver-Vehicle-Unit

The driver-vehicle-unit (DVU) consists of two major components: (1) Driver Perception and Decision-making Component and (2) Vehicle Mechanics Component (See Figure 3-22).

Perception and Decision-making Component

This component has two sub-components, i.e., *Information Acquisition Component*, and *Decision-making Component*. I*nformation acquisition* is a critical component for the robustness of this feedback driving system, as this component interprets driving surroundings and provides necessary information for *Decision Making* component, which in turn controls vehicle dynamics. If this component samples the wrong information, the right information too late due to lapse of attention, or fail to sample at all, c*rashes or flow disturbances* could result.

Factors that could influence driver's information acquisition process include *situational factors*, *environmental factors* and *driver's personal factors* such as age, gender or driving skill. These factors are postulated to affect a driver's perception threshold and attention level hence essentially affect effective reaction time during driving (See Figure 3-23).

Based on *individual driving strategy* (e.g., keeping desired time headway), *Decision-making Component* determines an appropriate control for the vehicle with the information provided by the *Information Acquisition Component*. The system may also fail during decision-making stage. For example, information may be used incorrectly, for instance, accepting an insufficient gap for lane changes. Also errors in control selection (i.e., accelerating or decelerating) and usage can also cause system failure and result in collisions. In addition, personal factors, such as age, skill, emotion, fatigue, alcohol or drugs could influence the Decision-making Component (Figure 3-23).

Vehicle Mechanics Component

At decision making stage, longitudinal control decisions, translated in terms of acceleration pedal position, or braking pressure, are passed to *Vehicle Mechanics* component. The outputs of *Vehicle Mechanics* component are vehicle accelerations and speeds based on such control decisions. Finally, these outputs are feed-backed to the system again as situational factors. Figure 3-23 illustrated a detailed diagram of the proposed framework.

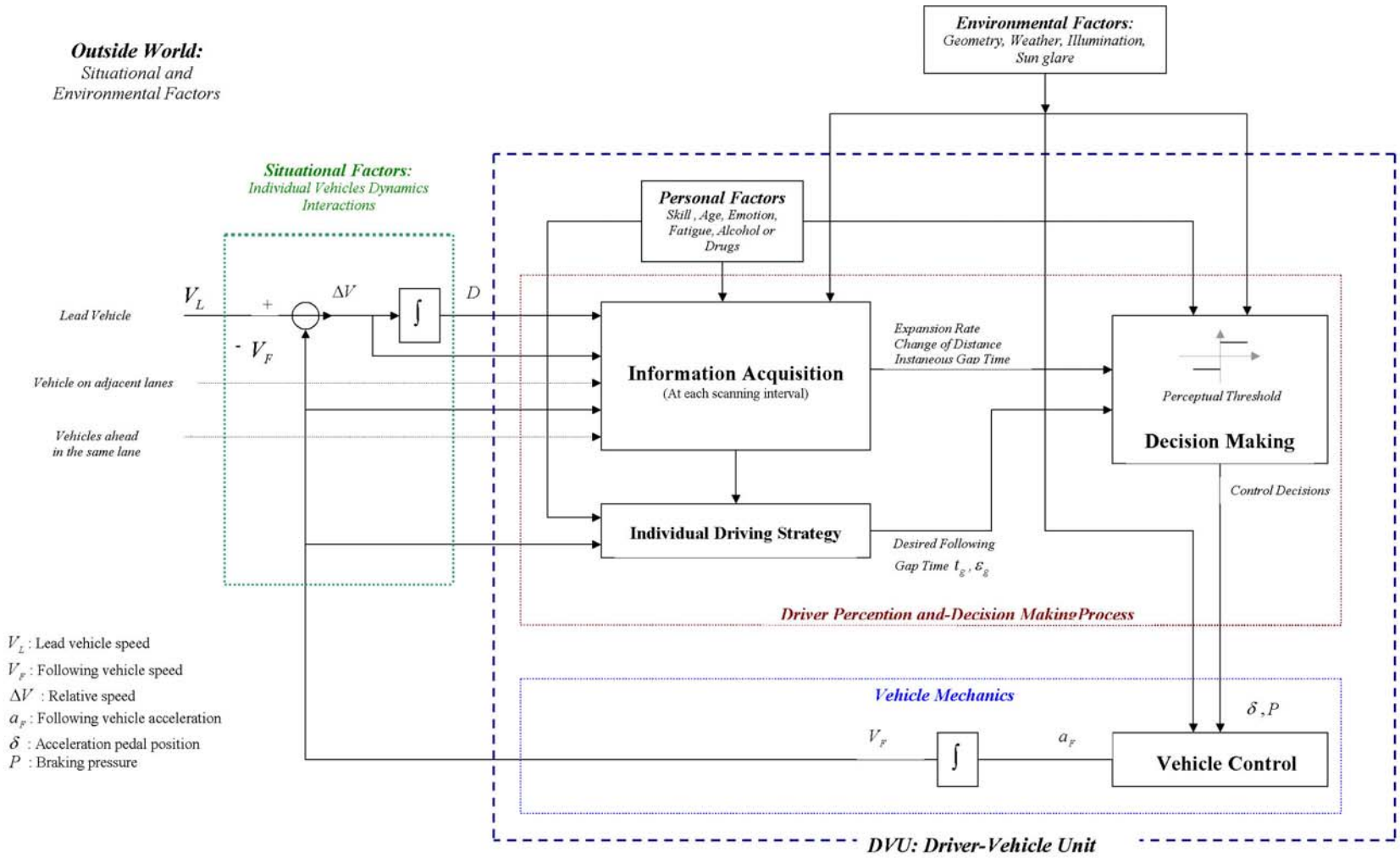

Figure 3-23. Detailed Block Diagram of Longitudinal Driving Task

3.2.4 Proposed Model

Assumptions and Hypothesis

A model is developed based on the proposed conceptual framework. At current stage of development, *situational factors* do not include multilane effects, while the impacts of *personal factors* and *environmental factors* on driver's perception-decision process are not explicitly incorporated in the model. It should be acknowledged that the proposed model is not a complete implementation of the proposed framework in its entirety, however, once experimental data and relevant research results from human factors or psychology studies become available, the model can be expanded to take into account these missing factors.

To be sure, the proposed model is essentially Gipps-like model while taking into account more realistic modeling of driver's perception-response process. Prior to elaborating on modeling details, it is worthwhile to preview some of the key assumptions or hypothesis employed in this model:

1) Each driver-vehicle-unit (DVU) has a *Desired Following Gap Time* t_g, which is the time headway he wishes to maintain while driving. However, due to human inability to keep exact following gap time, it is further assumed that a driver will allow an error of ε_g while maintaining his desired following gap time. This means, if the instantaneous gap time is within $[(1-\varepsilon_g)t_g, (1+\varepsilon_g)t_g]$, the driver would simply identify it with t_g.

2) Each DVU has a constant mechanical *response delay time* t_d. Note this *response delay time* t_d is part of driver's total *perception-response* time. This means, a driver has a fixed response delay time yet his perception time is variable depending on traffic situations such as relative speed and distance headway. This essentially results in a variable perception-response time that is time and traffic situation dependent.

3) When following a lead vehicle, it is very important for the following driver to perceive the relative motion and to take appropriate control actions to avoid collisions while still keeping up with the traffic (Hoffmann and Mortimer 1994). The visual stimulus to detect relative motion has been found to be related to a continuously changing optic array characterized by the visual angle θ subtended by the image of the lead vehicle on the retina, and the expansion rate $\dot{\theta}$ of this angle (Evans and Rothery 1974; Gibson 1982; Lee 1976; Lee and Reddish 1981; Michaels 1965; Michaels and Cozan 1963; Sun and Frost 1998). Mathematically, θ and $\dot{\theta}$ can be specified as (See Figure 3-24):

$$\tan(\frac{\theta}{2}) = \frac{W/2}{D(t)} \tag{0.0.28}$$

$$\frac{\sin(\theta)}{\dot{\theta}} = \frac{D(t)}{\Delta V} \tag{0.0.29}$$

where

θ : Visual angle subtended by the image of the lead vehicle on retina;

$\dot{\theta}$: Angular velocity, i.e., the expansion rate of θ ;

W : Vehicle width;

$D(t)$: Distance headway;

ΔV : Relative speed.

When θ is very small, Equation (0.0.28) and (0.0.29) can be approximated as:

$$\theta \approx \frac{W}{D} \tag{0.0.30}$$

$$\frac{\theta}{\dot{\theta}} = \frac{D(t)}{\Delta V} \tag{0.0.31}$$

Finally,

$$\dot{\theta} = W \frac{\Delta V}{D^2} \tag{0.0.32}$$

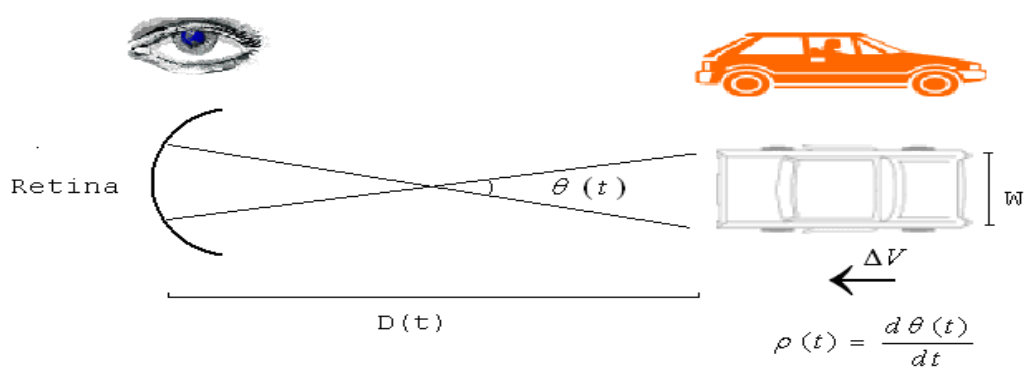

Figure 3-24. Visual Angle Subtended by the Image of an Object on the Retina and its Expansion Rate

In order to perceive relative motion, the angular velocity $\dot{\theta}$ must be above certain threshold value $C_{\dot{\theta}}$. This means, in order for a following driver to perceive relative velocity in relation to the preceding vehicle, $\frac{W \cdot |\Delta V|}{D^2} \geq C_{\dot{\theta}}$ must hold. A driver can not perceive relative motion when $\frac{W \cdot |\Delta V|}{D^2} < C_{\dot{\theta}}$, even if $|\Delta V| \neq 0$. Different values of this threshold have been reported in the literature ranging from 1~40 $\times 10^{-4} radian/\sec$ (Brackstone et al. 2000; Evans and Rothery 1973; Evans and Rothery 1977; Hoffmann 1968; Michaels and Cozan 1963; Wiedemann and U.Reiter 1970s).

Another visual cue that a driver uses to detect relative motion is *Just Noticeable Change (JNC) of Distance*. This is used to compensate the previous visual cue of expansion rate when the latter is below perception threshold. That is, when the expansion rate is below threshold, a driver can still perceive relative motion using *JNC* as a cue for detecting relative motion. This is expressed as:

$$|\frac{\Delta D}{D}| \geq C_D \qquad (0.0.33)$$

where ΔD is the accumulated change of distance headway, and D is initial distance headway, C_D is the *Change of Distance* threshold, commonly referred to as *Weber Ratio* in visual perception studies (Levinson 1998). For instance, when $\frac{W \cdot |\Delta V|}{D^2} < C_{\dot{\theta}}$ and $\Delta V < 0$, the following driver can not perceive relative motion using expansion rate as visual cue. However, since $\Delta V < 0$, he is continuously approaching lead vehicle with decreasing space headway D, thus at a certain point when the change of space headway ΔD becomes significant, i.e., $|\frac{\Delta D}{D}| \geq C_D$, the driver recognizes that he is approaching (slowly) to the lead vehicle.

In the proposed model, $C_{\dot{\theta}}$ and C_D are implemented based on the above logic. For each DUV, the threshold $C_{\dot{\theta}}$ and C_D are constant. However, these values are variable with different DVUs.

4) Driver inattention has been found to be one major contributing factor to rear-end collisions (Brown et al. 2000; Klauer et al. 2006; Senders et al. 1967; Sussman et al. 1985). In this study, this is modeled through a variable called *Scanning Interval*. This variable essentially is related to the frequency at which the driver samples traffic situation to his front view. Short scanning interval means the driver is alert to traffic dynamics thus can respond to any stimuli promptly, while long scanning interval means the driver is inattentive and might take long to react to changes of traffic states. Long scanning interval could be caused by allocation of visual focus to other views than direct front view, e.g., handling in-vehicle equipment, observing traffic in other lanes or looking at rear-view, or simply due to mind-idling (this is not uncommon during stop-and-go situation) .

Modeling Details

The proposed model follows the logic depicted in Figure 3-9. As is shown in this figure, DUV samples traffic information from its surrounding environment through ***Information Acquisition Component***, compiles sampled information to determine its current state, and compares with its desired state. This desired state is derived from ***Individual Driving Strategy Component***. Then a control decision is determined by ***Decision Making Component*** in terms of acceleration or deceleration to minimize any deviation between its current state and desired state. Finally, control decisions are implemented via ***Vehicle Mechanics Component*** after a mechanical response delay. These four components compose the proposed DUV model.

Information Acquisition Component (IAC)

The *Information Acquisition Component* (IAC) samples surrounding traffic environment every scanning interval. The inputs to this component include subject vehicle's instantaneous speed,

acceleration, preceding vehicle's speed and acceleration, and relative speed and distance headway between the subject vehicle and the preceding vehicle. IAC translates these inputs into three variables:

- *Visual Expansion Rate*
- *Change of Distance*
- *Instaneous Time Gap*

Visual Expansion Rate is computed as in Equation (0.0.32). *Change of Distance* is simply the difference between current distance headway and the distance headway at previous scanning interval. *Instaneous Time Gap* is derived by dividing current distance headway by subject vehicle's instaneous speed.

Driving Strategy Component (DSC)

As mentioned earlier, the driving strategy is to maintain a desired following gap time t_g subject to safety constraints. Due to human driver's inability to keep exact following gap time, it is further assumed that a driver will allow an error of ε_g while maintaining his desired following gap time. This means, if the instantaneous gap time is within $[(1-\varepsilon_g)t_g, (1+\varepsilon_g)t_g]$, the driver would simply identify it with t_g.

Decision Making Component (DMC)

Decision Making Component (DMC) determines an appropriate control maneuver (acceleration or deceleration or cruising) based on the information from *Information Acquisition Component* and *Individual Driving Strategy Component.* Specifically, at each scanning interval, DMC does the following Boolean checking:

1) True or false: Visual Angle Expansion Rate exceeds the threshold $C_{\dot{\theta}}$
2) True or false: Change of Distance exceeds the threshold C_D
3) True or False: Subject DUV is driving with its gap time outside of

$$[(1-\varepsilon_g)t_g, (1+\varepsilon_g)t_g]$$

If all of the three checking result "false", then the DUV is in a "subconscious" driving state without motivation for either accelerating or decelerating. This is because in this state, the driver is unable to perceive any relative motion (all perception thresholds not exceeded) while he is driving with a comfortable following gap time thus there is no need to accelerate to catch up with preceding vehicle or decelerate to avoid a looming collision. However, small displacements of gas pedal, wind or pavement friction could still effect an actual small acceleration or deceleration for the subject vehicle. Usually this rate is in the range of 0.5~0.8 ft/s^2 (Brackstone et al. 2000; Brackstone et al. 2002; McDonald et al. 1997; Sultan et al. 2004; Wang 2005). In this study, it is termed as *Oscillation Acceleration/Deceleration Rate* because except the preceding vehicle changes its speed drastically, the subject vehicle would keep employing this small rate until its perceptual threshold is exceeded and then the subject vehicle will reverse the sign of the acceleration rate until the perceptual threshold is exceeded again. To clarify this further, a typical real-life scenario is presented next.

Consider a preceding vehicle moving at constant speed while a following vehicle is catching up with it trying to maintain a desired following gap time subject to safety constraints. During certain time period, the relative speeds between these two vehicles are below perception threshold of the following driver thus the latter cannot perceive any relative motion between these two vehicles. He applies *Oscillation Acceleration Rate* "subconsciously" while closing in to the preceding vehicle until perceptual thresholds are exceeded either by expansion rate or by change of distance. The following driver then applies Oscillation Deceleration Rate and this time he is opening from the preceding vehicle until the perceptual thresholds are exceeded again. The closing and opening process keeps going on until the preceding vehicle changes its speeds drastically.

When neither of the above checking results "true", Gipps-like car following rules are used:

$$v_n(t+t_g) = \min\{v_n^a(t+t_g), v_n^b(t+t_g)\} \tag{0.0.34}$$

$$v_n^a(t+t_g) = v_n(t) + 2.5a_n t_g[1-\frac{v_n(t)}{V_n^{\max}}]\sqrt{0.025+\frac{v_n(t)}{V_n^{\max}}} \tag{0.0.35}$$

$$v_n^b(t+t_g) = -t_g b_n + \sqrt{t_g{}^2 b_n^2 + b_n\{2[x_{n-1}(t)-x_n(t)-s_0)]-t_g v_n(t)+\frac{v^2{}_{n-1}(t)}{\hat{b}_{n-1}}}\} \tag{0.0.36}$$

where

t_g is the driver's *desired following gap time;*

a_n is the maximum comfortable acceleration rate for vehicle n;

b_n is the maximum comfortable braking rate for vehicle n;

x_n, x_{n-1} are the position of vehicle n and n-1, respectively;

$\hat{b}_{n-1}$ is nth driver's estimation for $(n-1)th$ vehicle maximum comfortable braking rate;

V_n is the desired free flow speed of vehicle *n;*

s_0 is the distance headway at standstill.

Essentially Equation (0.0.34)(0.0.35)(0.0.36) reflects the speed the subject driver wishes to achieve within his desired following gap time. In these equations, t_g is added as time delay rendering the process a time-delay process. This is different from original Gipps car-following rules which use driver's reaction time as the time delay term. Moreover, t_g *in* Equation (0.0.34)(0.0.35)(0.0.36) should not be interpreted as driver's reaction time; rather it represents a relaxation time during which the driver *wishes* to relax his current speed to a safe speed in order to catch up with preceding vehicle while avoiding a potential collision. This actually characterizes aggressiveness, or safety potential of the subject driver.

Vehicle Mechanics Component (VMC)
A suitable acceleration or deceleration rate determined by *Decision Making Component* (DMC) will be implemented by *Vehicle Mechanics Component* after a mechanical response delay t_d .

3.3 Model Calibration and Validation

3.3.1 Calibration Methodology

The proposed model has the following calibrable parameters:

1) Maximum Comfortable Acceleration (ft/s^2) a_n
2) Maximum Comfortable Deceleration (ft/s^2) b_n
3) Oscillation Acceleration Rate (ft/s^2) a_{osc}
4) Oscillation Deceleration Rate (ft/s^2) b_{osc}
5) Desired Following Gap Time (sec) t_g
6) Error of Desired Following Gap Time ε_g
7) Scanning Interval (sec) t_{scan}
8) Mechanical Response Delay (sec) t_d
9) Perceptual Threshold of Visual Expansion Rate (radian/sec) $C_{\dot{\theta}}$
10) Weber Ratio C_D

As pointed out earlier, all of these parameters have direct behavioral connection or realistic physical meanings. In this study, these parameters are calibrated using least square fitting approach. This can be formulated as the following optimization problem:

$$\begin{aligned}
&\min \sum_{i=1}^{N} (x_i - y_i)^2 \\
&s.t. \\
&a_n^{lb} \le a_n \le a_n^{ub} \\
&b_n^{lb} \le b_n \le b_n^{ub} \\
&a_{osc}^{lb} \le a_{osc} \le a_{osc}^{ub} \\
&b_{osc}^{lb} \le b_n \le b_{osc}^{ub} \\
&\varepsilon_g^{lb} \le \varepsilon_g \le \varepsilon_g^{ub} \\
&t_g^{lb} \le t_g \le t_g^{ub} \\
&t_{scan}^{lb} \le t_{scan} \le t_{scan}^{ub} \\
&t_d^{lb} \le t_d \le t_d^{ub} \\
&C_{\dot{\theta}}^{lb} \le C_{\dot{\theta}} \le C_{\dot{\theta}}^{ub} \\
&C_D^{lb} \le C_D \le C_D^{ub}
\end{aligned} \tag{0.0.37}$$

where, x_i is the model predicted value whereas y_i is the actual trajectory observation indexed by i. The left-hand side and right-hand side constants of each constraint inequality correspond to the feasible lower-bound and upper-bound values of the respective. As indicated in this formulation, the objective function is the squared sum of residuals between the real-life trajectory and the model generated trajectory. Also the feasible region of parameter space is constrained with the lower-bound and upper-bound of each parameter determined from physical limits. For example, a feasible range for *Maximum Comfortable Acceleration* would be around -11 ft/s^2 (ITE 1999). Essentially this renders a *NP*-hard non-linear (also non-convex) constrained optimization problem. *Generalized Reduced Gradient* method(Pike 1986) is used for searching best parameters. Also, in order to get global optimal parameters instead of getting trapped with local minima, multi-start searching is employed. It is worthwhile to point out that other techniques, e.g., Generic Algorithm, or Neural Network are also feasible alternatives for calibrating parameters. However, the advantage of employing least-square minimization approach is that calibrated parameters would be the *maximum likelihood estimator* if the modeling error is identically and independently normal distributed (Gallant 1987). This is a common assumption both in the literature and in practice.

3.3.2 Validation Methodology

Measures of Effectiveness

The purpose of validation is to test the model's capability of replicating real-life scenarios with calibrated parameters. Essentially this involves comparing model generated vehicle trajectories to real-life trajectories using calibrated parameters. The following metrics are used to evaluate the deviation between model generated trajectories and real-life trajectories.

1) Root Mean Square Error (RMSE)
2)

$$RMSE = \sqrt{\frac{1}{n}\sum_{i=1}^{n}\left(x_i - y_i\right)^2} \qquad (0.0.38)$$

where

x_i is the model predicted value indexed by *i;*
y_i is the actual observation indexed by *i;*
n is the number of total observations.

3) Mean Percentage Error (MPE)
4)

$$MPE = \frac{1}{n}\sum_{i=1}^{n}\frac{|y_i - x_i|}{x_i} \qquad (0.0.39)$$

Validation against Non-Crash Data

The test track RTKGPS car-following data are used to validate the model against normal car-following behavior. This is accomplished by calibrating each DUV using only part of its real-life trajectory but validating it using the entire trajectory in full length. For example a DUV in the platoon has 15 minute-long trajectory at 0.1 sec resolution. One-minute data out of this entire 15

minutes trajectory is used to calibrate the DUV, and then the entire 15 minutes trajectory is used to validate the model.

Validation against Crash Data

Validation against crash data is accomplished by testing if the model can generate the crash event by collective simulation. This means, each DUV is calibrated individually using its preceding vehicle's real trajectory as the input; then all DUVs that involved in a crash (usually 5~6 vehicles with the last two directly crashing each other) are *simulated collectively* with only the platoon leader using real-life trajectory as the predefined input to the platoon as a whole. Other vehicles in the platoon are simply updated sequentially according to the proposed car-following rules. If the crash event can be generated as occurred in reality, then the validity of the model is verified.

3.4 Stability Analysis Methodology

Stability shows the recovery characteristics of car-following vehicles from a disturbance. Therefore, it is an indication of collision potential for a given traffic situation. Due to the nature of the proposed model, it is infeasible to carry out stability analysis analytically; rather it is accomplished through designed experimental tests. Specifically, two types of traffic disturbances were exerted to the leader of a platoon of 15 vehicles in order to analyze the stability and performance of the proposed model:

1) The platoon leader slowed down from 80 ft/s to 40 ft/s at a rate of -8 ft/s^2 due to a cut-in vehicle in front. This disturbance lasted 5s and the leader resumed its before-disturbance speed of 90 ft/s at 6 ft/s^2. This scenario represents a mild traffic disturbance;
2) The platoon leader came to a stop at an emergency deceleration rate of -16 ft/s^2 from 80 ft/s due to a queue backing up. The platoon leader also experienced a stop-and-go condition before the queue started clearing up. This scenario represents a severe traffic disturbance.

The speed profiles of the platoon leaders corresponding to these disturbances are given in Figure 3-25.

Note due to time limitations, the proposed stability test will not be performed but only listed here as necessary tasks for next phase research.

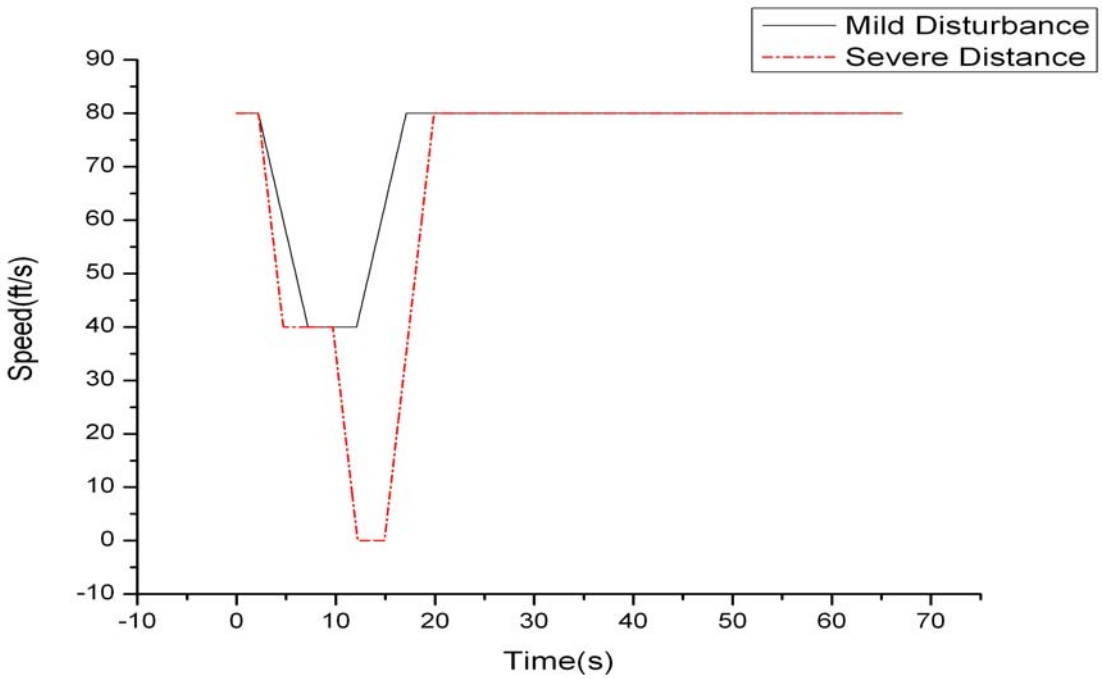

Figure 3-25. Speed Profiles of Platoon Leader Used in Mild and Severe Disturbance Scenarios

4 IMPLEMENTATION

4.1 Environment

In order to facilitate model calibration and testing, two programs were developed in this study. One is the CalibWizard program for automating parameter calibrations, whereas the other is the wxSim program for validating the proposed car-following model. Snapshots of these two programs are depicted in Figure 4-1 and Figure 4-2.

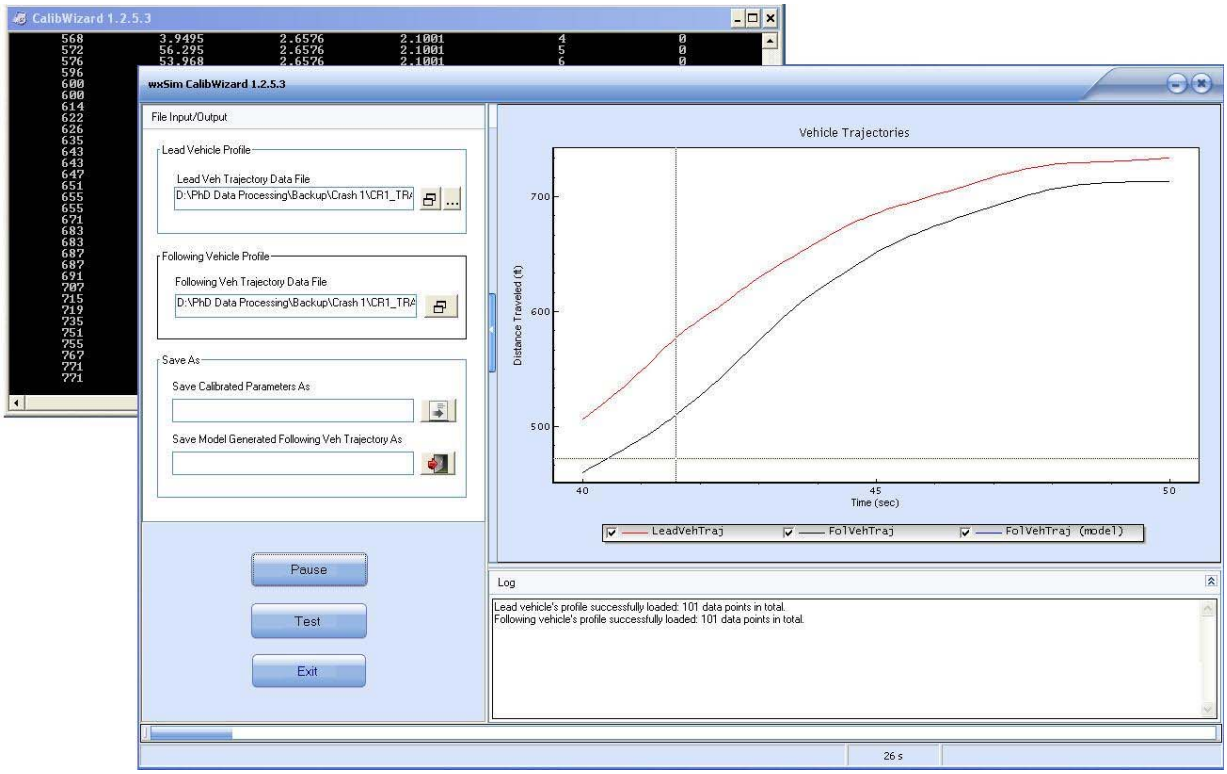

Figure 4-1. Snapshot of the CalibWizard Program Developed for Automating Parameter Calibration

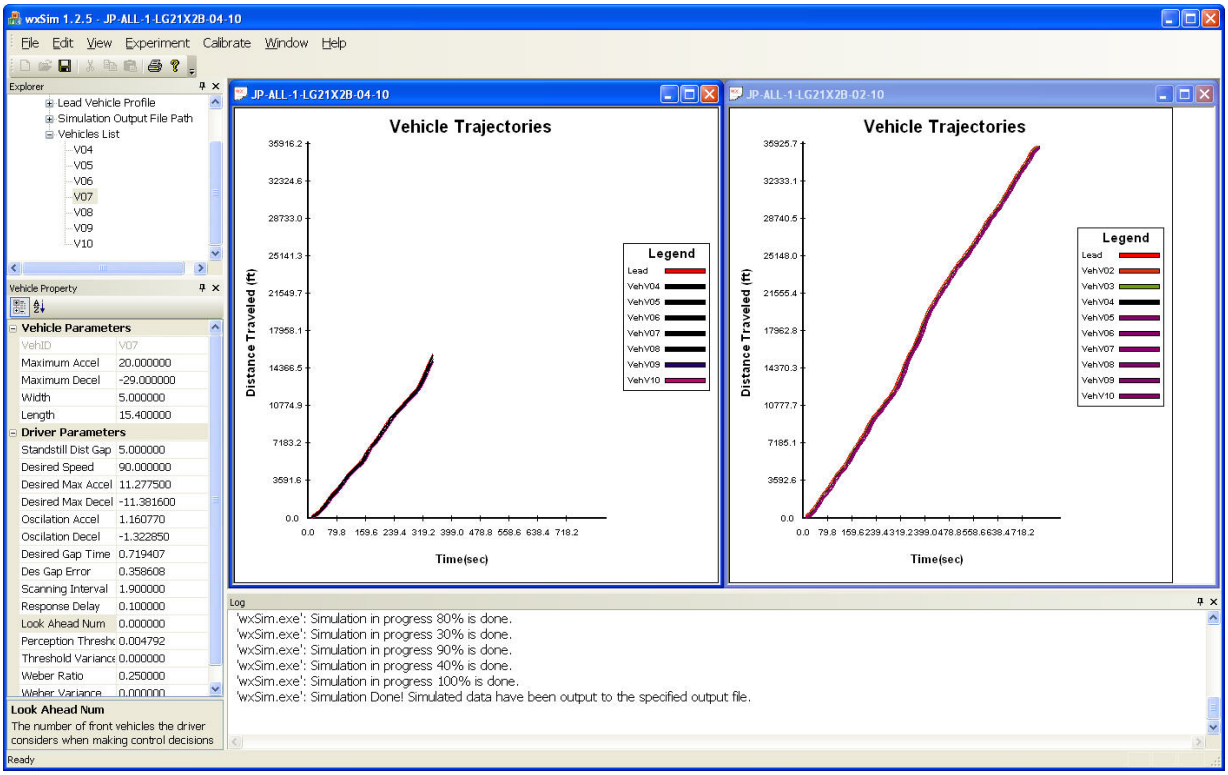

Figure 4-2. Snapshot of the wxSim Program Developed for Testing the Proposed Car-Following Program

CalibWizard Program

The CalibWizard program is developed in C++ using *Borland Visual Component Library* (VCL). This program implements the calibration methodology proposed in Section 3.3.1. The purpose of the CalibWizard program is to automate parameter calibrations for the proposed model. The inputs required by this program are trajectories of a lead vehicle and a following vehicle. Also CalibWizard program allows the user to specify the feasible region of parameters prior to running the program. Figure 4-3 shows the user interface for setting up upper-bound and lower-bound of each parameter. The output of this program is calibrated parameters, i.e., the optimal parameters minimizing the objective function as specified in Equation(0.0.37). Figure 4-4 illustrates a sample of calibration results. In this figure, the red line and black line are trajectories of the lead and the following vehicle respectively, while the blue line is the model predicted trajectory for the following vehicle after calibration. As shown in this figure, with calibrated parameters the black line and blue line matches well. This means the model can predict car-following behavior well after the calibration.

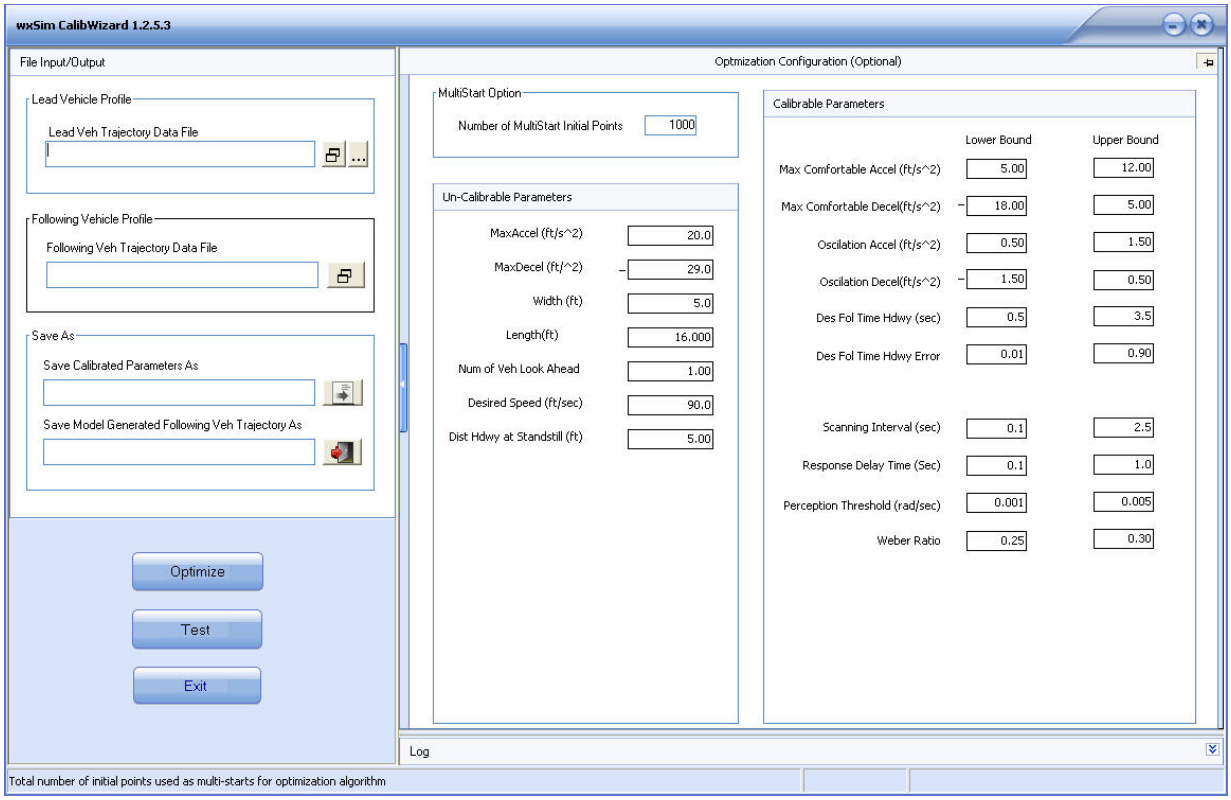

Figure 4-3. CalibWizard User Interface for Setting up Parameters Feasible Region

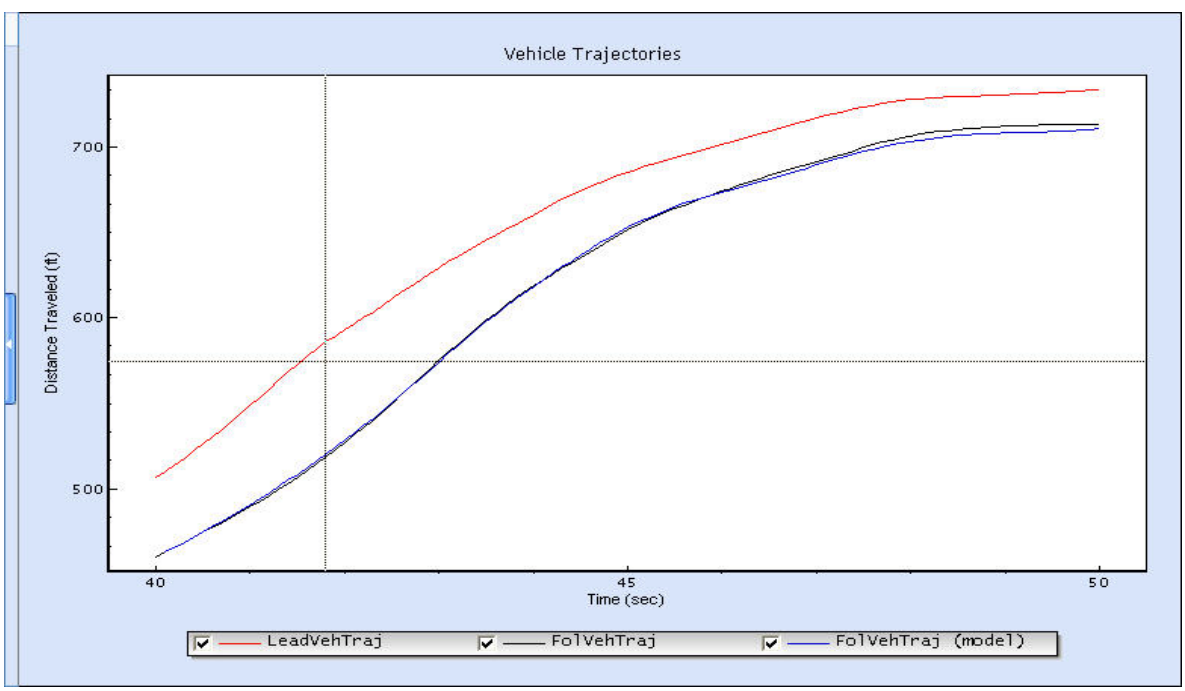

Figure 4-4. Calibration Results

wxSim Program

The wxSim program is developed in C++ using *Microsoft Foundation Class (MFC)* library. The purpose of the wxSim program is to provide a test-bed for testing the proposed car-following model. In other words, this program can be viewed as a "mini-simulator" that implements the proposed car-following model. Specifically, wxSim can simulate single-lane car-following dynamics for a platoon of vehicles. The inputs required by this program are the predefined trajectory of the platoon leader, and vehicle parameters for the following vehicles. The output of this program is the position, speed, and acceleration information at 0.1 second resolution for every vehicle in the platoon. Figure 4-5 shows the user interface when loading vehicle parameters. As shown in this figure, wxSim can load an existing parameter file that is generated by the CalibWizard program.

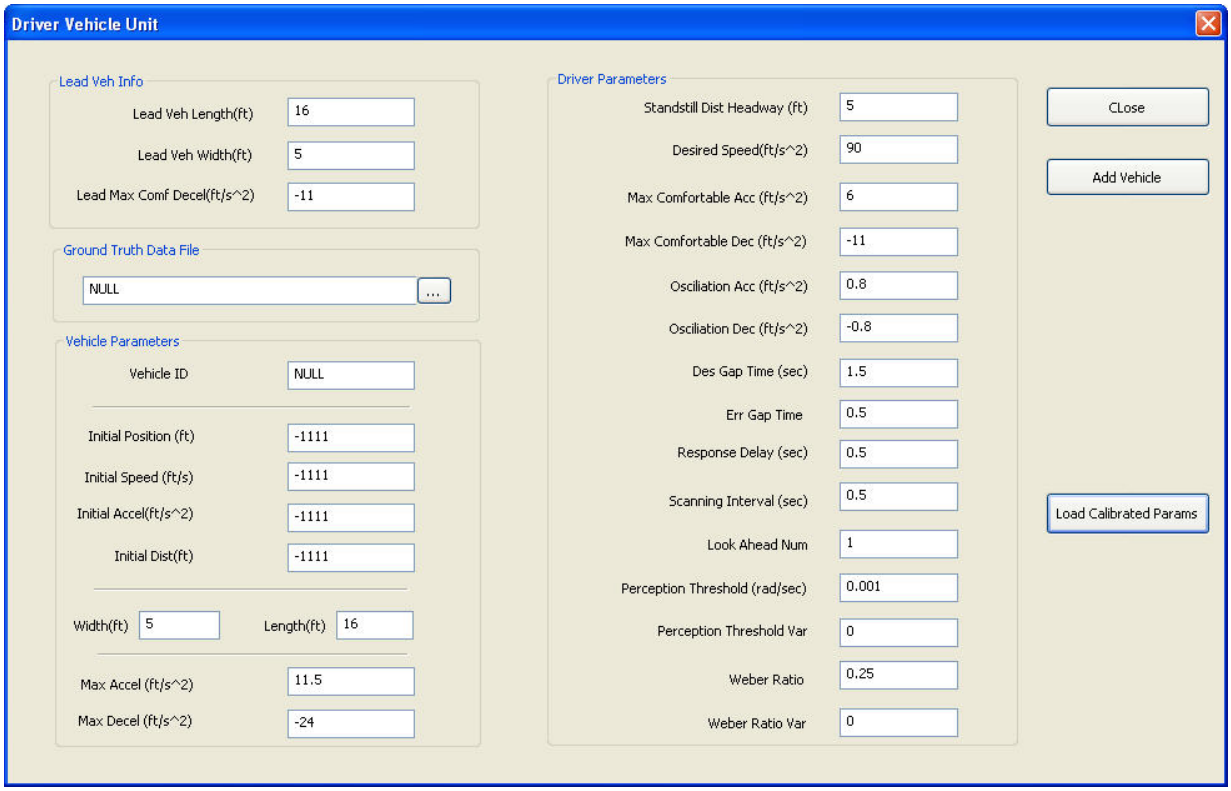

Figure 4-5. wxSim Loading Vehicle User Interface

4.2 Model Calibration and Validation Using Non-Crash Data

As mentioned earlier, the proposed model is calibrated and validated using both non-crash and crash data. In this section, the calibration and validation results using non-crash data are summarized. These data were collected using 10 test vehicles on a test track by University Hokkaido. Table 4-1 summarized the calibrated parameters for the following vehicles, i.e., this table includes 9 vehicles indexed from G02 to G10 that followed the platoon leader G01. As indicated in this table, the maximum comfortable acceleration rates range from 6.017 ft/sec^2 to 11.74 ft/sec^2, while maximum deceleration rates range from -7.95 ft/sec^2 to -21.4175 ft/sec^2. These values are consistent with real life physical constraints. Also the scanning interval ranges

from 0.1 second up to 1.9 second, characterizing the drivers' attention level with in the range of 1.8 seconds. Meanwhile the Weber Ratio coefficient appears uniform across driver with every driver has the same value of 0.25.

Table 4-1. Calibrated Parameters for the Following Vehicles in the Platoon (RTKGPS Data)

Param / VehID	a_n (ft/s^2)	b_n (ft/s^2)	a_{osc} (ft/s^2)	b_{osc} (ft/s^2)	t_g (sec)	ε_g	t_{scan} (sec)	t_d (sec)	$C_{\dot{\theta}}$ (rad/s)	C_D
G02	6.67013	-15.794	0.59168	-0.7858	1.26694	0.552616	1.2	0.2	0.004595	0.25
G03	8.42013	-21.4175	0.75521	-0.7552	1.95112	0.839229	1.9	0.3	0.003431	0.25
G04	7.0303	-12.1011	0.5095	-0.8136	1.25268	0.525128	0.6	0.1	0.004194	0.25
G05	11.1362	-7.95936	1.87943	-0.8792	0.234430	0.117432	0.8	0.2	0.003508	0.25
G06	11.7485	-14.7678	1.96256	-0.6328	1.65379	0.293513	1.2	0.1	0.004740	0.25
G07	11.3775	-17.6075	0.65737	-1.1163	1.21169	0.843909	0.3	0.3	0.004655	0.25
G08	6.01744	-17.3094	0.59419	-0.5977	1.34166	0.885887	0.1	0.1	0.004855	0.25
G09	11.5781	-15.6733	0.92256	-0.8127	1.62736	0.225286	1.1	0.1	0.004320	0.25
G10	11.3261	-14.1512	0.95337	-1.1093	1.04655	0.427004	0.7	0.1	0.003612	0.25

Figure 4-6 depicts the distribution of scanning intervals across the drivers. From this figure it is shown that different driver has different scanning interval while the maximum and minimum values being 1.9 second and 0.1 second respectively.

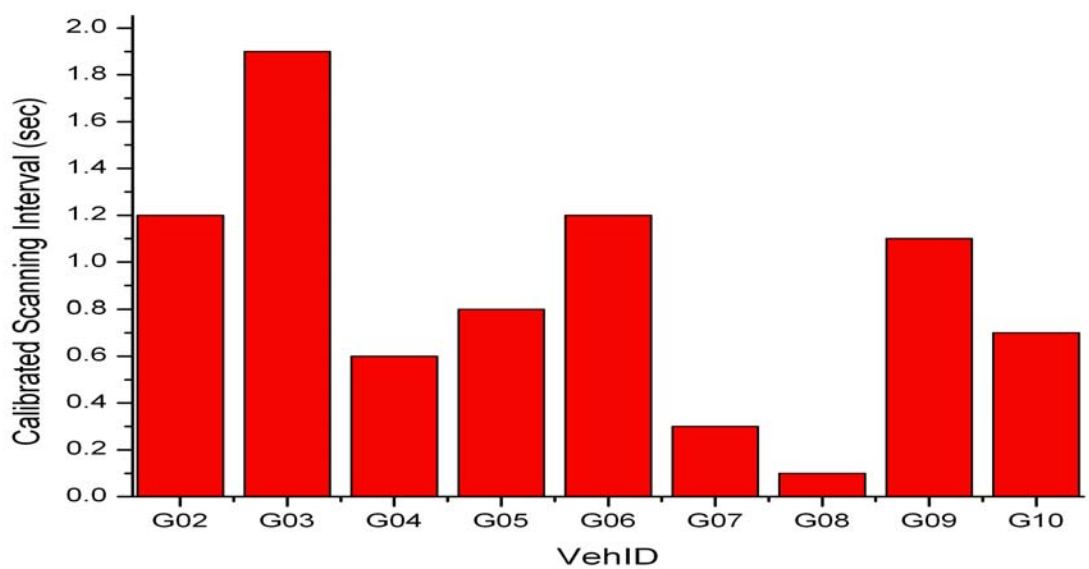

Figure 4-6. Calibrated Scanning Intervals

Table 4-2 specifically shows the statistics for the calibrated parameters. To be sure, this table includes the following statistics:

- *Mean ($\bar{X}$)*
- *Standard Deviation (SD)*
- *Standard Error of the Mean (SEM)*
- *25% Percentile*
- *75% Percentile*
- *Inter Quartile Range (IQR) (i.e., the difference between 25% and 75% percentile)*
- *Maximum*
- *Minimum*
- *Range*
- *Median*
- *Variance*
- *Coefficient of Variance (CV)*
- *Kurtosis*

Particularly, the standard deviation (SD) is calculated as $SD = \sqrt{Var}$, where $Var = \frac{1}{n-1}\sum_{i=1}^{n}(X_i - \bar{X})^2$, n is the sample size and $\bar{X}$ is the mean. The standard error of the mean (SEM) is calculated as $SEM = \frac{SD}{\sqrt{n}}$. Further, the coefficient of variance (CV) is calculated as $CV = \frac{SD}{\bar{X}}$.

Moreover, *kurtosis* is the measure for describing the degree of peakedness of a distribution, defined as a normalized form of the fourth central moment μ_4 of a distribution. This statistics is employed here to indicate if the underlying distributions for these parameters are similar to normal distribution. This means, if the *kurtosis* of a distribution is 0, this distribution has similar peakedness as normal distribution. On the other hand, positive *kurtosis* indicates relatively high peak (and called leptokurtic), while negative *kurtosis* suggests a relatively flat-topped curve (called platykurtic), in comparison to normal distribution.

Table 4-2 presents detailed statistics for the calibrated parameters. As shown in this table, maximum comfortable acceleration rate (a_n), oscillation deceleration rate (b_{osc}), error in keeping desired following gap time (ε_g), mechanical delay (t_d) and visual angle expansion rate threshold ($C_{\dot{\theta}}$), have negative kurtosis. This means the underlying distribution of these parameters are relatively flat-topped when compared to normal distribution. Likewise, other parameters have positive kurtosis, meaning the underlying distributions of those parameters are relatively peaked.

Validation results are summarized in Table 4-3 and Table 4-4. In Table 4-3, the platoon leader is vehicle G01 (actual leader), while in Table 4-4, the platoon leader is assumed to be vehicle G03. Figure 4-7 (a) illustrated the validation results with G01 as lead vehicle. Figure 4-7(b) illustrates the validations with G03 as lead vehicle. As indicated in these figures, when using G01 as lead

vehicle, the proposed model appears insufficient to replicate trajectories of the following vehicles. Specifically, after vehicle G03 (see Figure 4-7(a)), the deviations between ground-truth trajectories and model-predicted trajectories become significant. This prompted using G03 as lead vehicle to further examine the proposed model (see Figure 4-7(b)). Figure 4-7(b) and the statistics in Table 4-4 clearly indicate that the proposed can replicate vehicle trajectories to a high accuracy. This suggests that the raw trajectories assumed to be ground-truth contain certain errors that affected the model outputs. Overall, as shown in Figure 4-7(b) and Table 4-4, the proposed model is capable of replicating non-crash car-following situations accurately.

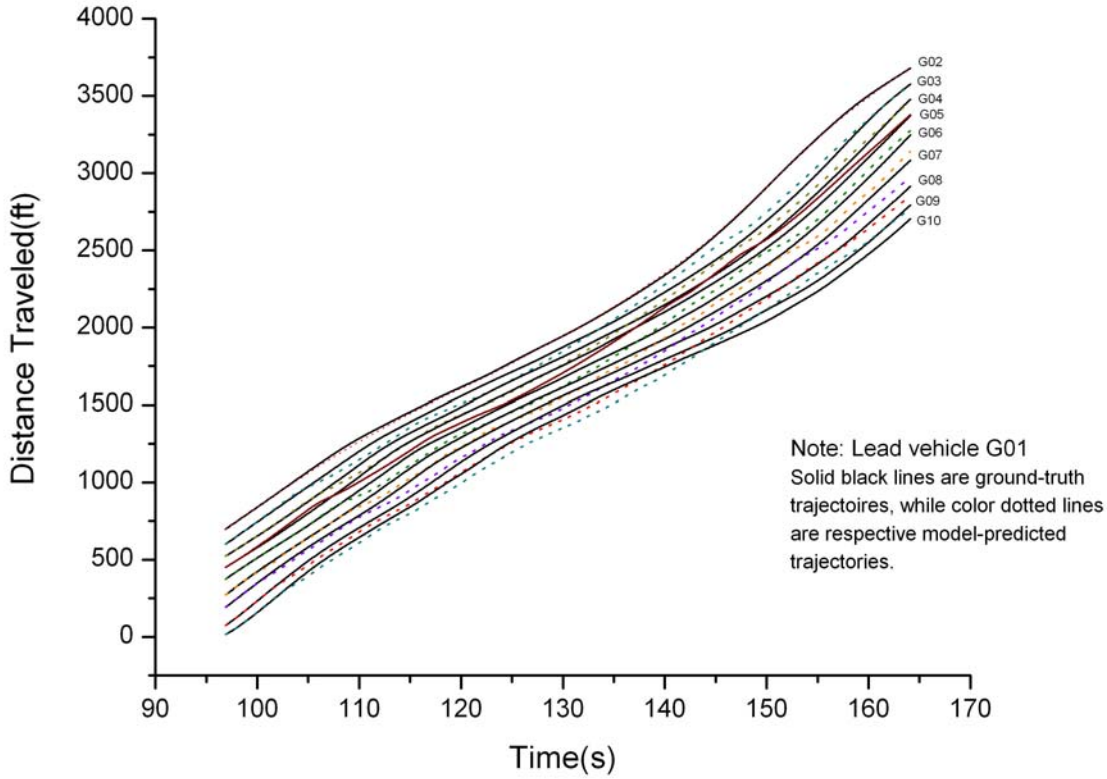

Figure 4-7 (a). Validation Results (Lead Vehicle G01 not Shown in the Figure)

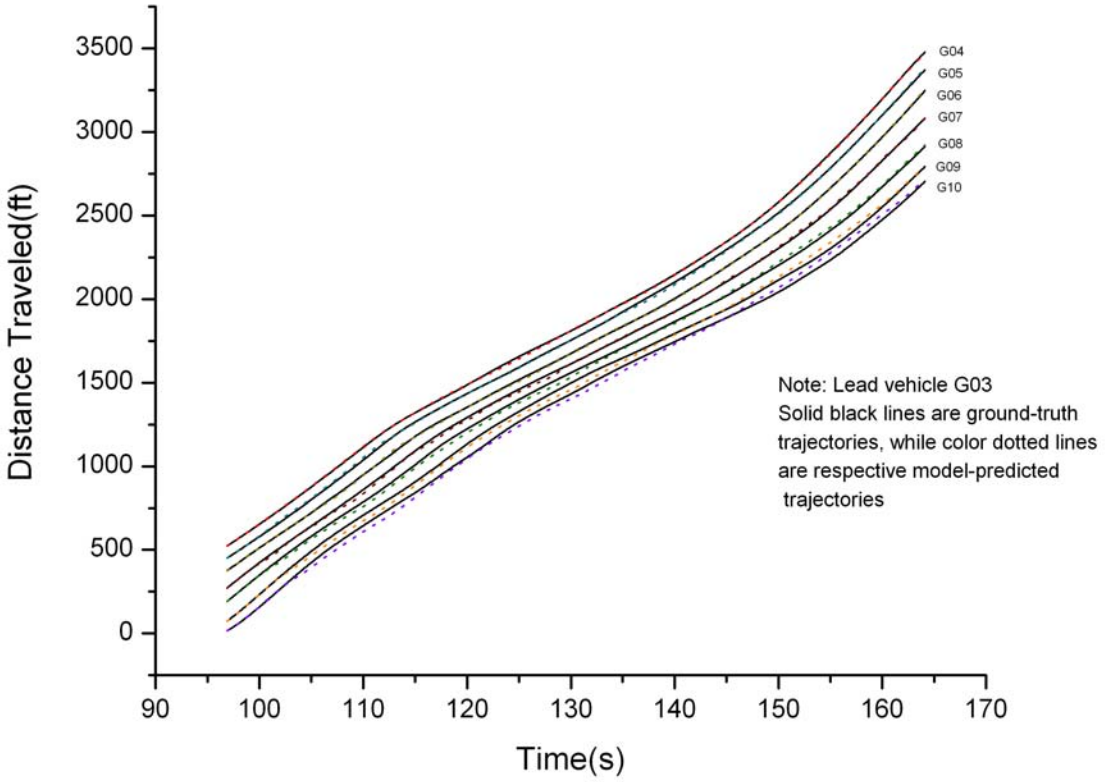

Figure 4-7 (b). Validation Results (Lead Vehicle is G03 not Shown in the Figure)

Figure 4-8 and Figure 4-9 illustrate the model-predicted speed profile vs. real speed profile for each individual vehicle in the platoon. Figure 4-8 shows the situation with G01 as platoon leader, while Figure 4-9 depicts the situation with G03 as platoon leader. As shown in these figures, the proposed model is accurate not only in replicating vehicle trajectories but also speed profiles over time.

Table 4-2. Statistics of Calibrated Parameters for Non-Crash Data (RTKGPS Data): Sample Size 9

Parameters \ Statistics	Mean	Standard Deviation	Standard Error of the Mean	25% Percentile	75% Percentile	Inter-Quartile Range	Minimum	Maximum	Range	Median	Variance	Coefficient of Variance	Kurtosis
Max Comft Accel a_n	9.47927	2.40595	0.80198	7.0303	11.3775	4.3472	6.01744	11.7485	5.73106	11.1362	5.78859	0.25384	-2.00512
Max Comft Decel b_n	-15.19791	3.75494	1.25165	-17.3094	-14.1512	3.1582	-21.4175	-7.95936	13.45815	-15.6733	14.09957	-0.24707	1.34193
Osc Accel a_{osc}	0.98065	0.55385	0.18462	0.59419	0.95337	0.35918	0.5095	1.96256	1.45306	0.75521	0.30675	0.56478	0.23958
Osc Decel b_{osc}	-0.83362	0.1814	0.06047	-0.8792	-0.7552	0.124	-1.1163	-0.5977	0.5186	-0.8127	0.03291	-0.2176	-0.38262
Desired Fol Gap t_g	1.28736	0.48314	0.16105	1.21169	1.62736	0.41567	0.23443	1.95112	1.71669	1.26694	0.23342	0.3753	2.59624
Gap Error ε_g	0.52333	0.28516	0.09505	0.29351	0.83923	0.54572	0.11743	0.88589	0.76846	0.52513	0.08132	0.5449	-1.50472
Scanning Interval t_{scan}	0.87778	0.54263	0.18088	0.6	1.2	0.6	0.1	1.9	1.8	0.8	0.29444	0.61818	0.37272
Mechnical Delay t_d	0.16667	0.0866	0.02887	0.1	0.2	0.1	0.1	0.3	0.2	0.1	0.0075	0.51962	-1.07937
Expansion Rate Thres $C_{\dot{\theta}}$	0.00421	5.6044E-4	1.8681E-4	0.00361	0.00466	0.00104	0.00343	0.00485	0.00142	0.00432	3.1409E-7	0.13305	-1.70277

Table 4-3. Validation Statistics (G01 is Platoon Leader)

Error Measure \ VehID		G02	G03	G04	G05	G06	G07	G08	G09	G10
Trajectory Profile (ft)	Mean Squared Error	56.0363	91.1307	50.05	61.81	73.8254	68.1181	81.09	83.30	84.03
	Mean Percentile Error	0.2%	0.4%	0.23%	0.29%	0.34%	0.31%	0.38%	0.38%	0.38%
Speed Profile (ft/s^2)	Mean Squared Error	2.69	6.11	6.29	6.77	8.607	9.38	6.89	7.31	7.938
	Mean Percentile Error	4.8%	10.5%	10.7%	11.7%	14.5%	16.6%	12.1%	12.7%	13.9%

Table 4-4. Validation Statistics (G03 is Platoon Leader)

Error Measure \ VehID		G02	G03	G04	G05	G06	G07	G08	G09	G10
Trajectory Profile (ft)	Mean Squared Error			84.102	71.2907	70.77	88.73	58.636	75.33	90.12706
	Mean Percentile Error			0.43%	0.33%	0.32%	0.43%	0.27%	0.34%	0.40
Speed Profile (ft/s^2)	Mean Squared Error			3.07	4.15	5.61	7.25	4.8	5.8	6.475
	Mean Percentile Error			5%	6.8%	9.2%	12.7%	8.3%	10.2%	11.1%

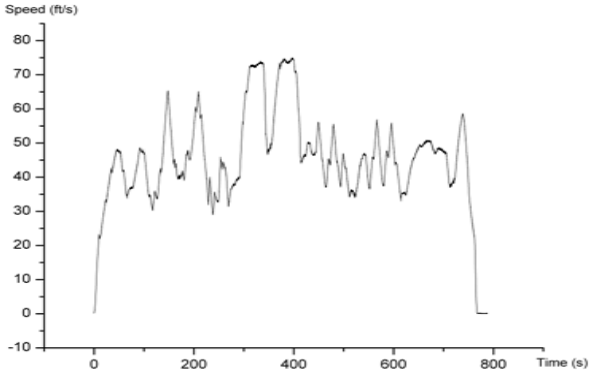

Figure 4-8 (a). Lead Vehicle (G01) Speed Profile

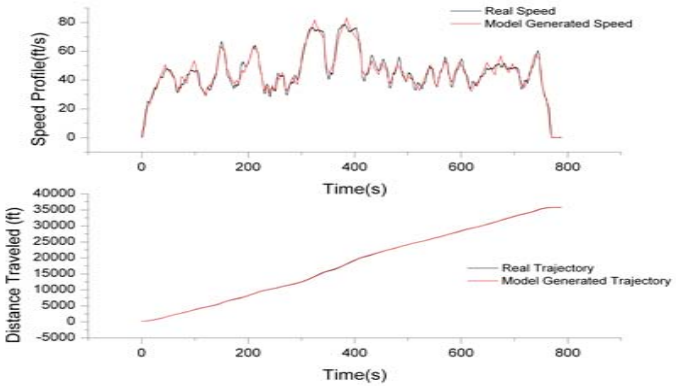

Figure 4-8 (b). Veh G02 Speed and Trajectory Profile: Real vs. Simulated

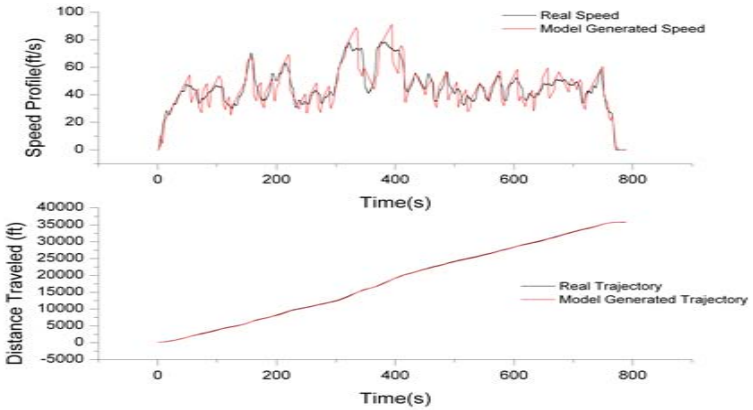

Figure 4-8 (c). Veh G03 Speed and Trajectory Profile: Real vs. Simulated

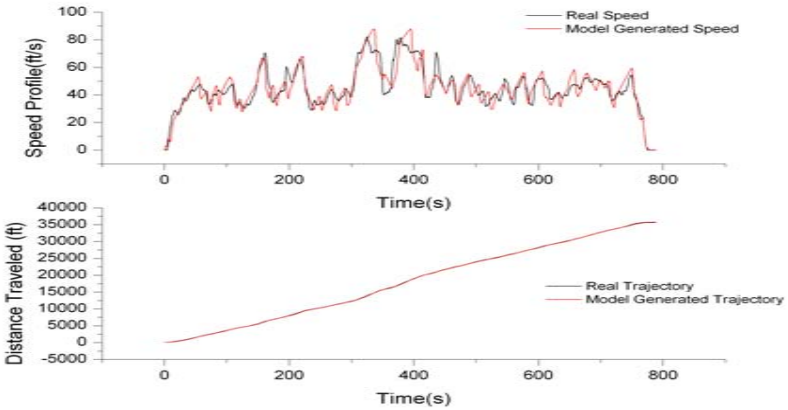

Figure 4-8 (d). Veh G04 Speed and Trajectory Profile: Real vs. Simulated

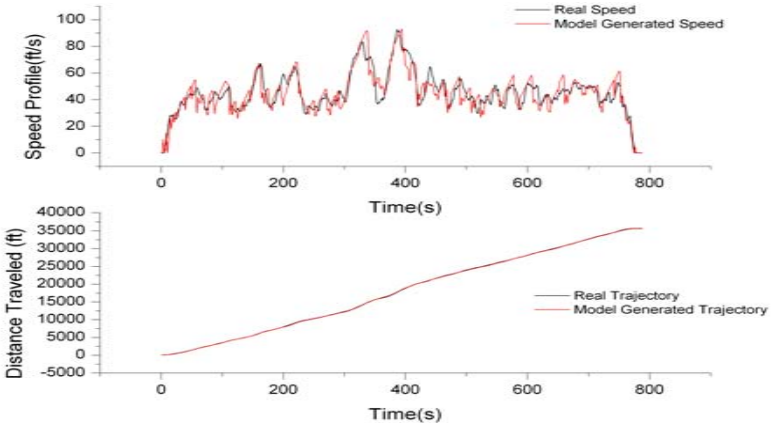

Figure 4-8 (e). Veh G05 Speed and Trajectory Profile: Real vs. Simulated

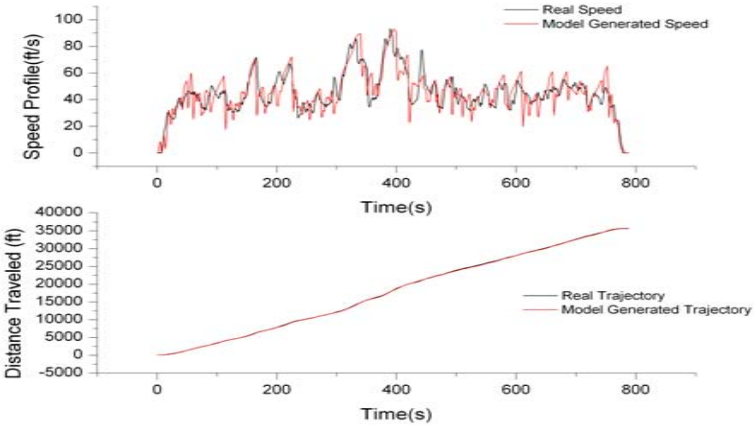

Figure 4-8 (f). Veh G06 Speed and Trajectory Profile: Real vs. Simulated

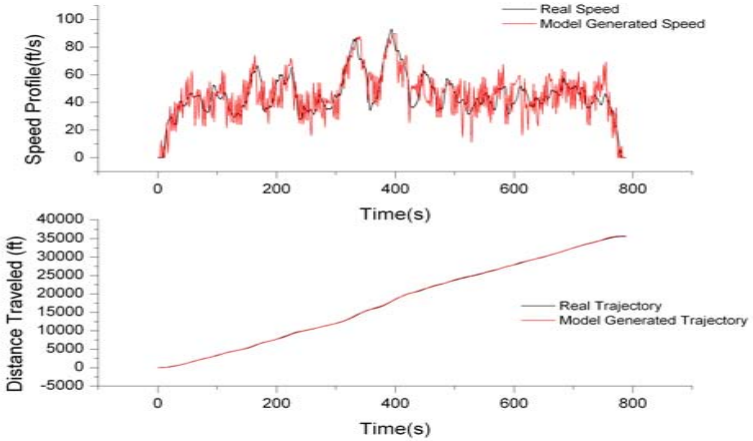

Figure 4-8 (g). Veh G07 Speed and Trajectory Profile: Real vs. Simulated

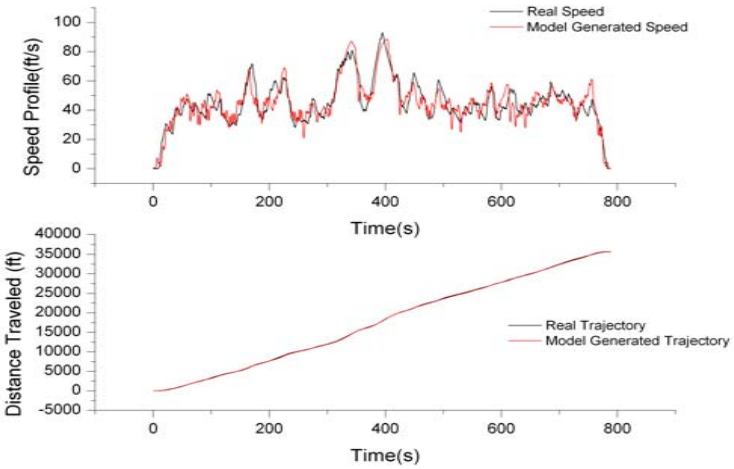

Figure 4-8 (h). Veh G08 Speed and Trajectory Profile: Real vs. Simulated

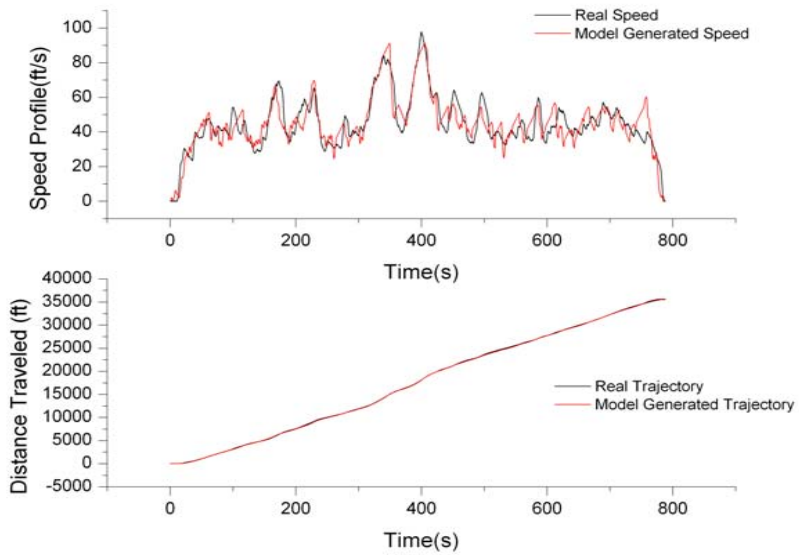

Figure 4-8 (i). Veh G09 Speed and Trajectory Profile: Real vs. Simulated

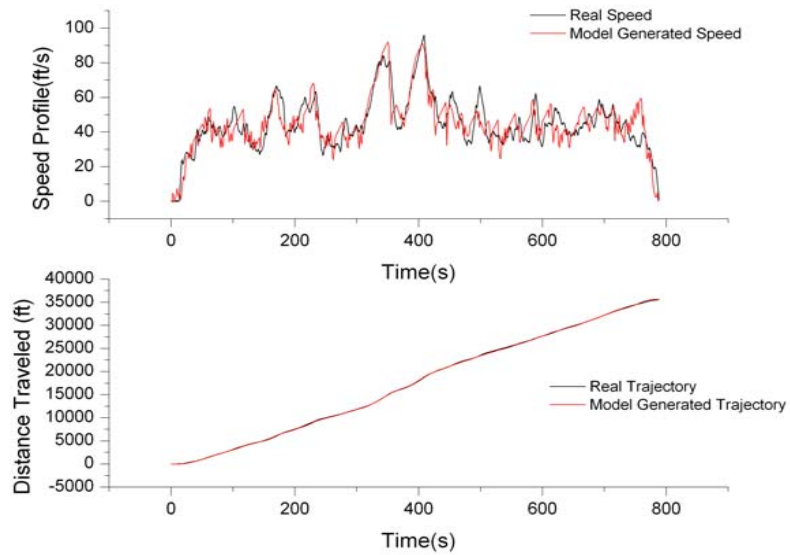

Figure 4-8 (j). Veh G10 Speed and Trajectory Profile: Real vs. Simulated

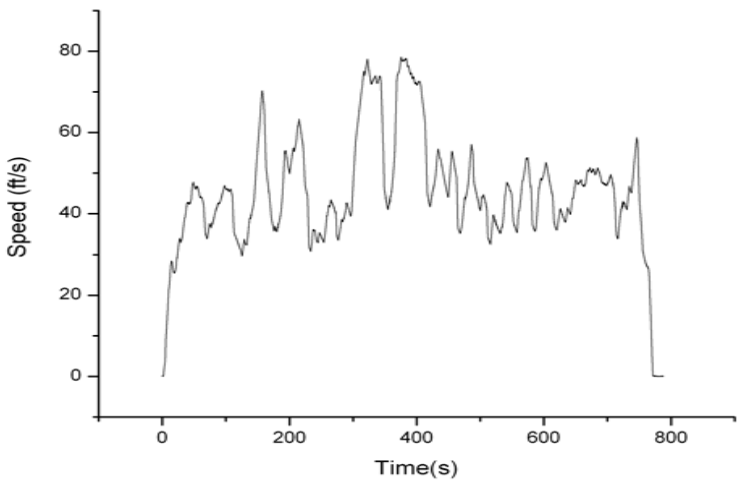

Figure 4-9 (a). Lead Vehicle (G03) Speed Profile

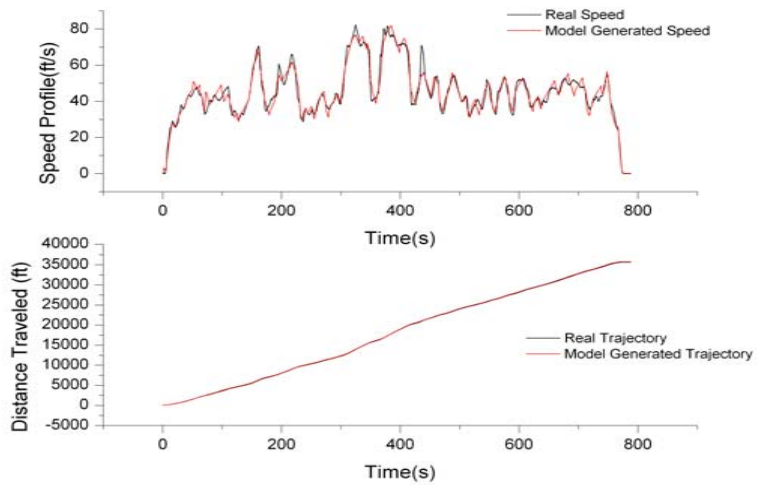

Figure 4-9 (b). Veh G04 Speed and Trajectory Profile: Real vs. Simulated

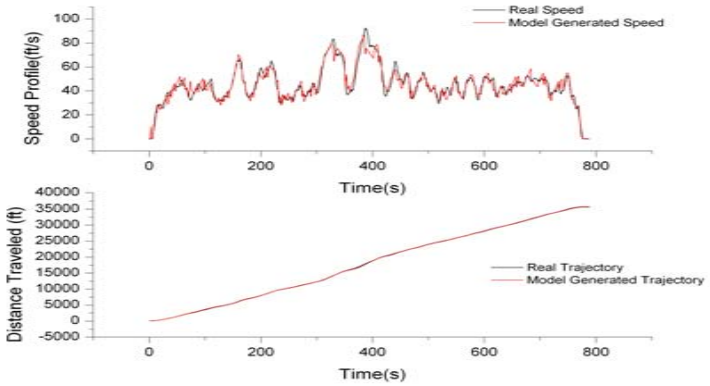

Figure 4-9 (c). Veh G05 Speed and Trajectory Profile: Real vs. Simulated

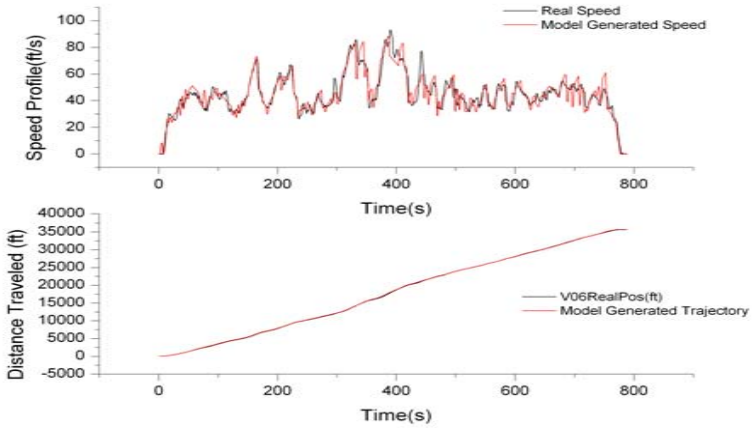

Figure 4-9 (d). Veh G06 Speed and Trajectory Profile: Real vs. Simulated

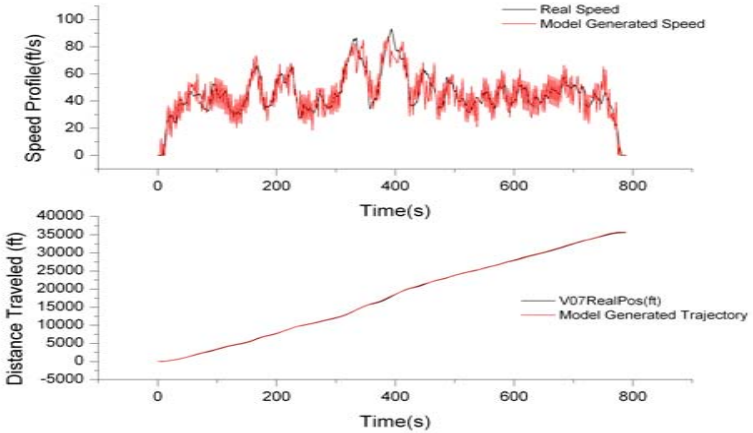

Figure 4-9 (e). Veh G07 Speed and Trajectory Profile: Real vs. Simulated

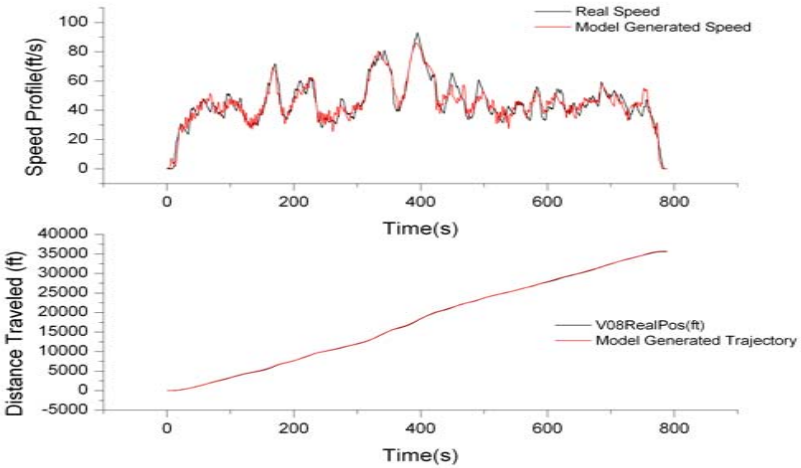

Figure 4-9 (f). Veh G08 Speed and Trajectory Profile: Real vs. Simulated

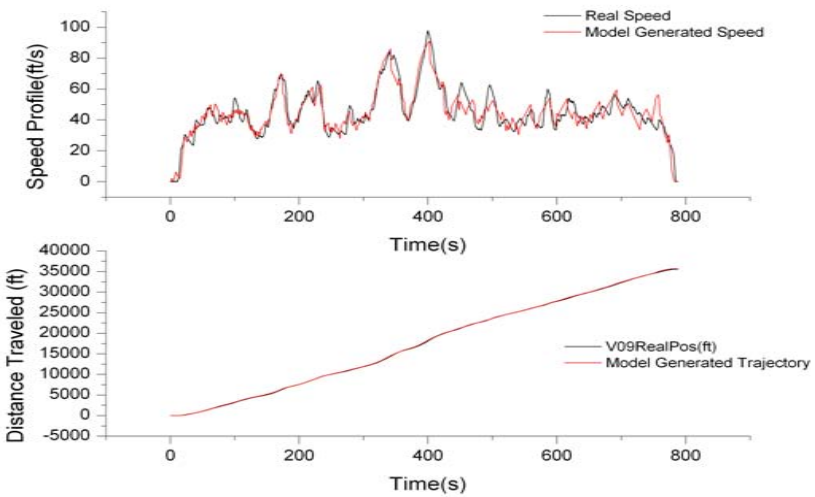

Figure 4-9 (g). Veh G09 Speed and Trajectory Profile: Real vs. Simulated

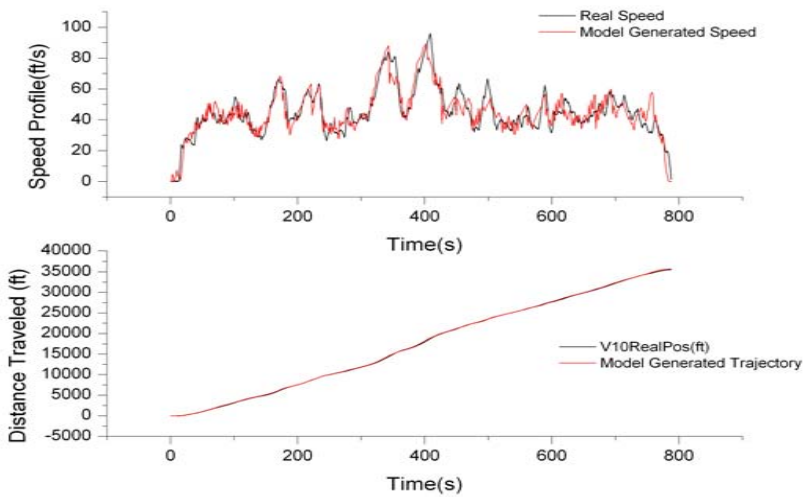

Figure 4-9 (h). Veh G10 Speed and Trajectory Profile: Real vs. Simulated

4.3 Model Calibration and Validation Using Crash Data

The proposed model is further tested using crash trajectories collected from the study site. This is summarized in this section. First of all, Table 4-5 overviews the crash cases collected in this study. As mentioned earlier, there are 11 crashes collected in this study. In Table 4-5, these crash cases are indexed with unique IDs from CR-01 to CR-11. For each crash case, a brief description documenting the time, lane position, and weather conditions are also provided. Finally, a total of 48 trajectories from these 11 crash cases are employed to calibrate and validate the proposed model.

Table 4-6 (a) ~ Table 4-6 (k) summarizes the calibrated parameters value for each crash case. Further Table 4-6(l) presents detailed statistics of calibrated parameters. The statistics presented in Table 4-6(l) include *Mean ($\bar{X}$), Standard Deviation (SD), Standard Error of the Mean (SEM), 25% Percentile, 75% Percentile, Inter Quartile Range (IQR), Maximum, Minimum, Range, Median, Variance, Coefficient of Variance (CV) and Kurtosis.* Definitions of these statistics can be found from earlier sections.

Figure 4-10 (a) ~Figure 4-10 (f) depict the distribution of *Maximum Comfortable Acceleration* (a_n), *Maximum Comfortable Deceleration* (b_n), *Oscillation Acceleration* (a_{osc}), *Oscillation Deceleration* (b_{osc}), *Desired Following Gap Time* (t_g), and *Scanning Interval* (t_{scan}). As suggested by these figures, the distributions are non-standard distributions with multiple local density clusters.

Figure 4-11 (a) ~Figure 4-11 (k) illustrates the validation results. From these figures, it can be seen that the proposed model can replicate the crashes cases with varying success. Table 4-7(a) ~Figure 4-7(i) summarizes the validation statistics. The statistics suggest the proposed model can replicate crash trajectories well.

Table 4-5. Summary of Crash/Near-Misses Cases Collected from Study Site

CrashID*	Time	Description
CR-01	Jul-12-2006-1615	Rear-end collision occurred on the leftmost lane; between Portland Ave and the flyover to I94WB; dry weather condition.
CR-02	Jul-07-2006-1828	Rear-end collision occurred on the rightmost lane; between Portland Ave and the flyover to I94WB; dry weather condition; prior to the collision, there were already two stalling vehicles on the right shoulder.
CR-03	Jul-17-2006-1741	Near-miss occurred on the rightmost lane; between Portland Ave and the flyover to I94WB; dry weather condition.
CR-04	Aug-08-2006-1827	Rear-end collision occurred on the rightmost lane; between Portland Ave and the flyover to I94WB;dry weather condition; 10 seconds prior to the collision, one vehicle conducted lane-change from the subject lane to the middle lane; the impact of the collision caused the lead vehicle run into the middle lane after being hit by the following vehicle.
CR-05	Aug-10-2006-1346	Rear-end collision involved three vehicles occurred on the rightmost lane; between Portland Ave and the flyover to I94WB; dry weather condition; the impact of the initial collision caused the lead vehicle run into the second vehicle in front.
CR-06	Aug-11-2006-1253	Near-miss occurred on the rightmost lane; between Portland Ave and the flyover to I94WB; dry weather condition; 20 seconds prior to the near-miss, one vehicle conducted lane-change from the subject lane to the middle lane.
CR-07	Aug-17-2006-1517	Rear-end collision occurred on the leftmost lane; between Portland Ave and the flyover to I94WB; dry weather condition; 18 seconds prior to the collision, one vehicle conducted lane-change from the subject lane to the middle lane.
CR-09	Aug-11-2006-1224	Near-miss occurred on the rightmost lane; between Portland Ave and the flyover to I94WB; dry weather condition.
CR-10	Aug-09-2006-1440	Rear-end collision occurred on the rightmost lane; between Portland Ave and the flyover to I94WB; dry weather condition.
CR-11	Aug-11-2006-1253	Near-miss occurred on the rightmost lane; between Portland Ave and the flyover to I94WB; dry weather condition.

*Note: CR-08 is discarded due to data quality.

Table 4-6 (a). Calibrated Parameters for Crash Case CR-01

Param / VehID	a_n (ft/s^2)	b_n (ft/s^2)	a_{osc} (ft/s^2)	b_{osc} (ft/s^2)	t_g (sec)	ε_g	t_{scan} (sec)	t_d (sec)	$C_{\dot{\theta}}$ (rad/s)	C_D
CR1-V07	5.2196	-15.5950	0.6181	-1.149	0.6428	0.221234	0.1	0.1	0.001608	0.25
CR1-V10	6.7733	-8.1295	1.4356	-1.0052	0.54896	0.8618	0.6	0.2	0.00148	0.25
CR1-V15	7.4417	-8.2163	1.4479	0.9220	3.49641	0.556951	0.5	0.2	0.003828	0.25
CR1-V21	10.5779	-17.7362	0.7926	-1.2003	1.04227	0.289067	1.0	0.1	0.003149	0.25
CR1-V16	11.4023	-17.9808	0.8403	-0.7310	0.86276	0.602460	0.1	0.6	0.003057	0.25
CR1-V30	7.3033	-17.9100	0.9642	-1.0377	0.92417	0.239240	0.1	0.3	0.002149	0.25

Table 4-6 (b). Calibrated Parameters for Crash Case #2

Param / VehID	a_n (ft/s^2)	b_n (ft/s^2)	a_{osc} (ft/s^2)	b_{osc} (ft/s^2)	t_g (sec)	ε_g	t_{scan} (sec)	t_d (sec)	$C_{\dot{\theta}}$ (rad/s)	C_D
CR2-V07	5.20537	-5.46103	0.71366	-1.02662	2.97501	0.731441	0.5	0.2	0.002284	0.25
CR2-V11	7.15034	-7.18871	0.8241	-1.0638	0.512	0.067	0.4	0.1	0.003884	0.25
CR2-V12	9.69792	-10.0495	0.832148	-0.8374	0.823	0.5633	0.1	0.8	0.004085	0.25
CR2-V17	5.00569	-14.5454	1.16516	-0.726947	1.16933	0.724187	1.3	0.1	0.00395	0.25
CR2-V14	5.13275	-16.7314	0.9176	-1.26093	0.50149	0.043839	1.1	0.1	0.003141	0.25

Table 4-6 (c). Calibrated Parameters for Crash Case #3 (near-miss)

Param / VehID	a_n (ft/s^2)	b_n (ft/s^2)	a_{osc} (ft/s^2)	b_{osc} (ft/s^2)	t_g (sec)	ε_g	t_{scan} (sec)	t_d (sec)	$C_{\dot{\theta}}$ (rad/s)	C_D
CR3-V07	5.05755	-5.1147	0.524801	-1.42519	2.95083	0.80677	0.2	0.5	0.003494	0.25
CR3-V08	5.35926	-17.3855	0.63041	-1.30114	0.808685	0.254759	0.5	0.1	0.001191	0.25
CR3-V11	7.24851	-17.5337	1.1217	-0.9863	1.33212	0.3178	1.5	0.3	0.002497	0.25
CR3-V12	8.07861	-13.839	1.30723	-0.7827	1.17393	0.3603	1.1	0.7	0.001472	0.25
CR3-V13	5.01651	-12.344	1.08981	-1.10926	0.5	0.6739	0.2	0.2	0.003561	0.25

Table 4-6 (d). Calibrated Parameters for Crash Case #4

Param / VehID	a_n (ft/s^2)	b_n (ft/s^2)	a_{osc} (ft/s^2)	b_{osc} (ft/s^2)	t_g (sec)	ε_g	t_{scan} (sec)	t_d (sec)	$C_{\dot{\theta}}$ (rad/s)	C_D
CR4-V10	8.65985	-13.6091	0.81548	-0.878659	1.21886	0.73883	0.7	0.2	0.001996	0.25
CR4-V11	6.16654	-11.2517	0.77564	-1.05767	0.512503	0.01458	0.1	0.1	0.001109	0.25
CR4-V15	5.80589	-7.37349	1.25725	-1.11798	0.604512	0.036597	0.2	0.1	0.00268	0.25
CR4-V06	10.4044	-17.4338	0.833563	-0.9829	0.563419	0.576477	0.3	0.1	0.002847	0.25
CR4-V07	7.62579	-9.64252	1.34475	-0.99593	0.668324	0.753714	0.3	0.5	0.003806	0.25
CR4-V08	5.17966	-16.7899	1.14871	-0.977156	0.732934	0.489315	0.4	0.7	0.003545	0.25

Table 4-6 (e). Calibrated Parameters for Crash Case #5

Param / VehID	a_n (ft/s^2)	b_n (ft/s^2)	a_{osc} (ft/s^2)	b_{osc} (ft/s^2)	t_g (sec)	ε_g	t_{scan} (sec)	t_d (sec)	$C_{\dot{\theta}}$ (rad/s)	C_D
CR5-V09	5.0113	-11.3918	0.715064	-1.15451	1.61744	0.3366	0.6	0.3	0.001802	0.25
CR5-V10	5.11611	-15.4427	0.972016	-1.04772	0.88986	0.32713	0.2	0.4	0.002001	0.25
CR5-V11	5.02854	-15.9801	0.500416	-1.47599	0.50	0.01397	0.1	0.1	0.001053	0.25
CR5-V12	7.16279	-7.34104	1.13632	-0.63045	1.3838	0.394832	0.2	0.1	0.004879	0.25
CR5-V14	5.8855	-15.0561	0.75055	-1.33418	0.51032	0.02795	1.2	0.1	0.001321	0.25

Table 4-6 (f). Calibrated Parameters for Crash Case #6 (Near Misses)

Param / VehID	a_n (ft/s^2)	b_n (ft/s^2)	a_{osc} (ft/s^2)	b_{osc} (ft/s^2)	t_g (sec)	ε_g	t_{scan} (sec)	t_d (sec)	$C_{\dot{\theta}}$ (rad/s)	C_D
CR6-V06	5.37958	-16.908	0.65425	-0.985391	1.36962	0.76002	0.1	0.2	0.004227	0.25
CR6-V07	5.08862	-16.2007	1.34076	-1.20773	0.798549	0.643009	0.8	0.7	0.003235	0.25
CR6-V08	6.11265	-11.333	0.980168	-1.34234	1.25661	0.492527	0.1	0.1	0.00208	0.25
CR6-V09	7.49804	-13.0374	0.683989	-1.37786	0.987522	0.47889	1.3	0.1	0.003007	0.25
CR6-V10	5.08268	-14.307	0.636397	-1.35954	0.985877	0.328891	0.9	0.1	0.001840	0.25
CR6-V13	7.98526	-15.099	1.07066	-1.15448	2.63164	0.65554	1.9	0.3	0.004358	0.25

Table 4-6 (g). Calibrated Parameters for Crash Case #7

Param / VehID	a_n (ft/s^2)	b_n (ft/s^2)	a_{osc} (ft/s^2)	b_{osc} (ft/s^2)	t_g (sec)	ε_g	t_{scan} (sec)	t_d (sec)	$C_{\dot{\theta}}$ (rad/s)	C_D
CR7-V11	10.8648	-14.1838	0.897911	-1.31366	2.72075	0.205	0.6	0.6	0.00463	0.25
CR7-V13	7.0585	-16.4174	0.567253	-0.706684	1.04676	0.561176	0.3	0.1	0.00491	0.25
CR7-V15	11.7824	-17.3214	0.746815	-1.12051	1.30864	0.65528	0.4	0.4	0.002160	0.25

Table 4-6 (h). Calibrated Parameters for Crash Case #9 (Vehicle 12 Near-Miss)

Param / VehID	a_n (ft/s^2)	b_n (ft/s^2)	a_{osc} (ft/s^2)	b_{osc} (ft/s^2)	t_g (sec)	ε_g	t_{scan} (sec)	t_d (sec)	$C_{\dot{\theta}}$ (rad/s)	C_D
CR9-V08	10.1018	-11.9763	0.904458	-0.591331	1.28302	0.705036	0.4	0.1	0.004125	0.25
CR9-V09	7.17724	-17.3314	0.863409	-1.29544	1.07958	0.12645	0.2	0.1	0.002461	0.25
CR9-V10	11.9895	-18	1.14515	-0.726738	0.66678	0.216653	0.1	0.5	0.00156	0.25
CR9-V11	5.08003	-17.8545	0.79764	-1.35317	0.71704	0.09286	0.3	0.1	0.0012	0.25
CR9-V12	5.07838	-17.8454	0.771117	-1.47018	1.16003	0.500683	0.4	0.2	0.001352	0.25
CR9-V13	9.76069	-13.7828	1.20541	-0.722878	2.65729	0.735353	1.0	0.3	0.00414	0.25

Table 4-6 (i). Calibrated Parameters for Crash Case #10

Param / VehID	a_n (ft/s^2)	b_n (ft/s^2)	a_{osc} (ft/s^2)	b_{osc} (ft/s^2)	t_g (sec)	ε_g	t_{scan} (sec)	t_d (sec)	$C_{\dot{\theta}}$ (rad/s)	C_D
CR10-V16	8.47219	-9.34061	0.750198	-0.92893	0.950778	0.505241	1.5	0.3	0.004756	0.25
CR10-V17	5.59099	-17.9188	0.721785	-0.954521	2.21373	0.349992	0.2	0.3	0.003929	0.25
CR10-V18	5.39594	-6.23301	1.06468	-1.2076	0.570416	0.526769	0.1	0.1	0.003271	0.25
CR10-V20	6.01945	-6.75353	1.01173	-0.921408	0.509564	0.407612	0.4	0.1	0.003810	0.25
CR10-V22	5.29439	-17.9999	0.506294	-1.49995	0.500	0.103976	0.5	0.1	0.001008	0.25
CR10-V23	9.13503	-17.5375	0.70823	-0.885052	2.75718	0.381457	0.3	0.1	0.001449	0.25
CR10-V24	5.6259	-17.9746	0.729097	-0.860297	0.534356	0.119953	0.3	0.4	0.001327	0.25

Table 4-6 (j). Calibrated Parameters for Crash Case #11 (Vehicle 11 Near-Miss)

Param / VehID	a_n (ft/s^2)	b_n (ft/s^2)	a_{osc} (ft/s^2)	b_{osc} (ft/s^2)	t_g (sec)	ε_g	t_{scan} (sec)	t_d (sec)	$C_{\dot{\theta}}$ (rad/s)	C_D
CR11-V07	6.83024	-15.0212	0.833716	-1.36683	1.00722	0.868822	1.1	0.2	0.003388	0.25
CR11-V08	5.49758	-17.5938	0.814961	-1.0597	0.9938	0.2548	0.1	0.7	0.001347	0.25
CR11-V09	6.1216	-17.2142	0.698301	-1.47106	0.9945	0.528	0.3	0.1	0.004821	0.25
CR11-V10	7.55394	-17.5678	0.670425	-0.795968	1.1161	0.337581	0.1	0.1	0.00181	0.25
CR11-V11	10.308	-17.9819	0.53748	-1.45306	0.5	0.2	0.2	0.2	0.001154	0.25

Table 4-6 (k). Statistics of Calibrated Parameters for Crash Data (I94 Crash Trajectories)
Sample Size: 48 Drivers

Parameters \ Statistics	Mean	Standard Deviation	Standard Error of the Mean	25% Percentile	75% Percentile	Inter-Quartile Range	Minimum	Maximum	Range	Median	Variance	Coefficient of Variance	Kurtosis
Max Comft Accel a_n	6.92531	1.95146	0.28167	5.2196	7.62579	2.40619	5.00569	11.7824	6.77671	6.14407	3.80821	0.28179	0.01718
Max Comft Decel b_n	-13.7712	4.11654	0.59417	-17.4338	-11.2517	6.1821	-17.99	-5.11	12.8852	-15.07755	16.94589	-0.29892	-0.82675
Osc Accel a_{osc}	0.87709	0.25366	0.03661	0.6983	1.06468	0.36638	0.50042	1.4479	0.94748	0.81979	0.06434	0.2892	-0.41101
Osc Decel b_{osc}	-1.0489	0.36772	0.05308	-1.30114	-0.92893	0.37221	-1.49995	0.922	2.42195	-1.05869	0.13522	-0.35058	17.13454
Desired Fol Gap t_g	1.1504	0.76785	0.11083	0.56342	1.25661	0.69319	0.5	3.49641	2.99641	0.96833	0.5896	0.66746	1.88519
Gap Error ε_g	0.42476	0.24519	0.03539	0.23924	0.60246	0.36322	0.01397	0.86882	0.85485	0.40122	0.06012	0.57724	-0.97086
Scanning Interval t_{scan}	0.52292	0.46184	0.06666	0.2	0.7	0.5	0.1	1.9	1.8	0.35	0.21329	0.88319	0.63199
Mechnical Delay t_d	0.2625	0.20999	0.03031	0.1	0.3	0.2	0.1	0.8	0.7	0.2	0.0441	0.79996	0.26576
Expansion Rate Thres $C_{\dot{\theta}}$	0.0028	0.00121	1.7524E-4	0.00161	0.00381	0.0022	0.00101	0.00491	0.0039	0.00293	1.474E-6	0.43365	-1.26009

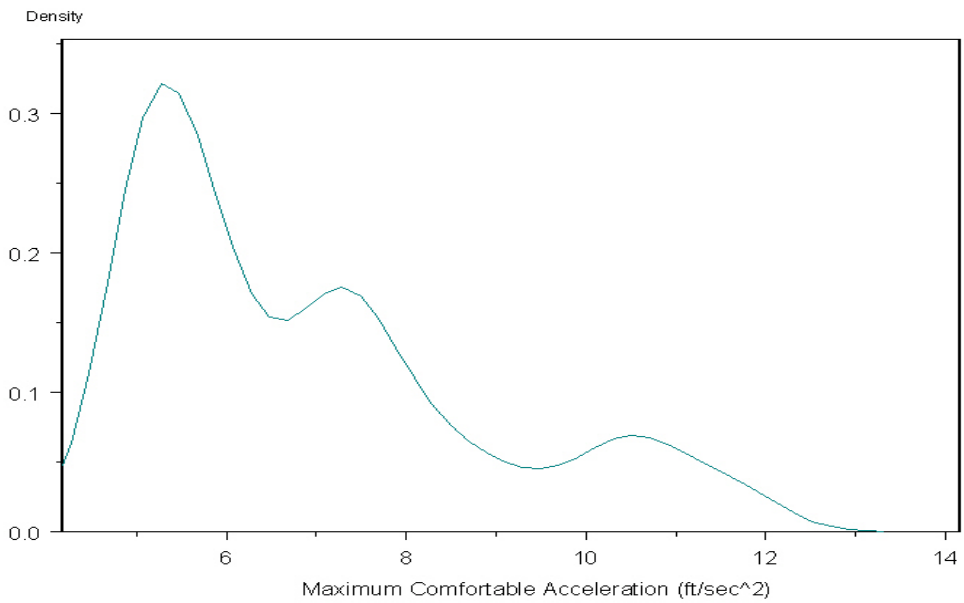

Figure 4-10 (a). Distribution of Calibrated Maximum Comfortable Acceleration

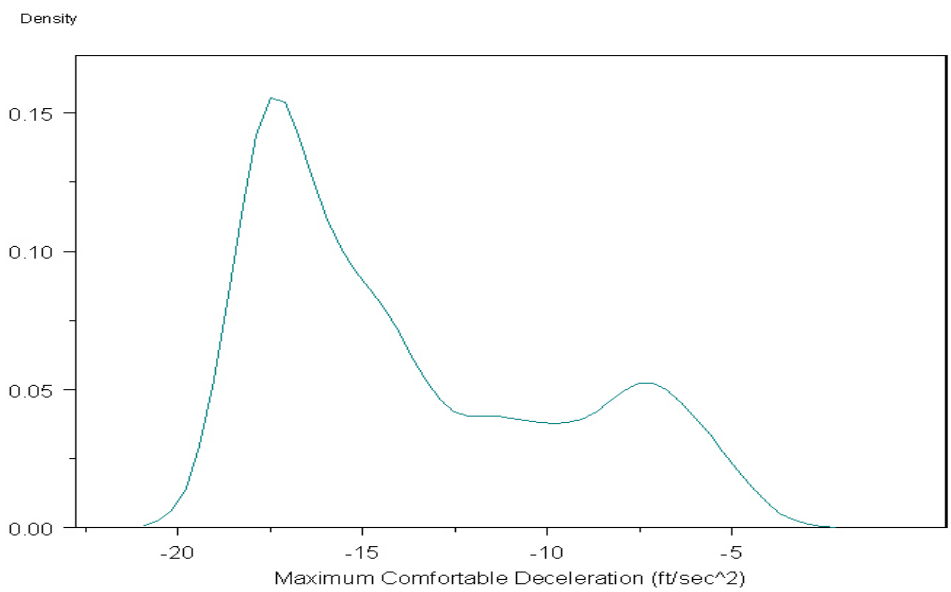

Figure 4-10 (b). Distribution of Calibrated Maximum Comfortable Deceleration

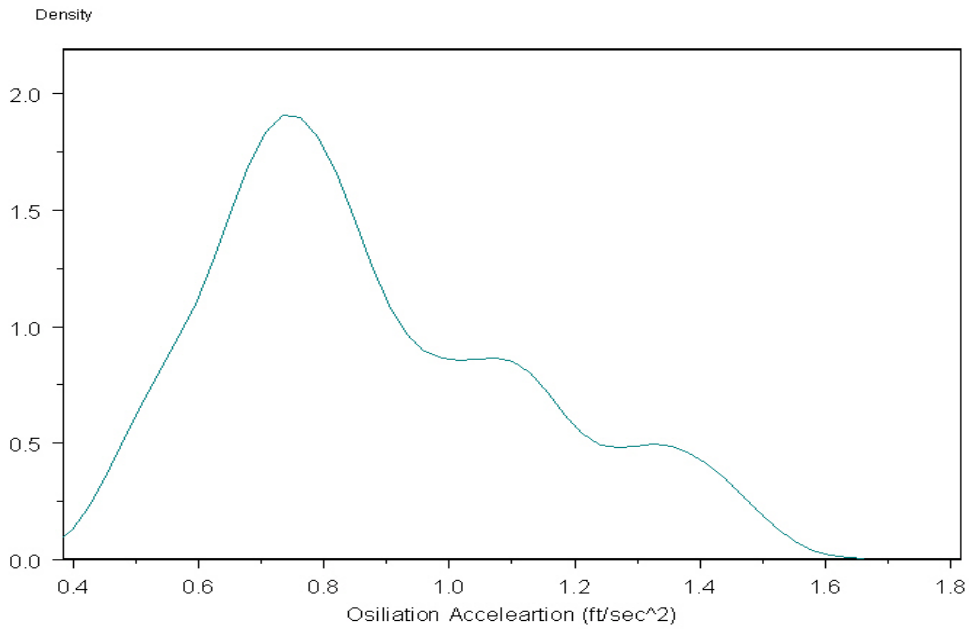

Figure 4-10 (c). Distribution of Calibrated Oscillation Acceleration

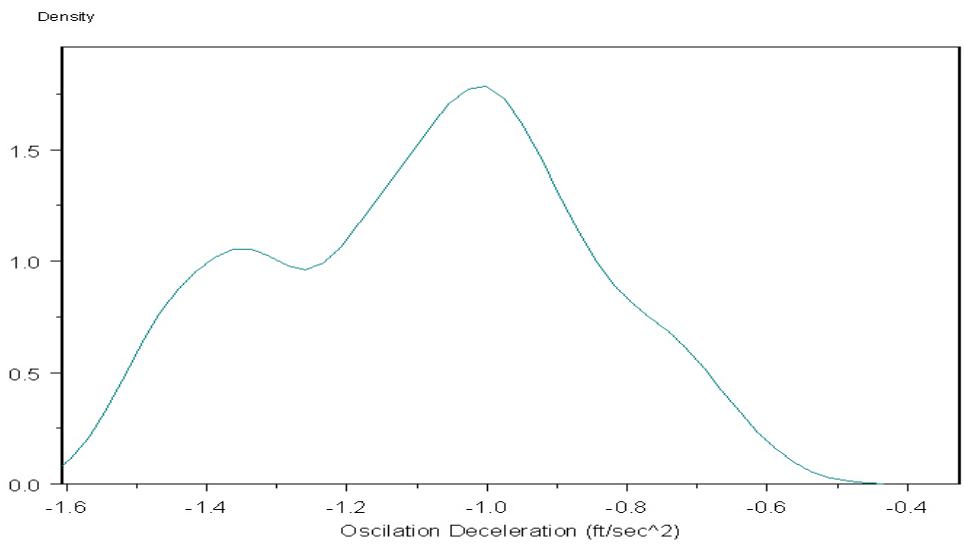

Figure 4-10 (d). Distribution of Calibrated Oscillation Deceleration

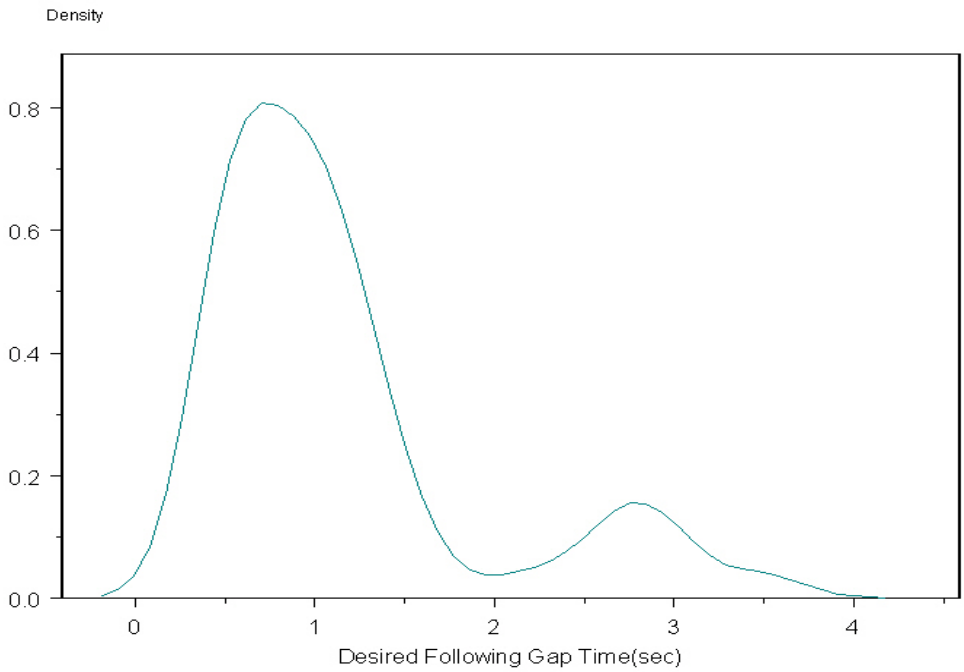

Figure 4-10 (e). Distribution of Calibrated Desired Following Gap Time

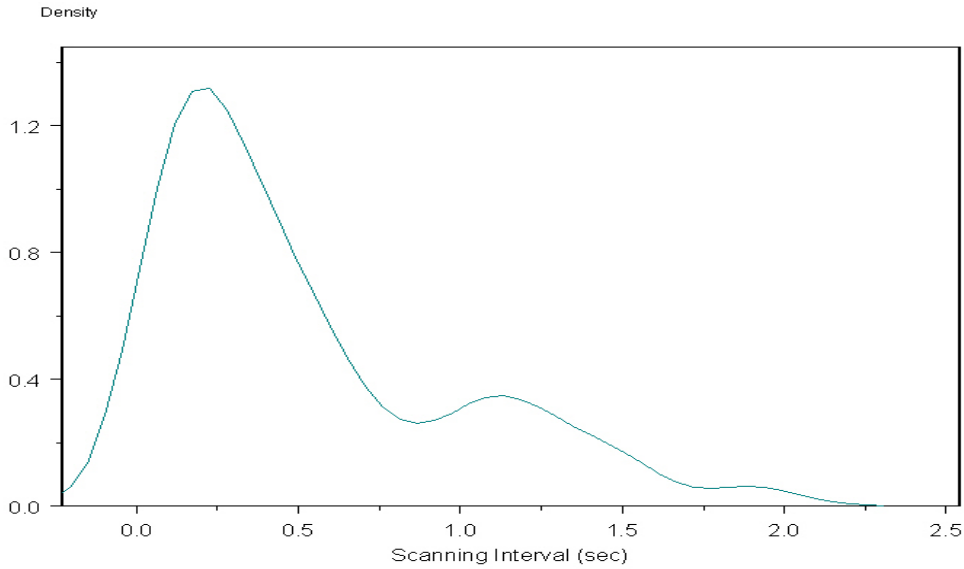

Figure 4-10 (f). Distribution of Calibrated Scanning Interval

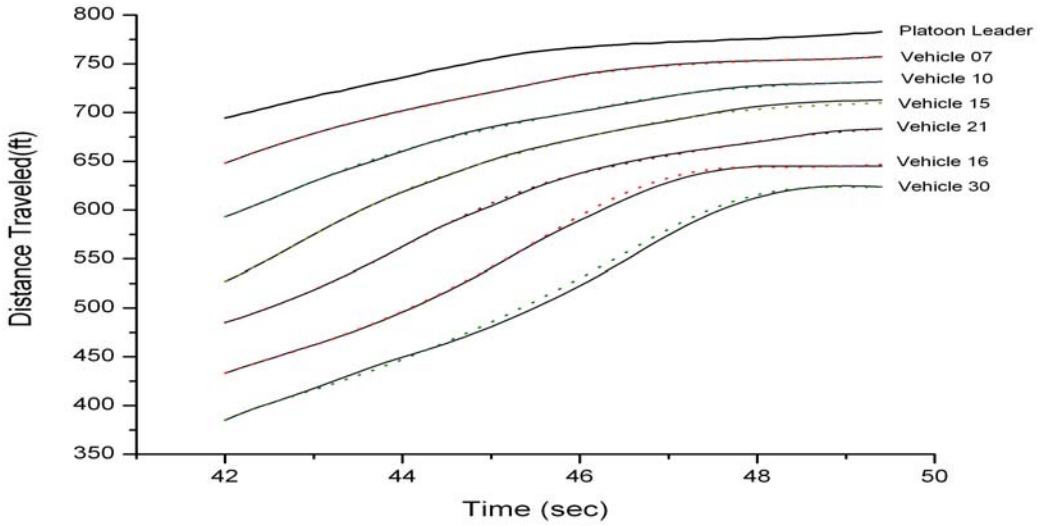

Figure 4-11 (a). Simulated Trajectories (Dotted Line) vs. Real Trajectories (Solid Line) for Crash Case CR-01

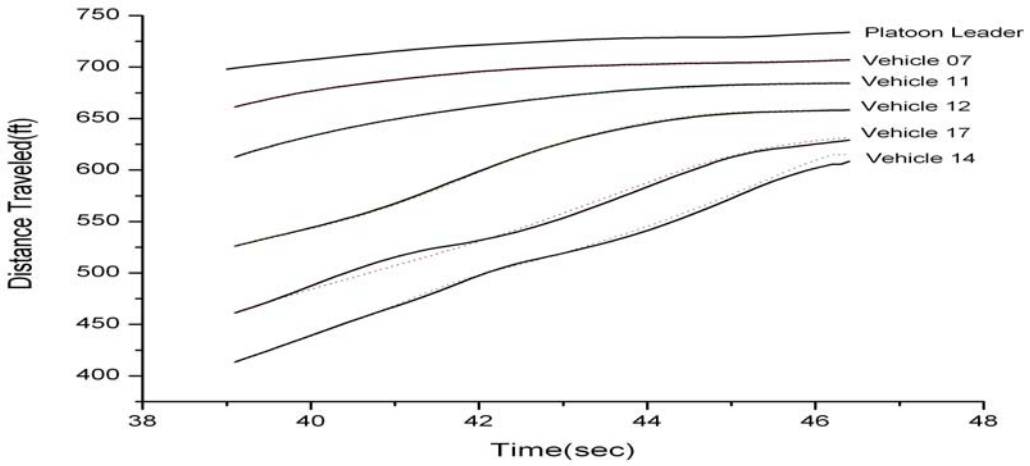

Figure 4-11 (b). Simulated Trajectories (Dotted Line) vs. Real Trajectories (Solid Line) for Crash Case CR-02

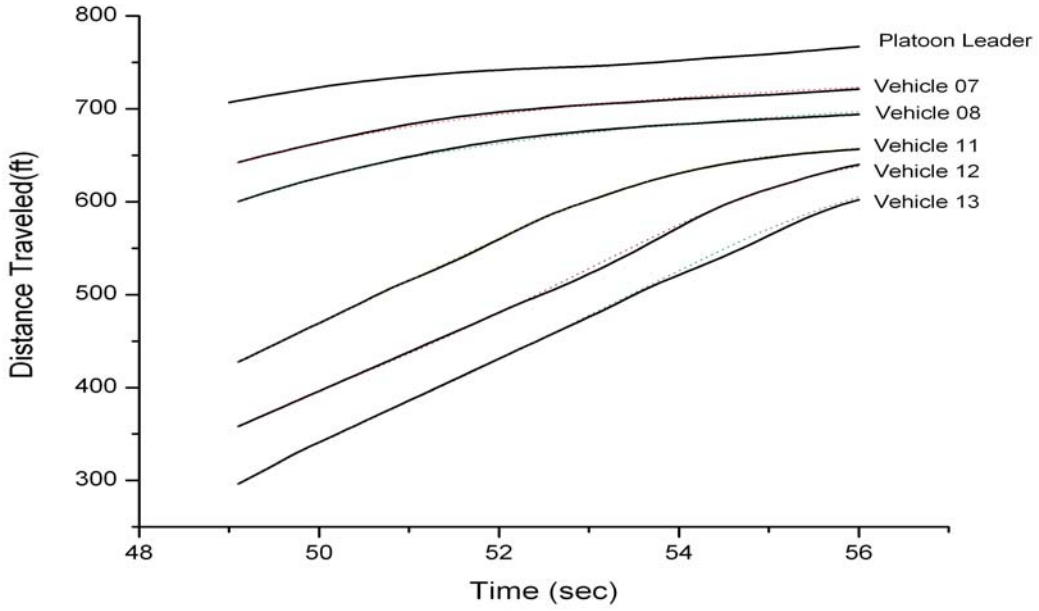

Figure 4-11 (c). Simulated Trajectories (Dotted Line) vs. Real Trajectories (Solid Line) for Crash Case CR-03

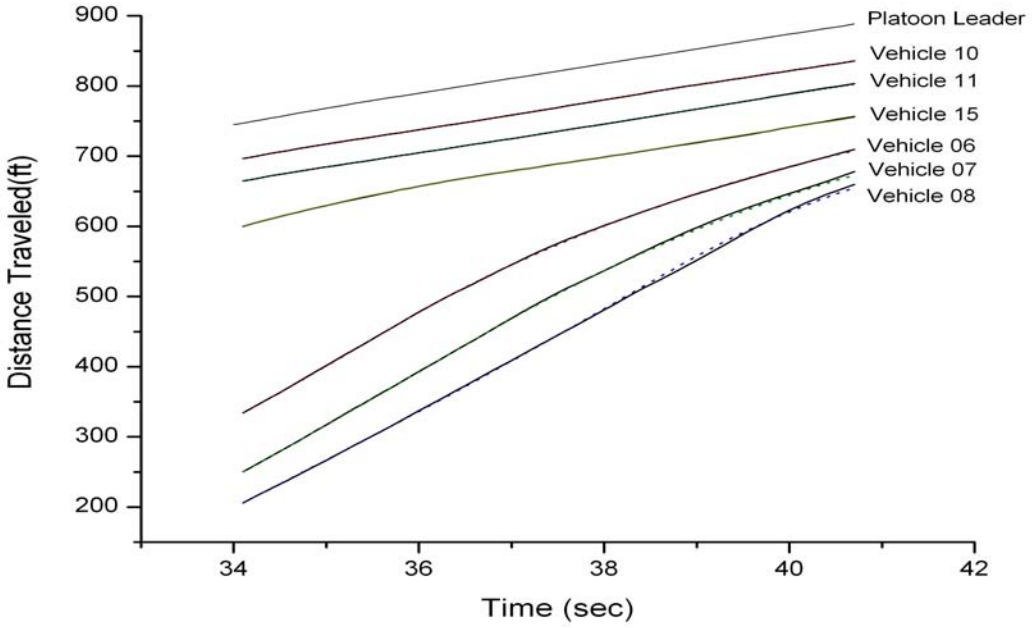

Figure 4-11 (d). Simulated Trajectories (Dotted Line) vs. Real Trajectories (Solid Line) for Crash Case CR-04

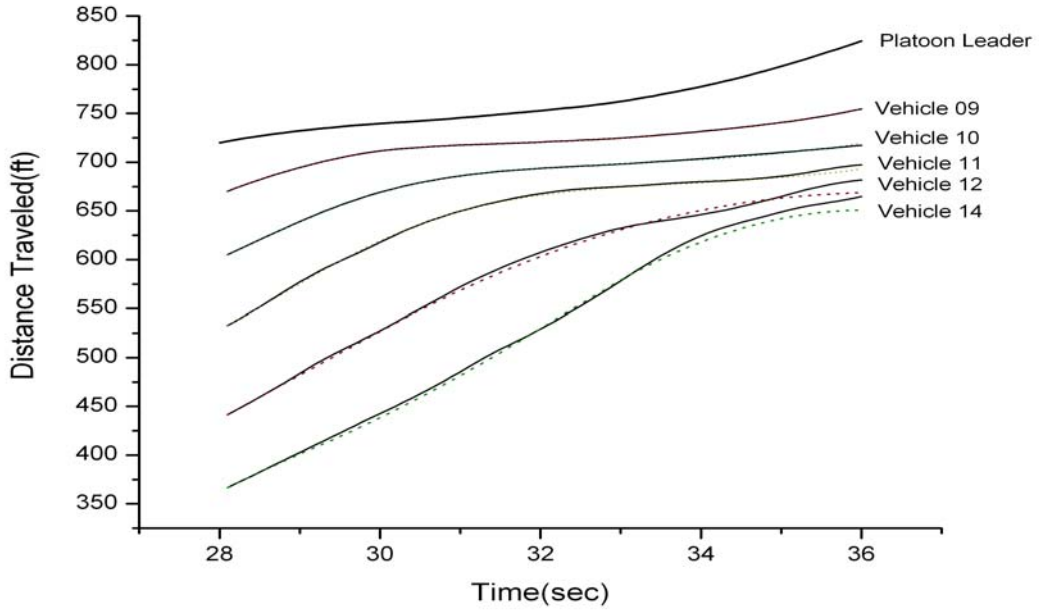

Figure 4-11 (e). Simulated Trajectories (Dotted Line) vs. Real Trajectories (Solid Line) for Crash Case CR-05

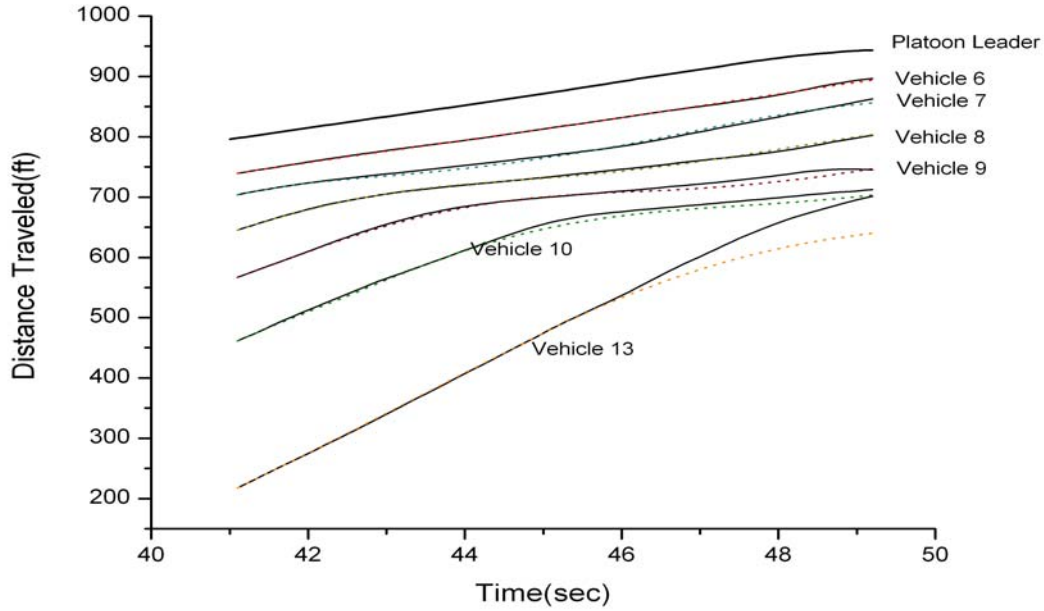

Figure 4-11 (f). Simulated Trajectories (Dotted Line) vs. Real Trajectories (Solid Line) for Crash Case CR-06

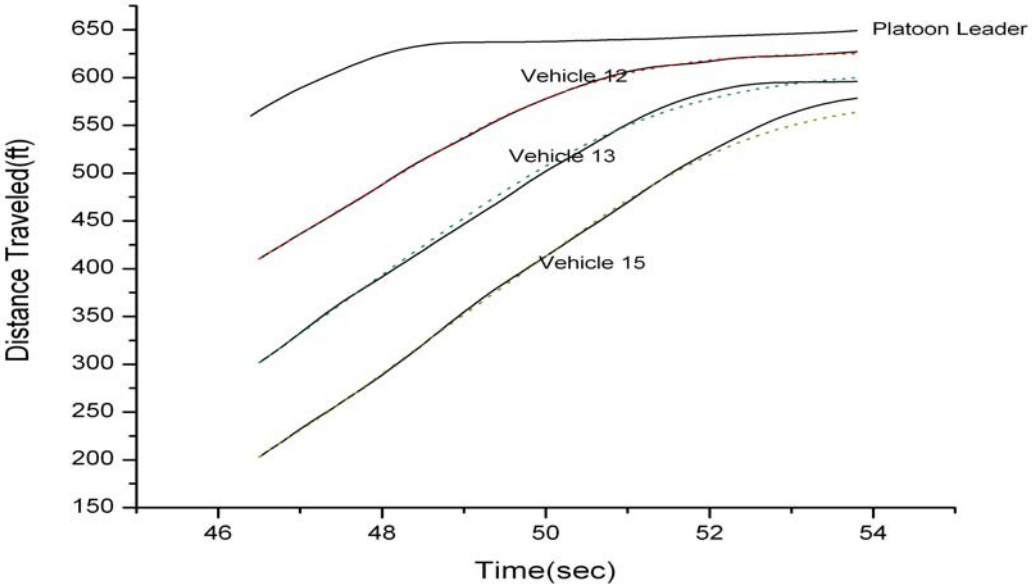

Figure 4-11 (g). Simulated Trajectories (Dotted Line) vs. Real Trajectories (Solid Line) for Crash Case CR-07

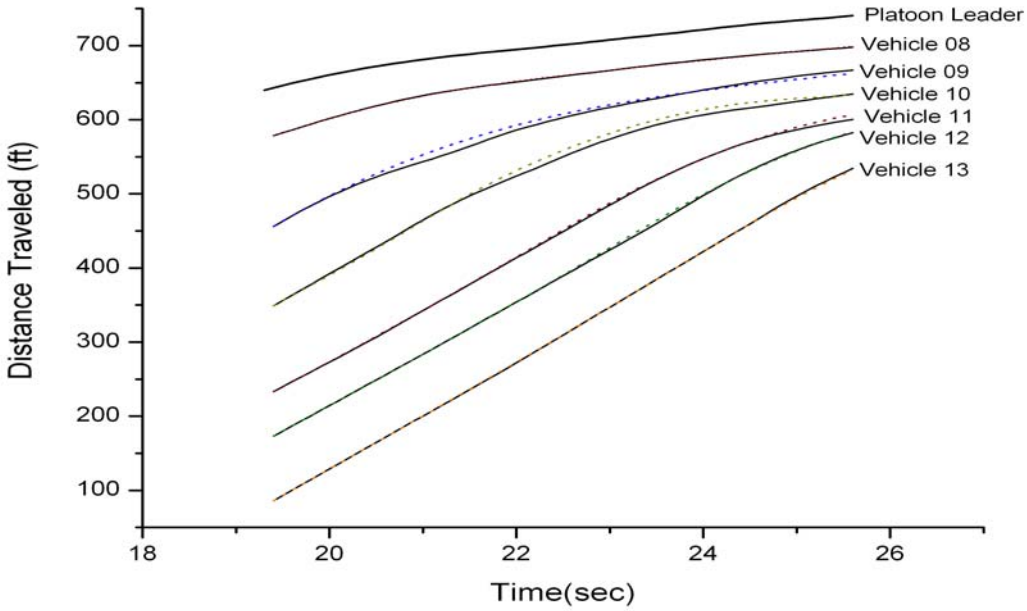

Figure 4-11 (h). Simulated Trajectories (Dotted Line) vs. Real Trajectories (Solid Line) for Crash Case CR-09

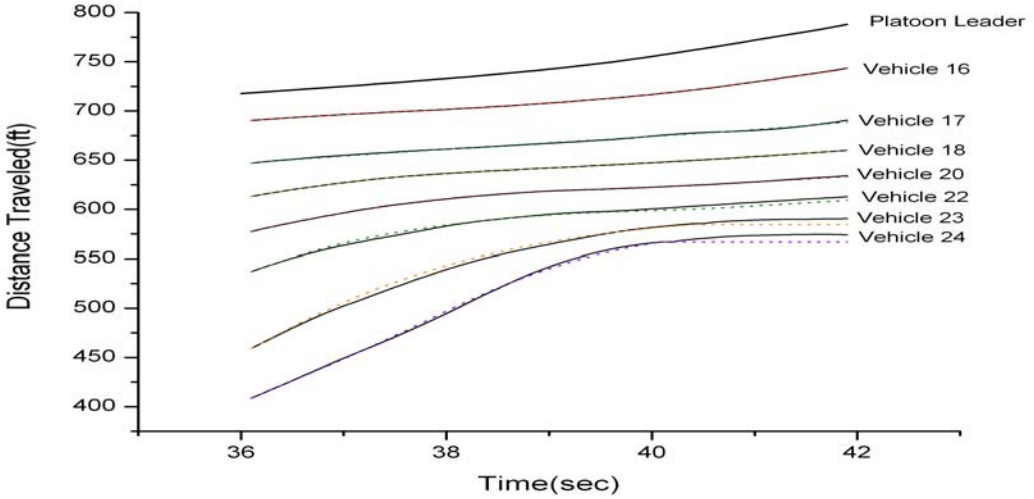

Figure 4-11 (i). Simulated Trajectories (Dotted Line) vs. Real Trajectories (Solid Line) for Crash Case CR-10

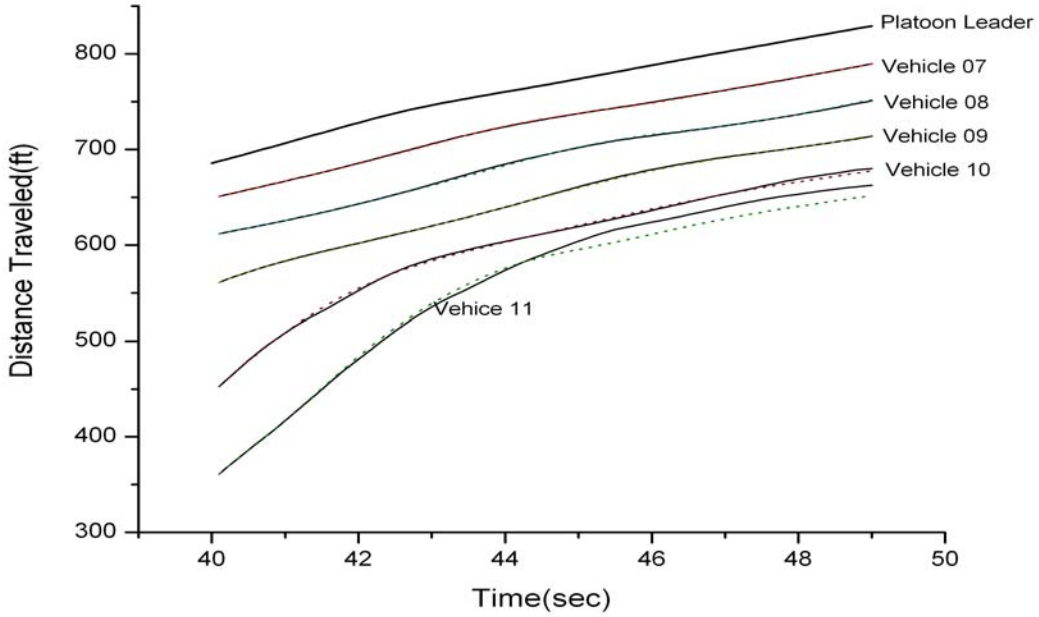

Figure 4-11 (j). Simulated Trajectories (Dotted Line) vs. Real Trajectories (Solid Line) for Crash Case CR-11

Table 4-7 (a). Validation Statistics for Crash Case CR-01

VehID / Statistics	CR1-V07	CR1-V10	CR1-V15	CR1-V21	CR1-V16	CR1-V30
Root Mean Squared Error(ft)	0.311786	0.426292	1.089	0.9823	0.909	1.57
Mean Percentage Error	0.0001987	0.000319	0.0009	0.0007	0.00076	0.00172

Table 4-7 (b). Validation Statistics for Crash Case #2

VehID / Statistics	CR2-V07	CR2-V11	CR2-V12	CR2-V17	CR2-V14
Root Mean Squared Error(ft)	0.31046	0.326983	0.795207	3.0301	2.4889
Mean Percentage Error	0.000259	0.00029322	0.000816	0.003409	0.002389

Table 4-7 (c). Validation Statistics for Crash Case #3 (Near-Miss)

VehID / Statistics	CR3-V07	CR3-V08	CR3-V11	CR3-V12	CR3-V13
Root Mean Squared Error(ft)	1.988913	1.889369	1.582747	2.294622	2.817635
Mean Percentage Error	0.001576	0.001476	0.00106312	0.00203	0.00269

Table 4-7 (d). Validation Statistics for Crash Case #4

VehID / Statistics	CR4-V10	CR4-V11	CR4-V15	CR4-V06	CR4-V07	CR4-V08
Root Mean Squared Error(ft)	1.494712	1.535204	1.531756	1.55131	1.936707	2.260162
Mean Percentage Error	0.000606	0.000747	0.000796	0.00091	0.001528	0.00212

Table 4-7 (e). Validation Statistics for Crash Case #5

VehID / Statistics	CR5-V9	CR5-V10	CR5-V11	CR5-V12	CR5-V14
Root Mean Squared Error(ft)	0.243963	0.475501	1.250859	3.123368	3.724632
Mean Percentage Error	0.0002053	0.0003767	0.001068	0.002827	0.0039415

Table 4-7 (f). Validation Statistics for Crash Case #6 (Near Misses)

VehID / Statistics	CR6-V6	CR6-V7	CR6-V8	CR6-V9	CR6-V10	CR6-V13
Root Mean Squared Error(ft)	0.872536	2.309686	1.421618	3.7837	4.790052	18.36
Mean Percentage Error	0.000554	0.001912	0.00115267	0.002818	0.0046065	0.0128

Table 4-7 (g). Validation Statistics for Crash Case #7

VehID / Statistics	CR7-V12	CR7-V13	CR7-V15
Root Mean Squared Error(ft)	0.629556	3.410964	4.464534
Mean Percentage Error	0.0006636	0.00421	0.004184

Table 4-7 (h). Validation Statistics for Crash Case #9 (Vehicle 12 Near-Miss)

VehID / Statistics	CR9-V8	CR9-V9	CR9-V10	CR9-V11	CR9-V12	CR9-V13
Root Mean Squared Error(ft)	0.5286	3.405369	3.593274	1.372389	1.068072	0.666442
Mean Percentage Error	0.0004551	0.003125	0.003566	0.001261	0.000986	0.00071246

Table 4-7 (i). Validation Statistics for Crash Case #10

VehID / Statistics	CR10-V16	CR10-V17	CR10-V18	CR10-V20	CR10-V22	CR10-V23	CR10-V24
Root Mean Squared Error(ft)	0.070623	0.43	0.1147	0.151982	1.57	2.40485	2.51
Mean Percentage Error	0.00005	0.0003865	0.000106	0.0001222	0.00149	0.00259	0.00229

Table 4-7 (j). Validation Statistics for Crash Case #11 (Vehicle 11 Near-Miss)

VehID / Statistics	CR11-V7	CR11-V8	CR11-V9	CR11-V10	CR11-V11
Root Mean Squared Error(ft)	0.288926	0.584416	0.520039	1.386115	6.756657
Mean Percentage Error	0.000257	0.000518	0.00049678	0.00146	0.006931

5 CONCLUDING REMARKS

Much research has been conducted in the development, implementation, and evaluation of innovative ITS technologies aiming to improve traffic operations and driving safety. As part of the process, micro-simulation has become an increasingly indispensable tool for assisting in system design and evaluation. It has become evident that existing micro-simulation models are deficient when evaluating sophisticated safety-related ITS techniques. This is because existing micro-simulation modeling only describes normative car-following behaviors devoid of weakness and risks associated with real-life everyday driving. Under existing simulation models, drivers are implicitly assumed to be ideal controllers with perfect perceptions of the surrounding driving complex, therefore resulting in collision-free simulations. To date, realistic car-following models pertinent to the true nature of driver behaviors are currently lacking. The goal of this research is to develop new car-following modeling capable of replicating real-life car-following behaviors with its risks and imperfections. The research capitalizes on real-life crash data collected from Twin Cities freeway as well as test track car-following data from Hokkaido University to assist model development, calibration and validation. The outcomes of this research will help advance the understanding of car-following behaviors while improving the micro-simulation modeling to facilitate assessing freeway safety concepts at high definition microscopic level.

Prior to closing it is worthwhile to point out that all parameters of the proposed model have a physical meaning and are identifiable from empirical data. However, as shown in previous sections, to identify parameters from empirical data is non-trivial and needs considerable effort including collecting and analyzing data. Further, at least within the scope of this study, it has been found out that the parameters follow non-standard distribution. This needs to be further explored to find out if it is due to small sample size or resulted from numerical distortion by the calibration process.

Existing commercial simulators such as AIMSUN or VISSIM provide flexible APIs that can be used to facilitate integrating the proposed model. Specifically, the *MicroSDK* of AIMSUN, or *External Driver Module* of VISSIM can be readily used to do this. However, since the proposed model in not collision-free, once integrated with a full-featured simulator environment, more issues need to be resolved before the simulator can be employed in actually safety evaluations or safety-related applications. One critical issue would be potentially long simulation running time or significantly increased number of replications in order to get meaningful safety indicators.

REFERENCES

Barcelo, J. (2001). *Microscopic traffic simulation: A tool for the analysis and assessment of ITS systems*. Transport Simulation Systems Internal Report (www.tss-bcn.com), Accessed 11/19/2008.

Brackstone, M., and McDonald, M. (1999). "Car-following: a historical review." *Transportation Research Part F:Traffic Psychology and Behavior*, 2, 181-196.

Brackstone, M., Sultan, B., and McDonald, M. (2000). "Some findings on the approach process between vehicles on motorways." *Transportation Research Record*, 1724, 21-28.

Brackstone, M., Sultan, B., and McDonald, M. (2002). "Motorway driver behavior: studies on car following " *Transportation Research Part F:Traffic Psychology and Behavior*, 5, 329-344.

Brown, T. L., Lee, J. D., and McGehee, D. V. (2000). "Attention-based model of driver performance in rear-end collisions." *Transportation Research Record*, 1724, 14-20.

Chakroborty, P., and Kikuchi, S. (1999). "Evaluation of the General Motors based car following models and a proposed fuzzy inference model." *Transportation Research Part C:Emerging Technology*, 7, 209-235.

Davis, G. A., and Swenson, T. (2004). *Identification and simulation of common freeway accident mechanism: collective responsibility in freeway rear-end collision.* CTS Report, Intelligent Transportation Institute, University of Minnesota, Minneapolis.

Edie, L. C. (1961). "Car-following and steady-state theory for non-congested traffic." *Operations Research*, 9(1), 66-76.

Edwards, J. B. (1998). "The relationship between road accident severity and recorded weather." *Journal of Safety Research*, 29(4), 249-262.

Ehlert, A. (2004). "The identification of some requirements for an improved car following model," Doctoral Dissertation, University of Newcastle upon Tyne, Newcastle Great Britain.

Evans, L., and Rothery, R. (1973). "Experimental measurements of perceptual thresholds in car-following." *Highway Research Record*, 464, 13-29.

Evans, L., and Rothery, R. (1977). "Perceptual threshold in car-following- A comparison of recent measurements with earlier results." *Transportation Science*, 11(1), 60-72.

Evans, L. C., and Rothery, R. W. (1974). "Detection of the sign of relative motion when following a vehicle." *Human Factors*, 16, 161-173.

Fritzsche, H. T. (1994). "A model for traffic simulation." *Traffic Engineering and Control*, 35(5), 317-321.

Gallant, A. R. (1987). *Nonlinear Statistical Models*, John Wiley & Sons, Inc., New York, NY.

Gazis, D. C., Herman, R., and Potts, R. B. (1959). "Car-following theory of steady-state traffic flow." *Operations Research*, 7(4), 499-505.

Gazis, D. C., Herman, R., and Rothery, R. W. (1961). "Nonlinear follow-the-leader models of traffic flow." *Operations Research*, 9(5), 545-567.

Gibson, J. J. (1982). *A theoretical analysis of automobile driving.* Reasons for Realism, E. Reed and R. Jones, eds., Lawrence Erlbaum Associates, Hillsdale, NJ, 199-136.

Gipps, P. G. (1981). "A behavioural car-following model for computer simulation." *Transportation Research Part B:Methodological*, 15(2), 105-111.

Greenberg, H. (1959). "An analysis of traffic flow." *Operations Research*, 7, 79-85.

Greenshields, B. D. (1934). "A study of traffic capacity." *Proceedings of Highway Research Board*, Washington D.C., 14, Part 1 448-477.

Helbing, D., and Tilch, B. (1998). "Generalized force model of traffic dynamics." *Physical Review E*, 58(1), 133-138.

Helly, W. (1959). "Simulation of bottlenecks in single lane traffic flow." *Proceedings of the symposium on the theory of traffic flow*, Research Laboratories, General Motors Corp., Detroit MI, 207-238.

Hoffmann, E. R. (1968). "Detection of vehicle velocity changes in car-following." *Proceedins:Australian Road Research Board*, 4, 821-837.

Hoffmann, E. R., and Mortimer, R. G. (1994). "Drivers' estimates of time to collision." *Accident Analysis and Prevention*, 26(4), 511-520.

Hourdos, J. (2005). "Crash prone traffic flow dynamics: Identification and real-time detection," Doctoral Dissertation, University of Minnesota, Minneapolis MN.

Hunuenin, F., Torday, A., and Dumont, A.G. (2005). "Evaluation of traffic safety using microsimulation." 5th Swiss Transport Research Conference (STRC), Monte Verita, Ascona, Switzerland.

ITE. (1999). *Traffic Engineering Handbook*, Prentice-Hall Engineering.

Jiang, R., Wu, Q., and Zhu, Z. (2001). "Full velocity difference model for a car-following theory." *Physical Review E*, 64, 017101.

Kerner, B. S. (1998). "Experimental features of self-organization in traffic flow." *Physical Review Letters*, 81(17), 3797-3800.

Khattak, A., Kantor, P., and Council, F. (1998). "The role of adverse weather in key crash types on limited access roadways: Implications for advanced weather systems." *Transportation Research Record*, 1621, 10-19.

Kim, Z., Gomes, G., Hranac, R., and Skabardonis, A. (2005). "A machine vision system for generating vehicle trajectories over extended freeway segments." 12th World Congress on Intelligent Transportation Systems, San Francisco, CA.

Kim, Z., and Malik, J. "Fast vehicle detection with probabilistic feature grouping and its application to vehicle tracking." 9th IEEE International Conference on Computer Vision (ICCV '03), Nice, France, 524-531.

Kim, Z., and Malik, J. "High-quality vehicle trajectory generation from video data based on vehicle detection and description." IEEE Trans. Intelligent Transportation Systems, 176-182.

Klauer, S. G., Dingus, T. A., Neale, V. L., Sudweeks, J., and Ramsey, D. (2006). *The impact of driver inattention on near-crash/crash risk: an analysis using the 100-car naturalistic driving study data. DOT HS 810 594*, National Highway Traffic Safety Administration, Washington D.C.

Kosonen, I. (1999). "HUTSIM-Urban traffic simulation and control model: Principles and applications," PhD Dissertation, Helsinki University of Technology, Helsinki, Finland.

Kosonen, I., and Ree, S. "The potential for microscopic simulation in traffic safety and conflict studies." *Proceedings of Conference on Road Safety on Three Continents*, Pretoria, South Africa.

Krauss, S. (1998). "Micorscopic modeling of traffic flow: investigation of collision free vehicle dynamics," PhD Dissertation, Universität zu Köln Köln, Germany.

Ledoux, C., and Archer, J. (1999). *Assessing the safety impact of intelligent transport systems*. Royal Institute of Technology, Stockholm, Sweden (http://www.infra.kth.se/ctr/publikationer/ctr1999_08.pdf), Accessed 8/15/2006.

Lee, D. N. (1976). "A theory of visual control of braking based on information about time-to-collision." *Perception*, 5, 437-459.

Lee, D. N., and Reddish, P. E. (1981). "Plummeting gannets: a paradigm of ecological optics." *Nature*, 293, 293-294.

Lee, J. D., McGehee, D. V., Brown, T. L., and Reyes, M. L. (2002). *Driver distraction, warning algorithm parameters, and driver response to imminent rear-end collisions in a high-fidelity driving simulator.* DOT-HS-809-448, NHTSA,USDOT, Washington D.C.

Levinson, W. H. (1998). "Interactive highway safety design model: Issues related to driver modeling." *Transportation Research Record*, 1631, 20-27.

Lubashevsky, I., Wagner, P., and Mahnke, R. (2003). "Bounded rational driver models." *European Physical Journal B*, 32(2), 243-247.

Marshal, R. E., and Mahack, K. (1998). "Determinants of headway selection." Transportation Research Board 77th Annual Meeting, Washington D.C.

McDonald, M., Brackstone, M. A., Sultan, B., and Roach, C. (1997). "Close following on the motorway: initial findings of an instrumented vehicle study." the 7th Vision in Vehicles Conference, Marseille, France.

Mehmood, A., Saccomanno, F., and Hellinga, B. (2001). "Simulation of road crashes by use of systems dynamics." *Transportation Research Record*, 1746, 37-46.

Michaels, R. M. (1965). "Perceptual factors in car following." *Proceedings of the Second International Symposium on the Theory of Traffic Flow: London 1963*, J. Almond, ed., The Organization for Economic Co-operation and Development (OECD), Paris, France.

Michaels, R. M., and Cozan, L. W. (1963). "Perceptual and field factors causing lateral displacement " *Highway Research Record*, 25.

Nagel, K., and Schreckenberg, M. (1992). "A cellular automaton model for freeway traffic." *Journal of Physical Institute of France*, 2, 2221-2229.

Newell, G. F. (1961). "Nonlinear effects in the dynamics of car following." *Operations Research*, 9, 209-229.

Pike, R. W. (1986). *Optimization for Engineering Systems*, Van Nostrand Reinhold Company, New York, NY.

Pipes, L. A. (1953). "An operational analysis of traffic dynamics." *Journal of Applied Physics*, 24(3), 274-281.

Ranjitkar, P. (2004). "Experimental analysis of car following dynamics based on RTK GPS data." *Proceedings of Infrastructure Planning 2004, Japan Society of Civil Engineers* (JSCE).

Rong, J., Wang, L., and Xu, X. (2006). "A variable response time lag analysis using car following data in urban expressway sections." CD-ROM 06-1611 Transportation Research Board Annual Meeting, Washington D.C.

Rothery, R. W. (1999). "Car Following Models." *Revised Monograph on Traffic Flow Theory*, N. Gartner, C. J. Messer, and A. K. Rathi, eds., Transportation Research Board (TRB), Special Report 165, Chap.4.

Senders, J. W., Kristofferson, A. B., Levison, W. H., and Ward, J. L. (1967). "The attentional demand of automobile driving." *Highway Research Record*, 195, 15-33.

Sultan, B., Brackstone, M., and McDonald, M. (2004). "Evidence for the use of deceleration/acceleration in car following." *Transportation Research Record*, 1883, 31-39.

Sun, H., and Frost, B. J. (1998). "Computation of different optical variables of looming objects in pigeon nucleus rotundus neurons." *Nature Neuroscience*, 1(4), 296-303.

Sussman, E. D., Bishop, H., Madnick, B., and Walter, R. (1985). "Driver inattention and highway safety." *Transportation Research Record*, 1047, 40-48.

Systematics, C. (2006). *NG-VIDEO User's Manual*. Federal Highway Administration, Washington D.C.

Todesiev, E. P. (1963). "The action point model of the driver vehicle system," Doctoral Dissertation, Ohio State University, Columbus, OH.

Toledo, T. (2003). "Ingegrated driving behavior modeling," Doctoral Dissertation, Massachusetts Institute of Technology, Boston, MA.

Torday, A., Baumann, D., and Dumont, A.-G. (2003). "Indicator for microsimulation-based safety evaluation." 3rd Swiss Transport Research Conference, Monte Verita, Ascona, Switzerland.

Treiber, M., Hennecke, A., and Helbing, D. (2000). "Microscopic simulation of congested traffic." *Traffic and Granular Flow '99: Social, Traffic and Granular Dynamics*, D. Helbing, H. J. Herrmann, and M. Schreckenberg, eds., Springer, Berlin, Germany.

TSS. (2005). *AIMSUN NG Manual.* TSS-Transport Simulation Systems. Barcelona, Spain.

Wang, J. (2005). "A merging model for motorway traffic." Doctoral Dissertation, The University of Leeds, Leeds, Great Britain.

Wang, L., Rong, J., and Xu, X. (2006). "Variable reaction time lag analysis using car-following data in urban expressway sections." Transportation Research Board 85th Annual Meeting CDROM, Washington D.C., Jan 22-26, 2006.

Wiedemann, R., and Rieter, U. (1970s). *Microscopic traffic simulation: the simulation system MISSION background and actual state*. PTV Vision, Germany.

Wiedemann, R., and U. Reiter. (1992). *Microscopic traffic simulation: the simulation system MISSION, background and actual state.* Project ICARUS(V1052) Final Report, Brussels, Belgium.

Xing, J. (1995). "A parameter identification of a car following model." *Proceedings of the 2nd World Congress on ATT*, Yokohama, Japan, 1739-1745.

Zhang, H. M., and Kim, T. (2005). "A car-folowing theory for multiphase vehicular traffic flow." *Transportation Research Part B:Methodological*, 39(5), 385-399.

Zhang, X., and Jarrett, D. F. (1997). "Stability analysis of the classical car-following model." *Transportation Research Part B:Methodological*, 31(6), 441-462.